MAREES TERRESTRES

BULLETIN D'INFORMATIONS

N° 94

15 JUIN 1985

Association Internationale de Geodesie

Commission Permanente des Marees Terrestres

Editeur Prof. Paul MELCHIOR

Observatoire royal de Belgique

Avenue Circulaire 3

1180 Bruxelles

TABLE DES MATIERES

PROCESSING AND ANALYSIS OF THE DATA

RESULTS OBTAINED WITH THE SUPERCONDUCTING GRAVIMETER ESP. WITH REGARD TO THE STUDY OF VERY LOW FREQUENCIES

ALGORITHMS FOR TIDAL LOADING COMPUTATION

* no paper prepared.

Preface

At the IUGG-Assembly in Hamburg, August 1983, it was agreed to continue the working group renamed to

"Working Group on Acquisition, Processing and Analysis of Earth Tidal Data"

The tasks of this group were enlarged by the topics

"Results obtained with the Superconducting Gravimeter esp. with regard to the study of very low frequencies"

and

"Algorithms for tidal loading computation"

It was decided to have a meeting of the working group to prepare a report for the 10th International Symposium on Earth Tides in Madrid, September 1985. This meeting took place at the "Institut für Theoretische Geodäsie", University of Bonn, Oct. 3.-5, 1984, and Prof. M. Bonatz was our accomodating host. The members of the working group and other interested colleagues took part, and altogether 21 scientists from 11 countries were present.

The content of this volume covers the topics of our meeting. The conclusions drawn are printed at first place, and they allow an overview over the following papers.

Here I should like to thank all participants for their contributions, and Prof. Bonatz for his hospitality. Finally we all acknowledge the support of the Deutsche Forschungsgemeinschaft, which enabled the participation of some of our colleagues.

Gerhard Jentzsch

Conclusions

On the basis of the previous report (New York, 1981, see proceedings of the 9th Int. Symp. on Earth Tides) the working group suggests the following conclusions:

1. Instrumentation and data acquisition

It should be noted that still no standardization is possible, but concerning the observations the following points should be taken into account:

- The timing accuracy should be better than + 5 s for each reading
- The dynamic range should cover at least 12 bits (corresponding to 4096 steps), no matter whether using digital or analogue recording (with chart stepper)
- Environmental parameters should be recorded. The type and number of parameters should be consistent with the requirement of the measurements. Air pressure should be recorded with an accuracy of at least 1 mbar. Regarding tilt measurements (esp. borehole tiltmeters) water table and ground water temperature should be recorded.
- Feedback systems should be used as an improvement of stability, esp. in the case of astatized instruments.

2. Preprocessing and analysis

- The sampling rate should be consistent with the storage capabilities and satisfy the Nyquist criterion. This applies to analog as well as to digital data. Digital data should be filtered numerically.
- The calibration of the instrument should provide the complete transfer function, e.g. amplitude factor and phase shift.
- Absolute calibration with in situ methods should be considered, esp. for gravimeters
- Checks of sensitivity disturb the record. Therefore, also computation methods should be considered in order to reduce the required number of sensitivity checks. In addition, the above recommendation regarding feedback will give much greater stability in sensitivity and therefore reduce the required number of sensitivity checks.

- In order to enable an easy program exchange between research groups and institutions the following information upon used computer programs should be given to the International Center (ICET): purpose, language, size, used computer. This information should be distributed by ICET at request.

3. Superconducting gravimeter

The working group realizes the progress achieved in recording with this instrument.

4. Tidal loading computation

- Using tidal charts based on a grid structure the true mass center should be taken into account, esp. approaching polar regions, if a point mass load method is used.

- Regarding local cotidal maps, the size of the ocean cells should be about a fifth of the distance to the instrument site.

- For theoretical load calculations for coastal stations a local seismic structure should be considered.

- The results of theoretical load calculations published should contain both the mass conservation and the non-conservation solutions.

- The results of overall loading computations with global models provided by ICET should be marked when the station is closer to the sea than 300 km. Then the results should be used only with special care.

5. Data bank

- The standard format for earth tide data is extended when tapes are used as storage medium. Then the first 20 columns are used as usual, and a record of 12 observations should be added covering a suitable number of digits (e.g a resolution of 1/100 gal is also possible).

- The data bank should be provided with data from every station. If that is not possible at least a copy of an analysis print-out should be made available applying a compatible method.

- The data of the data bank is available to everybody if permission of the donator is given.

PERFORMANCE OF TIDAL INSTRUMENTS AND DATA EVALUATION

Manfred BONATZ

Institut für Theoretische Geodäsie
BONN

During the last decade essential progress has been achieved concerning instrumental performance; in terms of internal precision gravimeters attain resolutions of 1...0.01 µGal, tiltmeters 0".0001 and strainmeters 10^{-10} respectively. Unfortunately the situation is not correspondingly favorable if we are looking for the absolute accuracy; at least for gravimeters it is still problematic to get a calibration to better than 0.5%. In this context it has to be stated, that calibration means determination of the whole response function of the instrument: intrumental scale and phase, both principally frequency dependant.

Beyond a certain instrumental resolution it becomes difficult clearly to distinguish between instrumental and geophysical perturbation effects. This is specially true for tilt and strain measurements as in both such cases very local influence affect the coupling of the sensors to the Earth's crust. In addition when performing high-precision measurements one observes a quantity of different phenomena, not only the tides of the solid Earth.

The recorded signal can be devided into two categories: signals due to instrumental imperfections and such due to geophysical processes (which additionally may also induce instrumental perturbation effects). To the first group belong effects caused by variations of temperature, airpressure, magnetic and electrical field, aging of matter etc. Geophysical signals are real physical quantities

in the dimension for which the sensor was designed: direct and indirect tidal effects, influences of tectonical or rockmechanical processes, of groundwater, airpressure etc.

Until now the analysis of the observed time series is more or less restricted to the tidal part of the signal: mainly by least-squares-techniques one determines the "observed" tidal parameters (amplitude and phase) using quantities of celestial mechanics (angular velocity of partial tides) as basis input. But looking at the distribrution of the residuals after the adjustments one can easily recognize, that they are (practically always) more or less away from a random distribution which had to be, if the underlying deterministic and stochastic model would sufficiently correctly represent the physical "reality". On the other hand: if the residuals after adjustment are not randomly distributed the basic assumption of the analysis is not fullfilled, which means that the estimated tidal parameters contain systematical errors.

It is already since a couple of years that this problematic situation has been discussed. The way out is called the "multichannel analysis". It means that parallel to the "tidal" observation some other relevant parameters are observed such that the data analysis can base upon a physically more realistic model taking into account the whole complexity of the observed physical processes. As a measure for the quality of the extended model the distribution of the residuals after analysis can be regarded, whether or not they are randomly distributed, respectively to which degree this claim has been fullfilled.

Except for some special investigations, there will be no more essential progress in the future, neither in tidal research (instrumental as well as interpretation) nor in investigations concerning such signals which are of tide induced or nontidal origin, if the problem of multichannel analysis is not solved.

This is what we need at present most urgently.

MULTICHANNEL RECORDING OF DIFFERENT EARTH TIDE COMPONENTS AT BUDAPEST STATION

Varga, P., Hegymegi L.

Eötvös Loránd Geophysical Institute of Hungary,

Columbus u. 17-23. Budapest, H - 1145

For recording different Earth tide components a new underground station was esteblished in NW part of Budapest in a cave - the total length of which is approximately 2.5 km. A small part of this cave recently - since April of 1981 - is occupied by the station /Fig. 1./. The instruments installed in this station are of about 40 meters from the entrance and also 40 meters under the surface of the Earth. This station was designed for two different purposes:

- to carry out absolute gravity measurements
- to record time variations with different kind of instruments. Until now registrations with gravimeters, pendulums and extensometer have been carried out

The central part of the station is the so called "absolute room" where in 1981 and 1983 the absolute gravity measurements have been carried out. In this room the recording systems - both analogous and digital - are installed. From this place can be done the distance regulation of gravimeters and extensometer. In this room are recorded the meteorological factors /humidity, air pressure/ as well. The absolute room is heated. The regulated temperature there is $25^{o}C$. The temperature of the other parts of the station is $12^{o}C$ like in the other parts of the cave. The annual variations are less then $1^{o}C$, the daily variations are of order $10^{-2}C^{o}$. Pendulums and recording gravimeters are installed in tunnels around the absolute room. Gravimeters with and without thermostatisation are used.

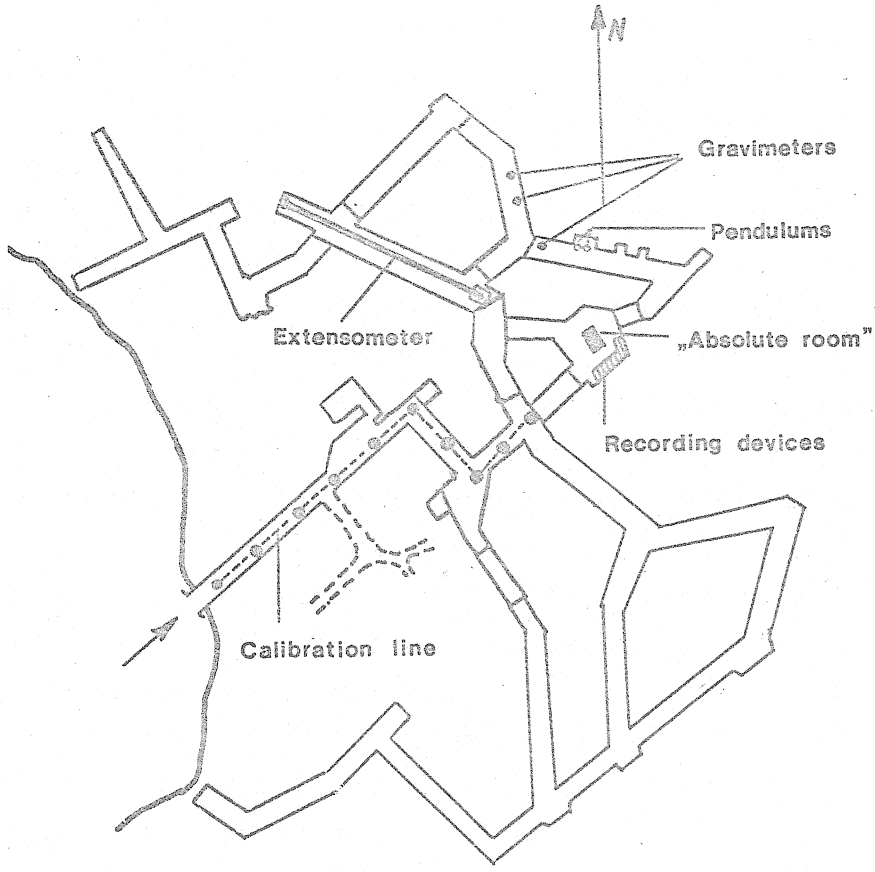

Fig. 1.

A 21 m long quartz tube extensometer, provided with capacitive transducer, is also in operation. This instrument is supplied with an automatic calibration device, which allows to determine the record scale with accuracy 2.5 %. It seems, that the most serious difficulty to get reliable gravimetric Earth tidal parameters is the calibration. To overcome this problem we used two different possibilities:

a./ an underground calibration line /Fig. 1./ of 1 mgal range within 35 meters has been established. The favourable feature of this small range line is, that the measurements can be carried out under thermostatised conditions

b./ comparison with absolute gravity measurements. Purpose of these determinations were to obtain a good absolute gravity value.

Therefore the observations were carried out during the minimum of tidal variations. The gravity difference of lunisolar origin was only 60-70 microgals. In spite of this unfavourable condition for the calibration of the recording instruments rather good calibration factor has been obtained for Askania gravimeter BN 07 /Fig.2./. The accuracy of this calibration was 1.5% and we hope to get better results when the absolute gravity measurements will be repeated at the time of maximal tidal variations.

To automatize the recording we completed a relative simple data acquisition equipment, which is based on a HP 41 CV calculator /Fig.3./. This system can collect output of 8 different instruments. Recently only two gravimeters and the extensometer is connected to this digital data acquisition system. The sempling rate is 1 minute for every instruments connected to this equipment. The HP 41 CV determines for every instrument on this basis a hourly value which is recorded on a digital casette recorder and printed on a line printer.

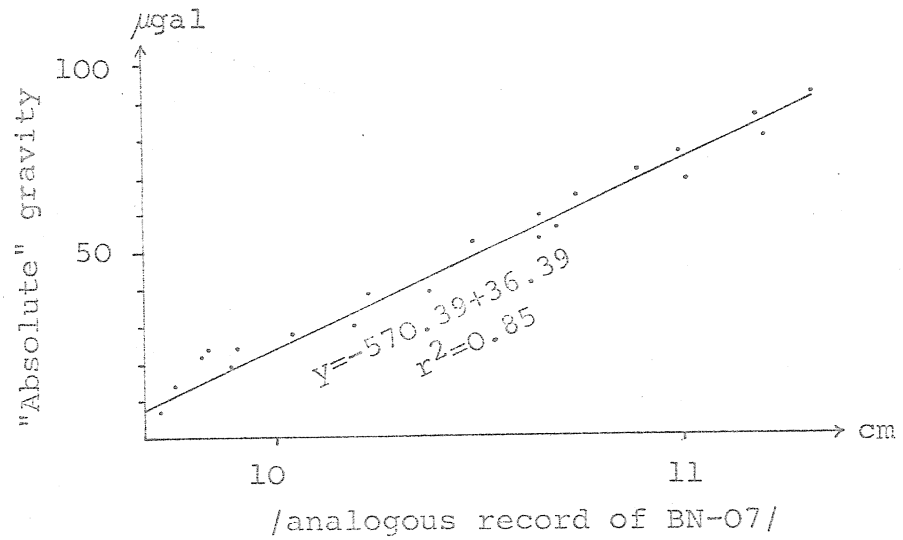

/analogous record of BN-07/

Fig. 2.

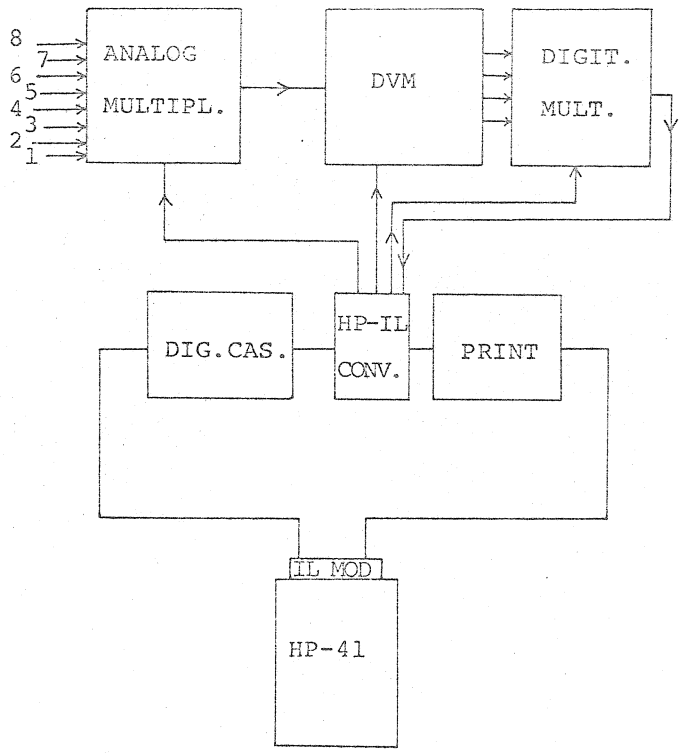

Fig.3.

The positive feature of this system is, that it is relatively cheap, works correctly, can be completed with rather simple knowledge in electrinics. The whole system is regulated with the HP 41 CV which carries out the processing of the collected data also.
A comparison of the calibration of the analogous and digital records is shown on Fig.4.

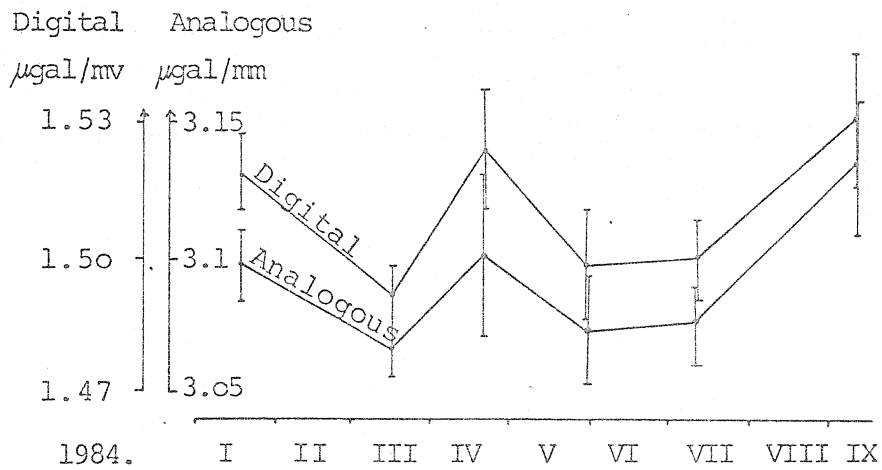

Fig.4.

Table 1.

STATION: BUDAPEST
Gravimeter: BN-07 19. 3. 1982. - 22. 11. 1982.
/5753 hourly observations/

	Amplitude factor	Phase
O_1	1.1565 ± 0.0022	$0^\circ.16 \pm 0^\circ.11$
K_1	1.1412 ± 0.0028	$0^\circ.15 \pm 0^\circ.14$
N_2	1.1681 ± 0.0070	$0^\circ.40 \pm 0^\circ.34$
M_2	1.1908 ± 0.0014	$0^\circ.63 \pm 0^\circ.07$
S_2	1.0672 ± 0.0873	$-4^\circ.05 \pm 4^\circ.50$

Extensometer

	Amplitude $\times 10^{-9}$	Phase	l/h	l/h (theoretical)
O_1	5.36 ± 0.36	$-1^\circ.3 \pm 3^\circ.8$	0.153	0.146
K_1	5.53 ± 0.33	$2^\circ.6 \pm 3^\circ.4$	0.130	0.186
N_2	0.55 ± 0.19	$8^\circ.0 \pm 20^\circ.3$	0.130	0.146
M_2	2.67 ± 0.17	$-10^\circ.3 \pm 3^\circ.7$	0.125	0.146
S_2	1.26 ± 0.16	$-16^\circ.5 \pm 7^\circ.1$	0.129	0.146

Until now we have at our disposal analysis results for gravimeter BN-07 and for the quartz extensometer /Table 1./. The accuracy of extensometric data can be improved. Naturally the analysed period in the case of extensometers is too short, to obtain good analysis results.
Concerning the gravimetric data it is to be noted that the M_2 residual determined on the basis of measurements in Budapest is in good agreement with the results of stations in this region /Fig. 5./.

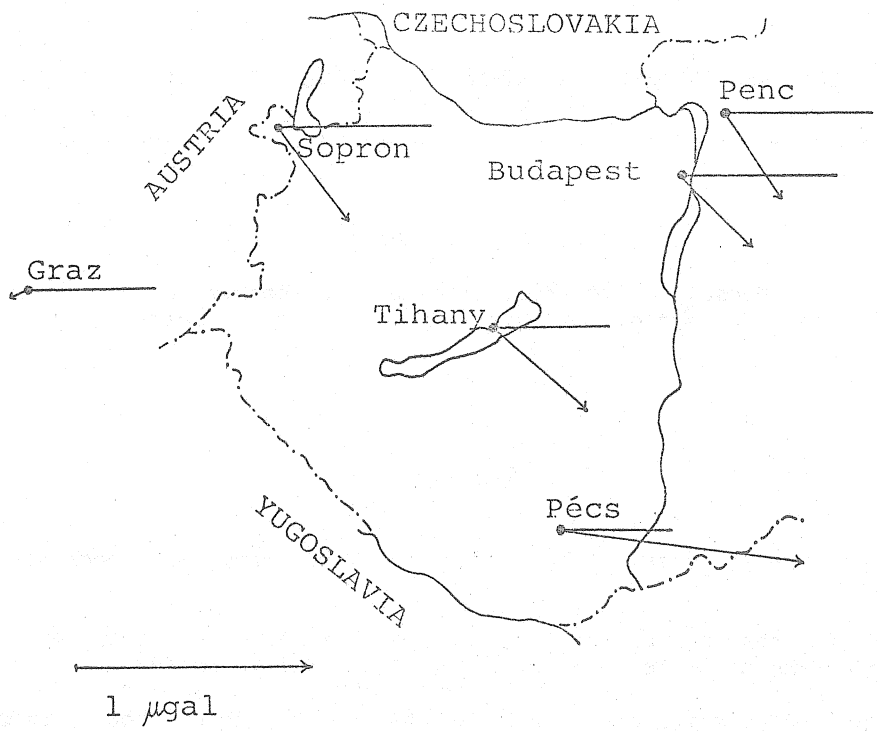

	M_2 RESIDUALS	
	Ampl.	Phase
Graz	0.06 μgal	$-179^{\circ}.57$
Sopron	0.51 μgal	$-51^{\circ}.44$
Tihany	0.57 μgal	$-50^{\circ}.73$
Budapest	0.25 μgal	$-45^{\circ}.99$
Penc	0.51 μgal	$-53^{\circ}.58$
Pécs	1.09 μgal	$-8^{\circ}.51$

Fig.5.

MEETING OF THE WORKING GROUP ON TIDAL DATA PROCESSING
Bonn, October 3-5, 1984.

TIDAL GRAVIMETERS: ENVIRONMENTAL EFFECTS, RESPONSE, AND DATA ACQUISITION

Hans-Georg Scherneck

Uppsala University, Institute of Geophysics
Dep. of Geodesy, Hällby; S-755 90 Uppsala, Sweden.

SUMMARY

Influences of site air pressure and temperature upon gravimeter observations are considered.

Two sources of phase shifts of the instrumental signal are investigated: the response of an analog filter and the creep of the sensor spring.

Finally, a simple data acquisition scheme which yields hourly samples of enhanced quality is presented.

INTRODUCTION

The fact that the instrumentally observed quantities of tidal gravity differ from the predictions based on tidal models due to instrumental effects is understandingly a major point of concern for the experimentators working in our subject. The objective is to identify, mathematically describe and remove the signal disturbances and distortions, and this process is to result in an observational time series which allows unbiased inferences to the tidal models. A realistic description of the experimental situation might be given in the form

$$y = C * g + D * x + e$$

where we want to retain the time variant part of the local acceleration g, or at least a frequency band limited part of it. The instrument readings y are dynamic responses to gravity as well as to a multiple of environmental effects x like the bouyancy forces of the sensor mass in the air, the temperature distribution over the sensor suspension and electronic circuits, or magnetic fields. The dynamic behaviour is indicated by the convolution operator *, the instrument being characterized by transfer functions C and D. e contains the signal drift and errors, or in a stronger sense those contributions to y which appear non-predictable.

This presentation is based upon experiments which were carried out with ASKANIA gravimeter GS-15 No.224 at Uppsala university. The instrument was isolated in a 1.5 m³ foam filled box within a 20 m³ room. This room is situated in an

underground depot driven 20 m into a granit hill. Air pressure and temperature in the site room was recorded simultaneously with gravity.

1. Air pressure and temperature effects.

Air pressure and temperature changes in the environment of an ASKANIA gravimeter affect the instrument readings; this has been reported in various papers, e.g. BONATZ (1965), WENZEL (1974). The spectral power of both processes increases towards low frequencies. Depending upon how well a gravimeter is isolated, related disturbances break even with the level of measurement resolution typically at semidiurnal or diurnal frequencies. In the case of the Uppsala site, the average temperature did not change by more than 0.05 K/day. Yet significant coherence with the residual gravity, i.e. observation minus body- and ocean-tide model, at frequencies < 10 °/h was found (c.f. fig. 1). On the other hand, a semidiurnal temperature oscillation of 0.01 K, which is believed to be caused by thermal convection in the site room, does not appear to be a major problem. The coherence diagramme in fig.1, however, might give a too optimistic result as a residual M2 effect could not be separated in the gravity spectrum. Coherence of the gravity residuals with air pressure at low frequencies is clearly evident. Air pressure variations own a sharper long period pronounciation, as concluded from the requirement of a 4'th order autoregressive process in order to whiten the spectrum (temperature was modelled with one order). From the size of the effects (the deduction is not given in detail; fig. 2 may suffice for comparison) it is suggested that only a minor part of the pressure effect is due to mass attraction and ground loading and that the major disturbance stems from an uncompensated bouyancy of the sensor mass in the surrounding air.

Without further effort, the study of long periodic tides with traditional gravimeters will not be feasable. One way of proceeding is to attempt to determine the sensitivity operator (transfer function) of the instrument accounting for the environmental effects by solving the multi-channel problem

$$\underline{\underline{C}}_{pT}(k-j)\ \underline{h}_{pT}(j) = \underline{C}_{g,pT}(k)$$

using e.g. the Levinson-algorithm (CLAERBOUT 1976, chap.7).

The competing requirements on such a system for obtaining a satisfying prediction filter solution h (c.f. JENKINS and WATTS 1968), like the amount of samples input versus the length of the filter, the signal bandwidth and power distribution versus the sampling frequency, but also the requirements on the stationarity of the time series could not be met simultaneously. Our predicted disturbance overestimates high frequency and underestimates low frequency variations. In attempts to solve more than 48 filter coefficients, the solution became unstable. The result obtained using 36 filter coefficients is shown in fig. 2.

Returning to the S2 wave we give here the following results from standard least square harmonic analysis (Schueller programme in "Chojnicki-mode") of 3500 hourly samples taken at our site:

observed amplitude	10.7 μgal
observed amplitude factor	(1.175, 0.002i) +- 0.003
" after filter phase lag compensation	(1.175, 0.005i)
predicted ocean loading effect:	0.18 μgal, 14°
" " " " (delta-scale):	(0.019, 0.005i)
air pressure effect (0.3 μgal/mbar)	0.068 μgal, -10°
" " " (delta-scale):	(0.006,-0.001i) +- 0.003
Molodenski reference model + inertial corr.:	(1.163, 0.0i)
residual	(-0.013, 0.001i)

S2 determinations are almost avoided in the literature due to the sensitivity of the instruments to atmospheric effects. Our result however would be consistent with the local M2 result (observed load effect = 2/3 predicted effect) if we can discard the site S2 temperature effect as a cause for the observed residual.

Another instrument (ASKANIA GS 11) of our department recording in a mine at 400 m depth shows a residual (no correction for pressure and temperature) of (0.015, 0.035i) on the delta-scale after subtraction of the Schwiderski ocean load solution. Obviously, deep siting does not guarantee absence of environmental effects.

2. Phase delays.

Two sources of phase lags of the instrument's signal in respect to the ambient acceleration were investigated: an analog low pass filter and the rheologic behaviour of the sensor springs.

Because of the microseismic background, analog filters are used for cleaning signals to be given to chart recorders or, in the case of digital data acquisition, for rejecting signal power above the sampling Nyquist frequency. Inevitably, such filters induce phase lags. E.g. a three pole Chebychev filter causes a phase lag of 0.16° for semidiurnal frequencies if the filter's 3-dB-point occurs at 0.018 Hz (c.f. fig.3). This effect is significant for M2 determinations (our accuracy: 2σ =0.04 μgal). A method is suggested to compute the filter phase lag by a combination of circuit analysis, using the nominal values of the electronic components, and a step response experiment to refine the component values (see remarks in fig.3). The method succeeds if the resistors of the RC-network are equal within 1 or 2 %. The characteristic step response values (slew rate, ripple features) are readily computed from the characteristic polynomial. The filter design equations can be found in GEFFE (1976). The method offers adventages in accuracy compared with direct step response transform methods or real time long period response experiments. Our ad-hoc estimation indicates at least an accuracy of 5 % for the phase lag determination. Possible flaws could arise from the finite resistances of capacitors (electrolytic devices should be avoided in any case) and the operational amplifier input stage.

Anelastic creep of the gravimeter springs and possibly also the sensor suspension frame are responsible for a but small discrepancy between sensitivity values obtained in short term calibration experiments and the sensitivity valid in the long term (tidal) spectral band. Determination of the rheological properties of astatized gravimeters was given by DUCARME (1975), mainly accounting for the damping of the system using a Kelvin-body as a model (MELCHIOR, 1978, chap.9.8). In this study, where the nonastatized ASKANIA system is concerned, we attribute the non-elastic behaviour to internal friction of solid state material. In order to determine the material creep strength and the dominant relaxation time (c.f. NOWICK and BERRY 1972, pp 46-57), a step response experiment was performed utilizing the electromagnetic calibration system of the GS 15. Experimental control and and sampling was fully microcomputer operated. A series of the response to 22 steps (+/- current polarisation) of 4.27 h duration and 275 μgal amplitude each, sampled at 15 s interval (12 bit resolution, 400 μgal dynamic range) was analyzed after subtraction of known Earth and ocean tide effects, the instrumental drift (6'th order polynomial), and a pure best fitting rectangular wave. Finally, all samples of equal delay in respect to the switching cycle were averaged with weights of either plus or minus one, depending upon the step polarity. With the switching period given, the averaging operation rejects residual tidal frequencies by -20 dB or more, but is sensitive to quarterdiurnal effects. The curve thus obtained (c.f. fig.4) shows exponential character and is supposed to represent the creep function. Within an interval of 16 minutes after switching, the series is perturbed due to the response delay of the analog filter. A

pessimistic assumption for the creep function during this interval is included in fig.4b.

We conclude: $\Delta = 0.5 \ldots 0.9 * 10^{-3}$ and $\tau = 1200 \ldots 600$ s.

From a diagramme for the phase shift of semidiurnal frequencies induced by a Zener body (μ=1, Δ, τ), we obtain negligible values of less than 0.01°. An increase of sensitivity in the relaxed state (tidal frequencies) by a fraction of Δ from the partially unrelaxed response due to short (< 1 h) calibration pulses is indicated, being significant provided that accuracies of better than 1:1000 are acheived.

3. Data acquisition.

A simple algorithm is presented for digital real time sampling of tidal signals, providing hourly or semi-hourly records R:

$$R_j = \sum_{k=-K}^{K} w_k \; r_{j+k} \; / \; \sum w_k \qquad (3.1)$$

where the r(j+k) are the quantized samples at times 3600j + 10k seconds. Hanning weights w, K=45, provide effective rejection of periodicities less than 150 s (e.g. thermostatic disturbances, a common problem with the GS 15 gravimeter). (3.1) implies no true convolution; the system employing it remains idle during 45 (15) minutes. Thus, the R's are sensitive to spectral aliasing. However, studies of the noise power distribution over the spectral range above the Nyquist frequency of the R's suggest the feasability of (3.1): the noise power decreases with increasing frequency by at least -10 dB until the Hanning filter attenuation takes over (c.f. fig.5). Remote earthquakes might distroy the quality of one or two samples in 500...1000.

Due to the short digitisation interval of 10 s for the r's, the antialiasing analog filter described in section (2) and fig. 3 is suitable. Lower digitisation rates demand a lower knee frequency, which consequently leeds to increased phase shifts and increased demands on accuracy when the filter characteristics are to be computed. The reader is referred to ASCH (1983) for comparison with the features and implications of a direct sample-and-store data acquisition strategy.

The sum in (3.1) reduces the quantisation noise variance by
$\sum w(i)^2 / (\sum w(i))^2 = 0.016$. Therefore, (3.1) should be computed with 1.5 figures beyond the decimal point if the r's resolution is unity. The reader is referred to ZUERN (1974) for further implications.

The procedure outlined offers the following adventages:

1. The sampling process can be realized with a commercial personal computer, provided an analog-digital converter and a good quartz clock are supported. System development costs can be kept low.
2. The sampling programme can be extended to allow operation on user demand during the idle time spans, e.g. for calibration experiments.
3. Programming and operation can be done conveniently.
4. The output data rates are extremely low. Values can be collected in blocks before they are sent to e.g. a cassette unit.

More than 90% of the data used in this article was sampled with the aid of an inexpensive personal computer[1]. One of 10,000 samples was lost due to a bad

---

[1] Scandia-Metric ABC-80

place on the tape. The weakest point of the system is its sensitivity to power failures or, respectively, the effort required to maintain power buffers of sufficient quality.

CONCLUSIONS

Site effect modelling accounting for air pressure and temperature variations has not given satisfying results yet.

A convenient method for obtaining the phase shift of an analog filter was outlined. Accuracies better than 5% can be achieved. Typical analog filters used as anti-aliasing filters before digital data sampling yield significant phase shifts in the tidal bands.

Anelastic creep effects upon the response of the ASKANIA gravimeter springs can be neglected.

Given a low-noise environment in the spectral range between 0.5 and 15 cyc/h, hourly samples, a rate sufficient for most kinds of tidal analysis, can be collected from disjunct weighted averages employing an ordinary personal computer.

REFERENCES

ASCH, G., 1983: Digital data acquisition and preprocessing of tidal data.
BIM No.89, pp 5742-5758.

BONATZ, M., 1965: Der Einfluss der Aussentemperatur auf den Gang des ASKANIA Gravimeters GS 11 No.116.
Zeits.Vermess.12 90 pp 497-506.

CLAERBOUT, J.F., 1976: Fundamentals of geophysical data processing.
McGraw-Hill.

DUCARME, B., 1975: A fundamental station for trans-world tidal gravity profiles.
Phys.Earth Planet.Inter.11, pp 119-127.

GEFFE, P.R., 1976: How to build high-quality filters out of low quality parts.
Electronics Vol.49, No.23, pp 111-113.

JENKINS, G.M., and D.G. WATTS, 1976: Spectral analysis and its applications.
Holden Day, San Francisco.

MELCHIOR, P., 1978: The tides of the planet Earth.
Pergamon Press.

NOWICK, A.S., and B.S. BERRY, 1972: Anelastic relaxation in crystalline solids.
Academic Press, New York, London.

WENZEL, H.G., 1974: Der Einfluss von Luftdruck und Lufttemperatur auf gravimetrische Erdgezeitenbeobachtungen.
Mitteilungen Inst.theor.Geodaesie Hannover.

ZUERN, W., 1974: Detectability of small harmonic signals in digitized records.
J.Geophys.Res. Vol.79 No.29, pp 4433-4438.

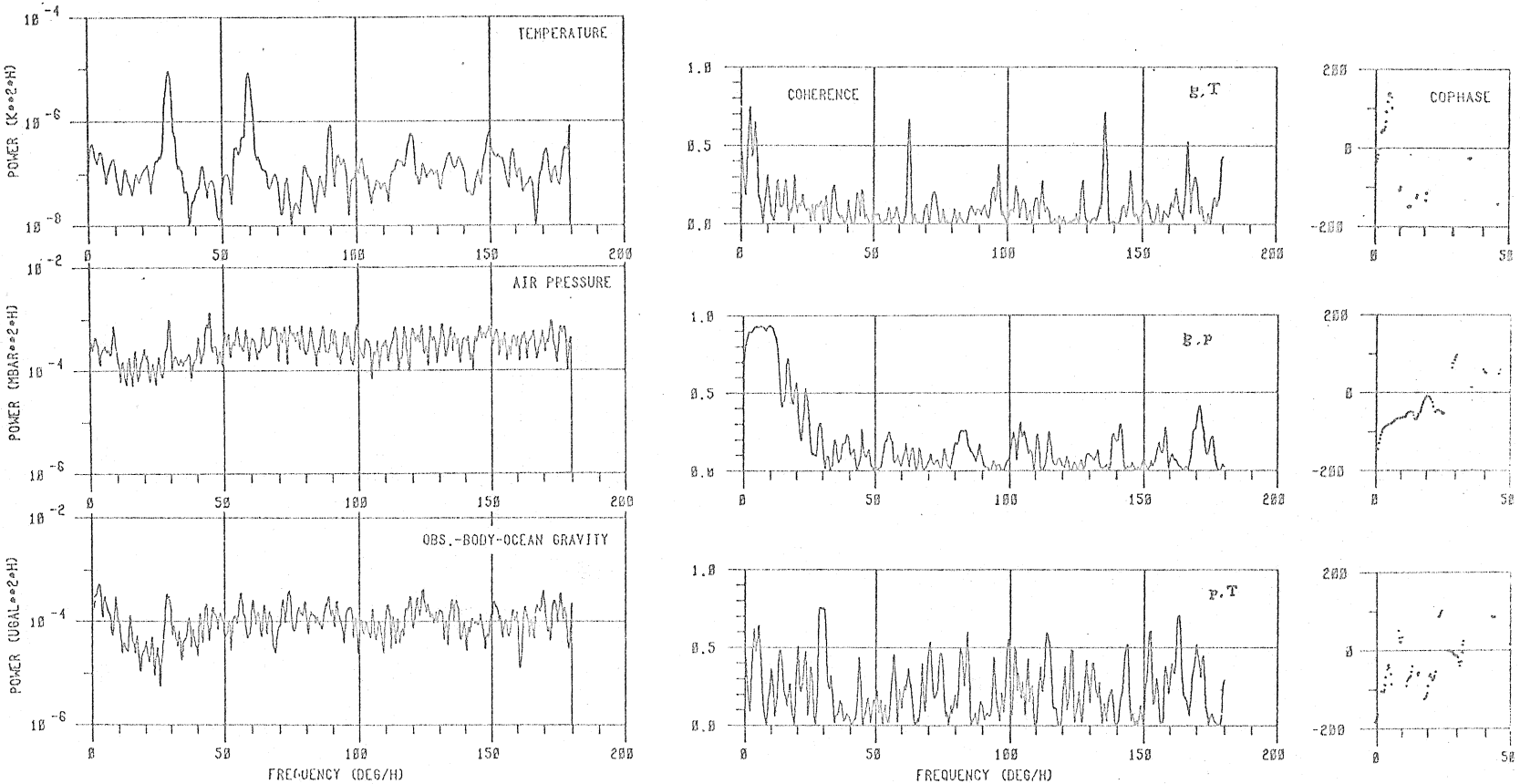

Fig.1: Relations between simultaneous series of site temperature, air pressure and residual gravity in the spectral domain. Significant coherence is limited to low frequencies because the instrument's isolation from its environment becomes less effective as periods increase. From the cophase between air pressure and gravity which turns to a static value (-180 deg.) only at extremely low frequencies one can infer that a dynamic response model would have to span over more than 100 hours.

The dominant features in the temperature power spectrum are supposed to be related to thermal convection in the site room. The fundamental effect is semidiurnal. The gravimeter appears to be weakly affected.

All series except temperature were whitened using a maximum entropy method before the co-spectra were computed. As sinusiods were present in the lower half of the spectra, the reliability of the co-spectra is degraded in their upper half due to high frequency noise exaggeration.

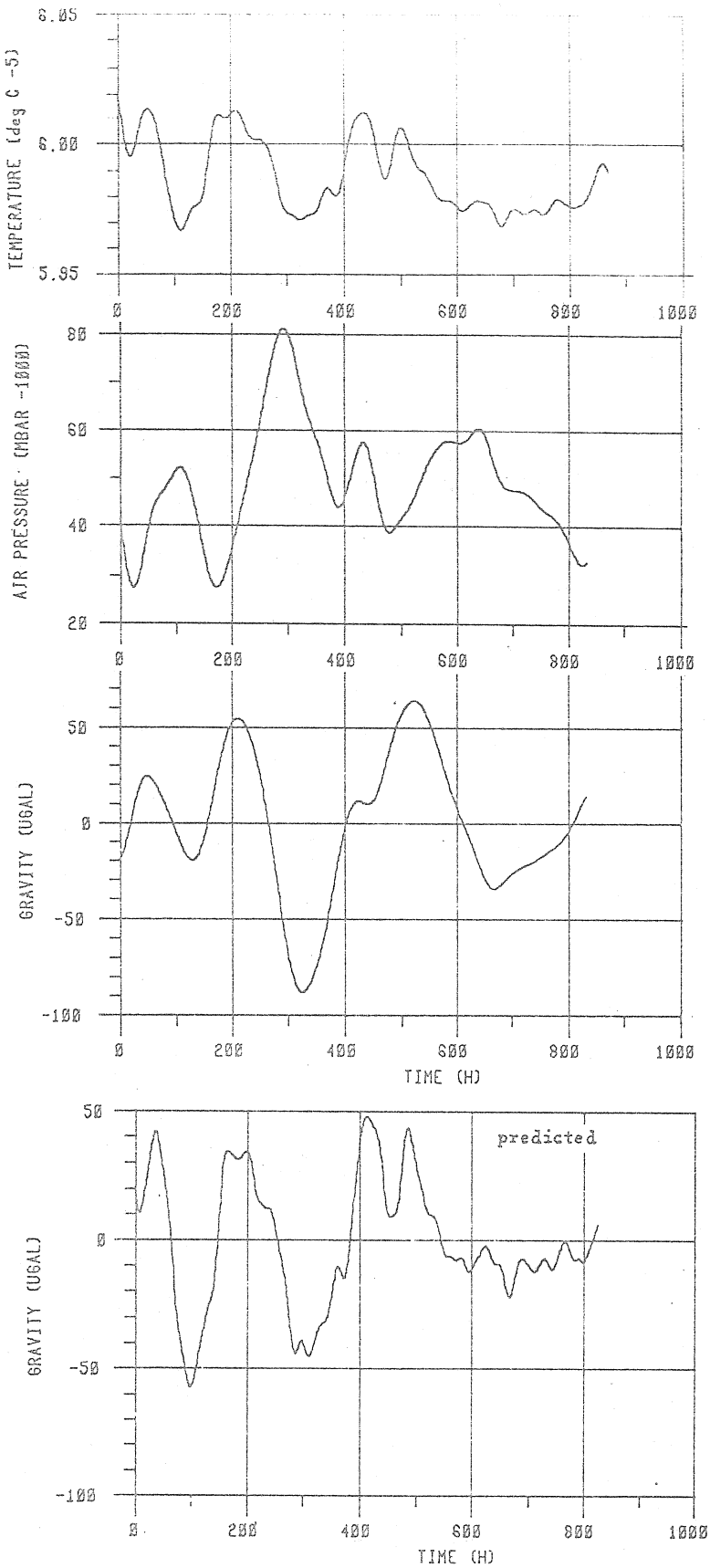

Fig.2: On the basis of the three time series of site temperature, air pressure and residual gravity a two-channel filter can be constructed for a prediction of constituents of the instrument's trend. The bottom plot resulted using a filter with 36 coefficients. The result suggests the need of considerable improvement of the signal analysis method employed.

3–Pole Filter Response

Response Spectrum

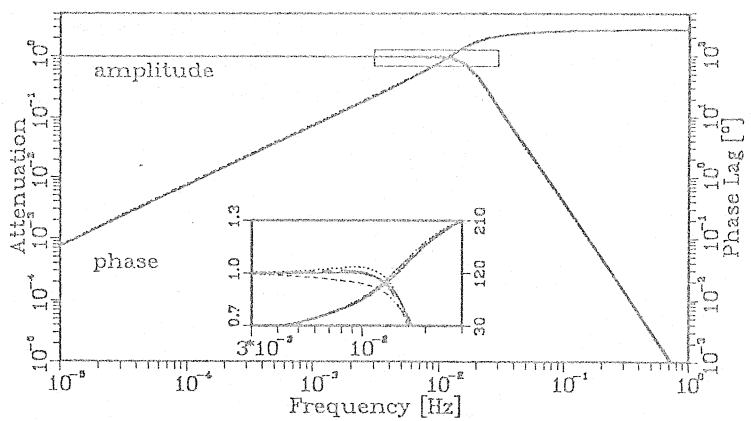

$C_1 = 3.4\ \mu F$
$C_2 = 10.0\ "\quad R = 4.3\ M\Omega$
$C_3 = 0.38\ "$

vary $\{C_1, C_2, C_3\}$ by + 10 %

Unit Step Response

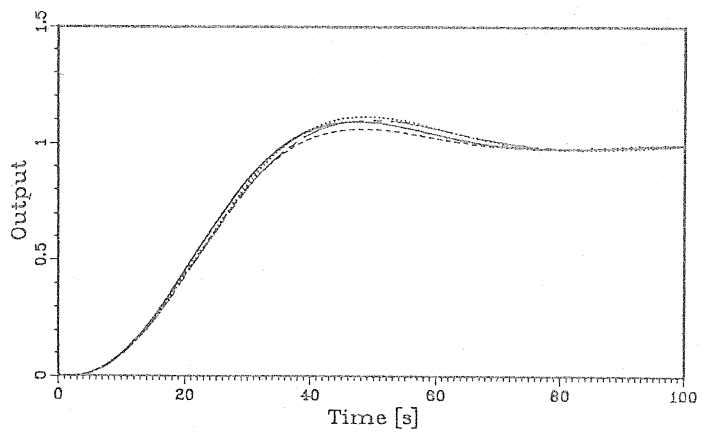

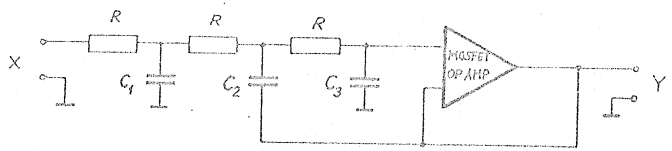

System characteristic polynomial: $y(p) = h(p) \times (p)$

$$h(p) = \left[R^3 C_1 C_2 C_3 p^3 + 2R^2 C_3 (C_1 + C_2) p^2 + R(C_1 + 3C_3) p + 1\right]^{-1}$$

Step response:

$$y(t) = -\lambda_1 \lambda_2 \lambda_3 \sum_{j=1}^{4} e^{\lambda_j t} / \prod_{k \neq j} (\lambda_j - \lambda_k)$$

with λ_j = roots of $h(p)^{-1}$, $j = 1,2,3$ and $\lambda_4 = 0$

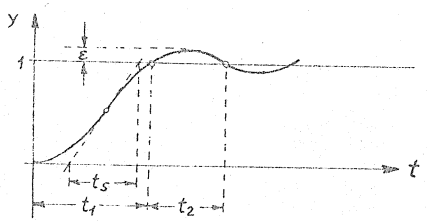

Characteristic step response values used for fine-adjustment of C_1, C_2, C_3: $\underline{\eta} := \{t_1, t_2, t_s, \varepsilon\}$

Choose all R within 1 %.

Determine $\hat{\eta}$ for approximate $\{C_1, C_2, C_3\}$.

Determine $\partial \eta_i / \partial C_j$.

Observe η in experiment.

Solve $\partial \eta_i / \partial C_j \; \Delta C_j = \eta_i - \hat{\eta}_i$.

Fig. 3

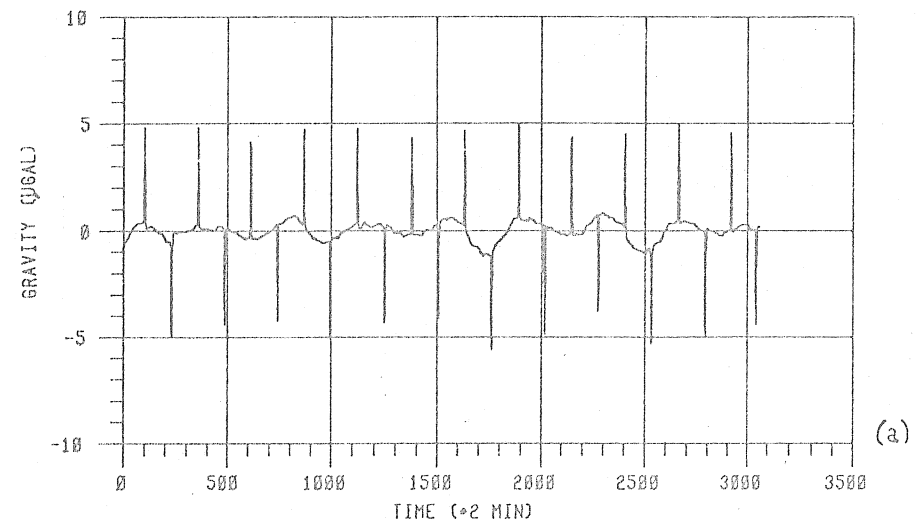

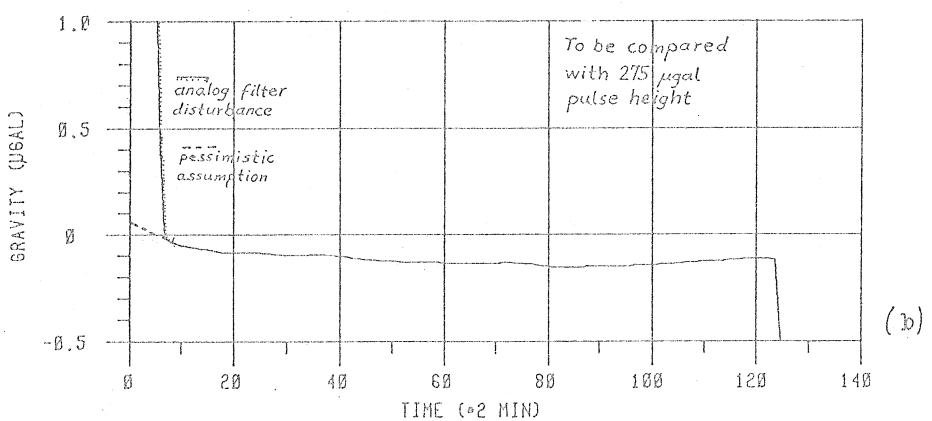

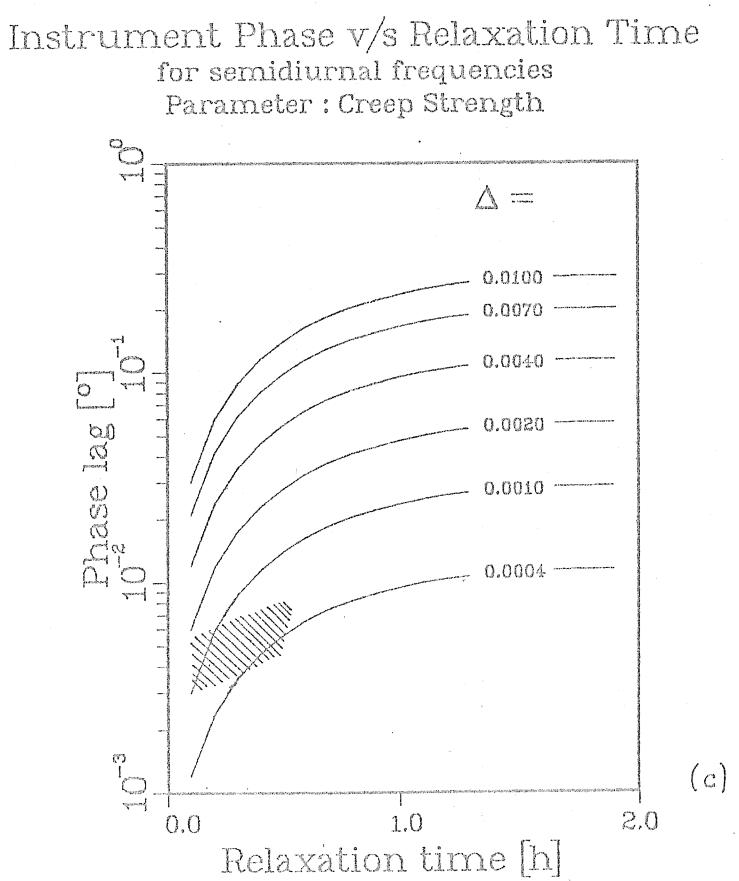

Fig.4: The creep function of the gravimeter spring is obtained from an average of its response to a rectangular wave train feeding the electromagnetic calibration system. The curve in plot (a) displays the response signal after removal of a best-fitting rectangular wave, the known tidal effects, and the instrumental drift. The remaining spikes occur due to the jagged response of the analog filter. Plot (b) represents the average reponse to a step (going from +275 ugal to zero). Provided the gravimeter spring can be modelled with a Zener-body, the phase shift at semidiurnal frequencies compatible with the creep function (b) can be obtained from plot (c). Our results fall within the hatched area.

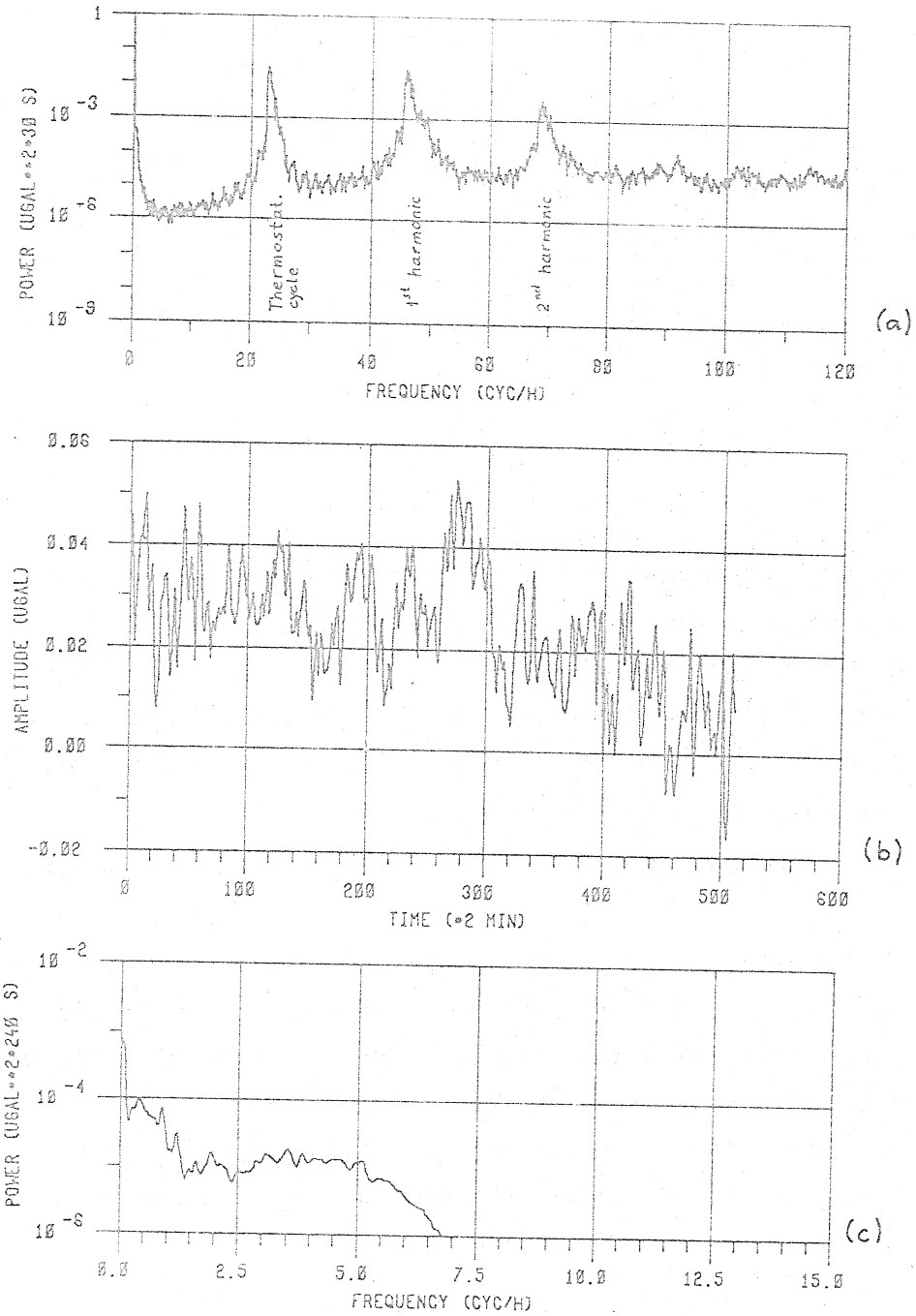

Fig.5: The feasability of the simplified data acquisition algorithm (see text) has been tested on a series of 30,000 samples at 15 seconds interval. A similar Hanning filter was used, however now performing true convolution rather than weighted averaging. Plot (a) displays the spectrum of the 15-s-series with the thermostatic disturbances (23 cyc/h) clearly appearing. The filter output is shown in plot (b). Its spectrum is attenuated beyond the Nyquist frequency of hourly samples (0.5 cyc/h).

Remarks: Before computing the spectra, the series were differenced with the operators (1,-0.75) in the case of (a) and (1,-1) in the case of (c). This implies spectral normalisation by an expression $(1+h^{**}2+2h\cos(\pi f/f_y))^{**}-1$ for an operator (1,h) which flattens out the true slopes of spectrum (c).

RECORDING AND PROCESSING OF TIDAL DATA ET STATION PŘIBRAM

Bohumil Chan

Geophysical Institute Czech. Acad. Sci., Prague, CSSR

1. INTRODUCTION

Recording of the Earth tides in Přibram has its long tradition. First observation here realised prof. Köhler as early as 1910 at the 32nd level of "MARIE" ore mine in the depth of 1109 m under the Earth surface. For the tilt-meter we used the horizontal Zöllner pendulum. After prof. Köhler retired recording of the Earth tides in Přibram continued under the auspices of prof. Čechura during the period of 1925-1940.

When the Czechoslovak Academy of Sciences was created in 1953, recording of the Earth tides in Přibram has been restored by dr. Picha, head of the gravimetric department of the Geophysical Institute. This time the measurements were made at the 30th level of the ore mine "VOJTĚCH"/depth 1000 m/. Later on, during the International Geophysical Year of 1958, the monitoring station was set up the 36th level of the ore mine "ANNA" in the depth of 1300 m, becoming thus the station in the deepest location of all the world. Quality and accuracy of results from this station led even to international comparison measurements.

During years access to the station was more and more difficult and finally relocation of the station to a more convenient place was inevitable.

2. PRESENT STATE OF THE STATION PŘIBRAM

2.1. Relocation of the station

A suitable solution of all problems has been found in 1977 when Geophysical Institute took over a former fan building and installation of the ore mine "PROKOP" with an oblique ventilation level some 170 m long. The length of this tunnel with its gradient of about 25 ^{o} makes possible to walk directly into the 1st or 2nd level of the mine / 67 or 91 m below the Earth surface/,

where there is ample space for all the necessary tilt meter instruments.

2.2. Building adaptation

The original old building was reconstructed and refurbished. Most of the work has been finished and the station now consists of an entrance hall, socoal facilities, two recordings rooms and two offices for the permanent staff. Access to the underground tunnel is through the entrance hall. For a safe passage to the lower underground levels a new steel stairway will be mounted to the oblique tunnel.

2.3. Experimental equipment

For the registration of the Earth tides, and any other Earth movements as well, two Ostrovski-photoelectric tiltmeters with the remote control and the analogue recording have been installed in the underground chambers. The remote control and data recording device is located in the smaller recording room at the station on the surface. In the larger one, a thermal chamber for two or three tidal gravimeters is provided; so far two are installed - BN 27 and in our institute modified GS 11 - both with the analogue output. All the analogue records are digitalized by a modified plotter HP 7225 A or by a special device "Digitizer", developed and made in the Research laboratories Czech Acad.Sci. Digital data are processed on Hewlett-Packard HP-85 personal computer system.

3. PROSPECTS FOR FURTHER DEVELOPMENT

Regarding the long tradition and the good results of the tide recording in Pribram we are commited to continue in this measurements there with the help of the modern technique. The staff of this station is now pursuing two main directions :

a/ expansion of the present recording techniques and instruments;
b/ automatization of data collecting and processing.

Ad a/: The present equipment of the station will be in a short time supplemented by two compensation tiltmeters of our own construction. They are basically similar to older types described in our literature, but they are lighter and smaller with a higher degree of reliability. In the same time reconstruction of the GS-11 gravimeter is in preparation with the ultimate goal to make out of it a compensation digital instrument. In the long run an addition of instruments for the extensometric measurements is also planned.

Ad b/: The other direction is aimed at reducing the cumbersone work of data collecting and processing. Eventually all the scientific instruments will be provided with the analogue- to-digital convertors, data will be recorded on a magnetic tape and processed on the computing system directly at the station.

4. OTHER TIDAL OBSERVATORIES

Besides the main tidal station in Příbram there are two other observatories in Bohemia region :

- station LAZEC in Southern Bohemia is located in a horizontal gallery of a former grafite mine. The tunnel is 300 m long and regardless the fact, that the recording chamber is only 23 m below the surface, the results obtained there are of very good quality. This station is equipped with two compensating tiltmeters.

- station JEZEŘI is in the depth of 131 m below the surface at the end of 400 m long horizontal gallery in the hill-side of Krušné hory - mountains. It is in operation since 1982 and its primary task is to monitor any Earth movements especially in connection with the coal strip-mining in its vicinity. Registration is made by four photoelectric tiltmeters of Ostrovski type with the analogue output.

5. CONCLUSION

The Earth tides stations of the Geophysical Institute Czech. Acad. Sci. are now in midst of a large modernisation effort. Applications of modern electronics offers bright prospects for continuation of Earth tides measurements in quality pertinent to our predecessors during past 70 old years. We feel obliged to continue in the long tradition of Příbram station in bringing new qualitative results which would augment the men's knowledge of our Earth and we sincerely invite you to come to Czechoslovakia and to join in our endeavour.

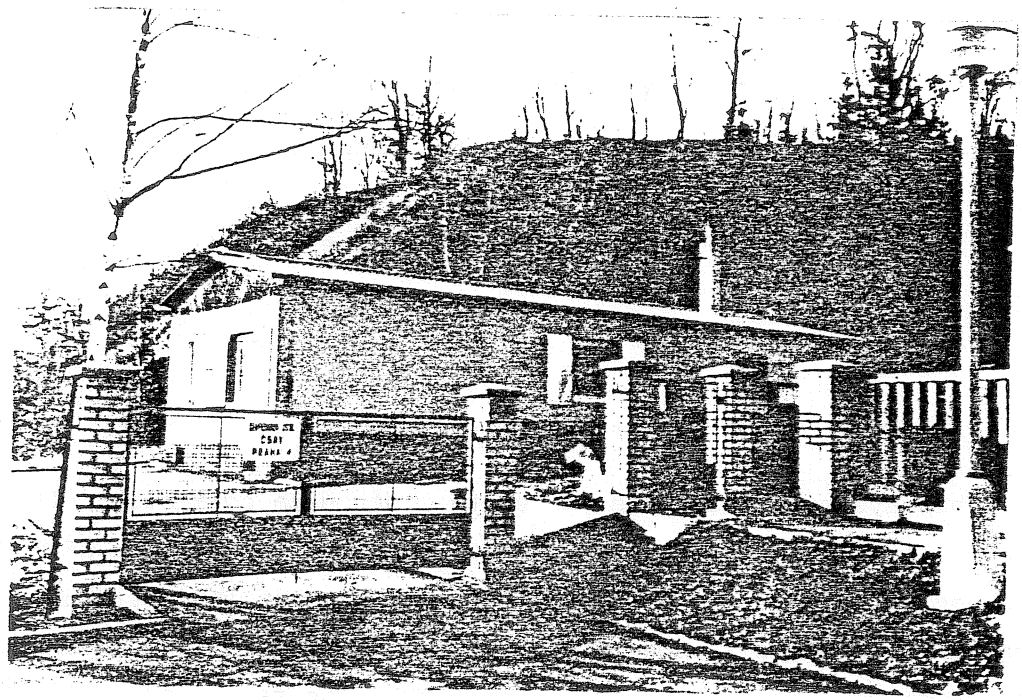

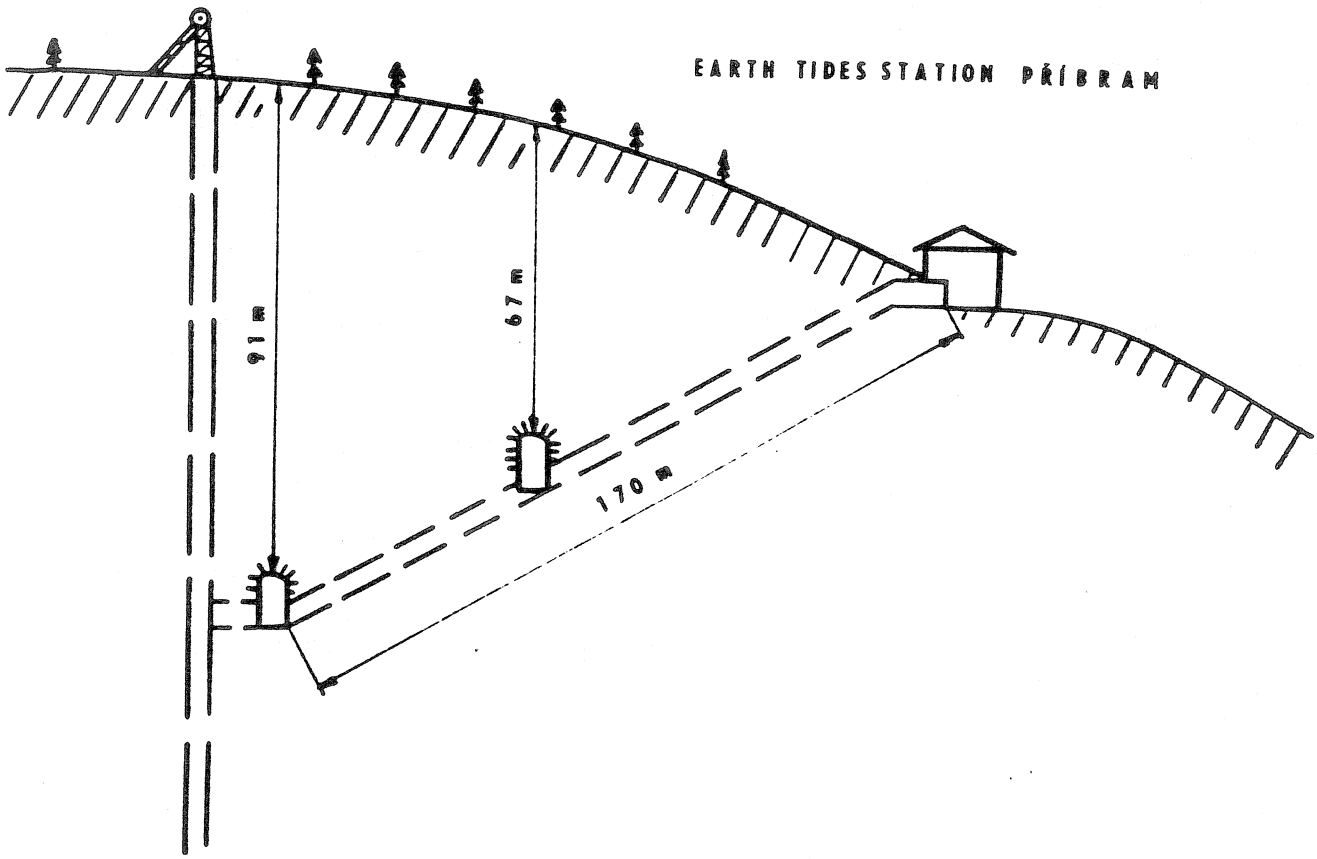
EARTH TIDES STATION PŘÍBRAM
91 m
67 m
170 m

A TAPE RECORDING SYSTEM FOR EARTH TIDES DATA COLLECTION

Tao Guoqiang, Chen Zhenbang, Jiang Xingyi

Institute of Geodesy and Geophysics
the Chinese Academy of Sciences

ABSTRACT

This system is designed for earth tides data collection. It is developed and enlarged on the basis of TP801 single board computer of model Z80 CPU, matching with hardwares such as A/D converter, microprinter and a general audio frequency cassette recorder, etc ... With the aid of the degined softwares, a system consisting of a real-time clock, digital printer and tape recorder for collecting earth tides data is composed.

The sampling work of this system is done per second and is stored every two hours on the tape. The clock may display hour, minute and second or year, month and day and its speed may be adjusted by pushing a key. The printed output full-hour value and the digital voltmeter on the instrument panel serve as visual monitoring for the working state of this system.

I. *THE FUNCTIONS OF THIS SYSTEM*

This tape recording system for data collection is a multi-function real-time control recording system. It's working principle is shown on figure 1.

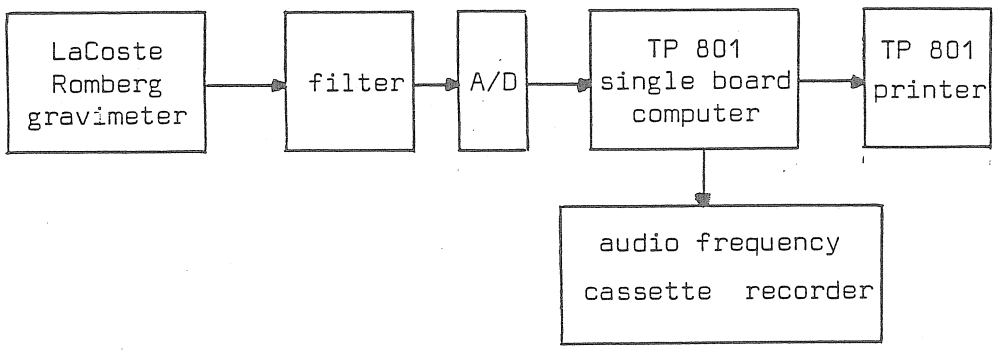

Fig. 1. Working principle diagram of the tape recording system for data collection.

1. *The real-time data collected*

Time is a most important factor. In this system, by combining hardwares and softwares, a digital clock will be interrupted one time per second and used to control real time. This clock has great priority and takes overall plans about the order of each work to be carried out. Six luminous diodes on the single board computer display hour, minute and second or year, month and day.

The sampling will be done one time per second, a datum will be stored up every 20 second and 180 data may be laid up in the random access memory (RAM). The records are arranged as follows according to time sequence :

15.00 (hour), 21th Feb. 1984

+1236
+0785
+0325
+0041
-0056 180 times
-0120
-0932
-1354
⋮

16.00 (hour), 21th Feb. 1984

-1125
-0741
-0212 180 times
+0147
+0659
+1043
⋮

There are altogether 360 data in two hours, which takes up 720 stored units plus time information transferred and stored up on the audio frequency casket tape. In this way the work of data collection is completed.

2. *Print-out*

After one minute of full hour operation in this system, the mean value of ten time of the sampling data will be printed out by the TP 801 P printer before and after 5 second of the full hour operation, which (the mean value) serve as the visual record, the reference value and also the normal work monitoring for this system. The printing is done one time in an hour and its form is as follows :

01 hour	21th day	03 month	-0005
02 hour	21th day	03 month	-0028
03 hour	21th day	03 month	-0057
04 hour	21th day	03 month	-0156
05 hour	21th day	03 month	-0749
06 hour	21th day	03 month	-0432
07 hour	21th day	03 month	+0021
08 hour	21th day	03 month	+0054
09 hour	21th day	03 month	+0147
10 hour	21th day	03 month	+0845

3. *The audio-frequency cassette recorder*

Every two hours (hour in even number) the data and time information stored in the RAM are transferred are stored up on the audio-frequency casket tape. The transmitting speed is 300 baud. Transfer and store up on the tape takes about 2 minutes. In the fore-said process many times of sampling need to be carried out and even one datum should not be left out. Thus it needs better arrangement of multistage interruption and suitable layout of interruption programme.

II. *HARDWARES DESIGNED*

The hardwares are composed of filter, A/D converter, TP 801 single board computer, micro printer and recorder. Among hardwares TP 801 single board computer has been enlarged. Its block diagram is given on figure 2.

1. *A/D converter*

Gravity information is a slowly changing voltage. After filtering, the range of its change is ± 200 mv. We have adopted double integrating $3\frac{1}{2}$ digits digital meter to serve as A/D converter. Its range is 0 - ±199 mv and resolution 100 μv. The accuracy of reading is ±0.2 % in full scale and its input impedance is 100 MΩ. Because the change of information is slow, we always consider that A/D conversion is completed; but when taking the sample, its code output is BCD code. By adding the bit of sign, it has 14 bits in all.

2. *The enlarged single board computer*

In accordance with the requirements of the functions of this system, we have adopted TP 801 single board computer and enlarged it.

(1) To adopt Z-80CPU

(2) A Chip of Z-80CTC serves as transfer and storing of the tape, and another chip CTC_1 of Z-80 as digital clock which may have a time of interruption per second. After dividing the crystal oscillation frequency by two, it is

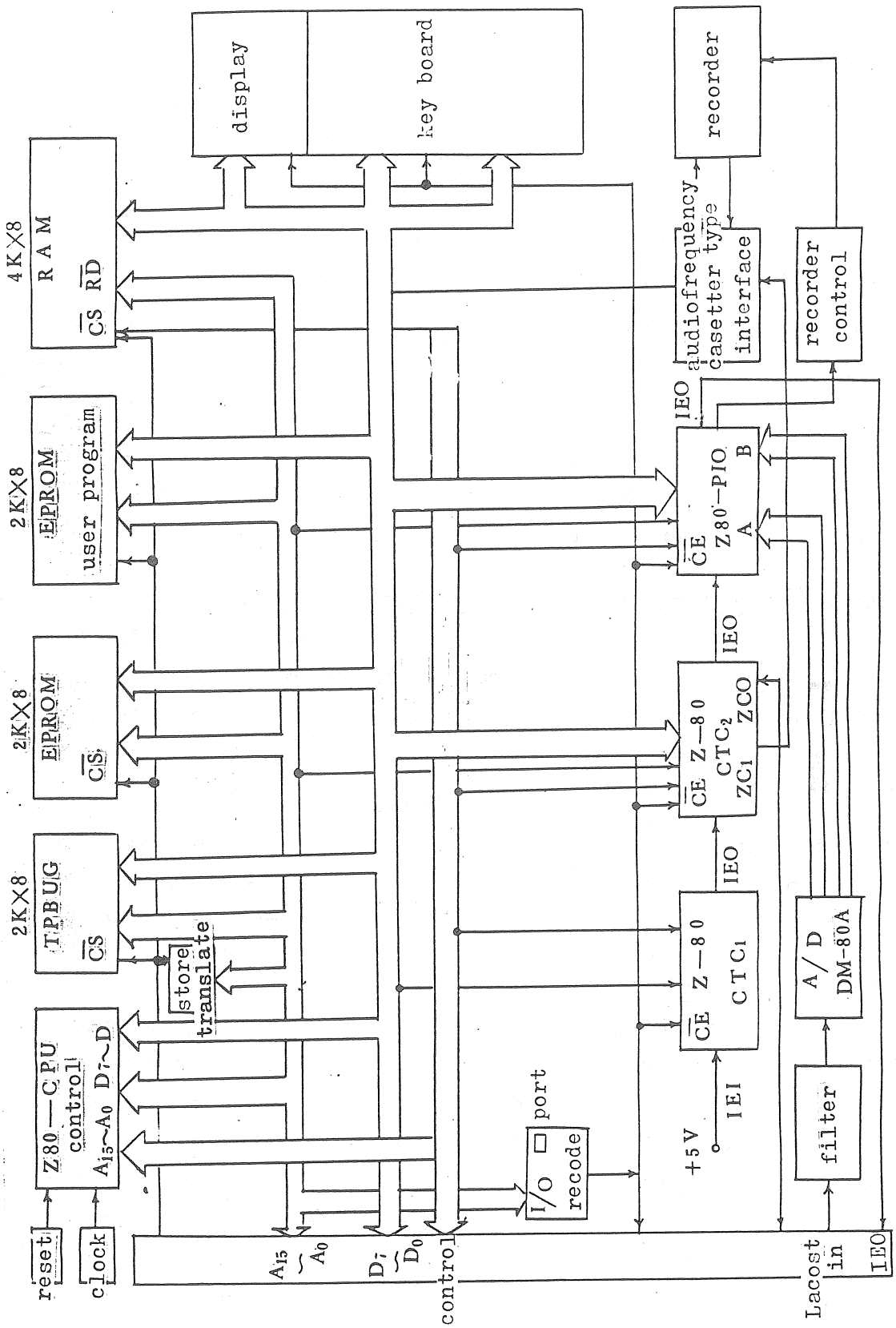

Fig. 2. Main block.

1.9968 MHZ. There are two counting channels used in CTC_1. The coefficient of the scaler is 256. In this way we have obtained the second signal.

1996800 256 156 50 = 1C/S

(3) Z-80 PIO has two independent 8-bit I/O part which serves as the passing in and out for data collection and control. The two parts A and B are all used for the mode of bit control.

(4) There is a 4KB static reading and writing memory RAM.

(5) There is a 4KB ROM (or EPROM), in which 2KB is used as software programme for systematic work.

(6) The keyboard has 16 digital keys and 12 command ones. Among them the functions of the six keys A, B, C, D, E and F have been redefined in this system. They are used for conveying the time initial value and correcting the time.

(7) Indicator : There are six LED indicating the time of hour, minute and second and also date of year, month and day.

3. *The audio frequency cassette tape recorder and interface*

Under the control softwares, the interfaces of single board computer and audio frequency casket tape recorder may accomplish series-parallel and parallel-series conversion by using Z-80-CPU, Z-80-CTC and other hardwares, i.e. it accomplishes the work of data reception and transmission.

Owing to that Z80-PIO has adopted the mode of bit control, PB7 is used as the output of the start stop control signal of recorder. This output signal is passing through the control circuit and the relay which the controls the power source of the recorder. The type of the recorder is SANYO-M2405H.

4. *TP801P matrix point printer*

After hardware connecting TP801P micro-matrix-point printer with the TP801 single board computer, it is used as a data output device of hard copy under the control of CUP. It has an interface logic and driving circuit and a 2KB stationary controlled stamping programme TPMP which takes up the address bus 2KB of the single board computer. By using programme execution mode and CALL instruction, we transfer a command with the mode of subroutine and the required content is printed out.

III. *THE DESIGN OF SOFTWARES AND THE FLOW DIAGRAM*

According to the requirements of the functions of this system, we use assembly language to write about 1.5KB of software programme which chiefly includes : the initialized program, keyboard analysis and function execution program, CTC timing interruption and tape transfer and storing program, and digital clock program, etc ...

As for the tape transfer and storing system, we have adopted the standard of Kansas City and the form of Intel Hex to express the form of data block record.

The flow diagram is chiefly divided into three parts : the first is the initialized one which sets up initial value for the work and flag unit, puts up the mode of bit control for PIO port and places interruption vector and scaling; the second is mainly defining the functions of the six character keys A, B, C, D, E and F; and the third to take the mean value of ten times of the sampling date will be printed out before and after of the full hour. The start and stop of the record is done in every two hours, which are transfered and stored up on the tape. Its flow diagram is given on the figure 3.

IV. *CONCLUSION*

This data collecting system is designed for the observation of earth tides with LaCoste Romberg model G gravimeters. Owing to its perfect functions, small size, light weight and convenient in use, it is the best general-purpose system, which is also suitable to be used in recording slowly changing quantities of informations such as the gravity, tilt, deformations, displacement, temperature, frequency, etc ..., and especially those recorded on the tape are easy for us to carry out analysis and handling, and to put them back again in the computer by using the single board computer.

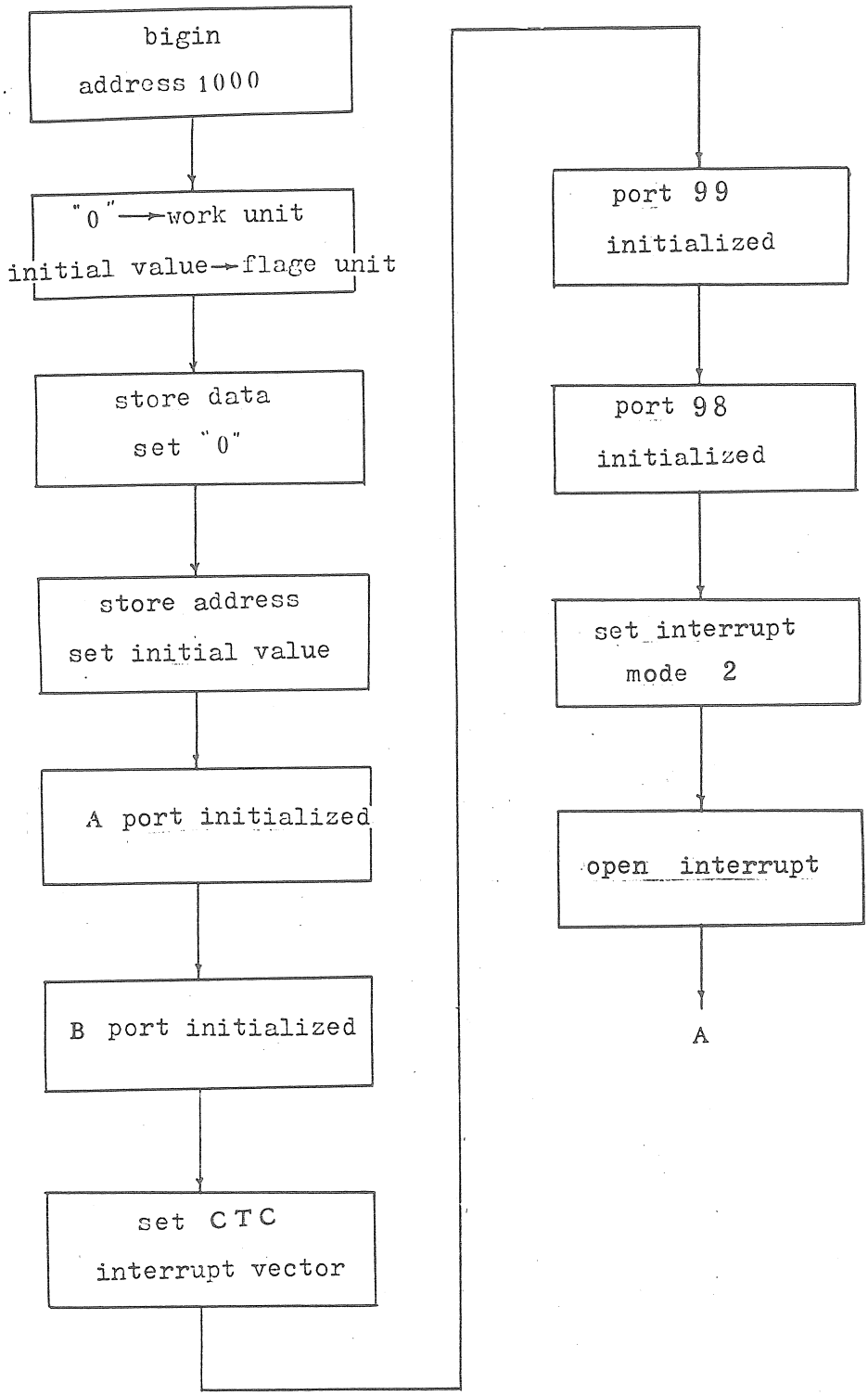

(1)

Fig. 3. Flow diagram

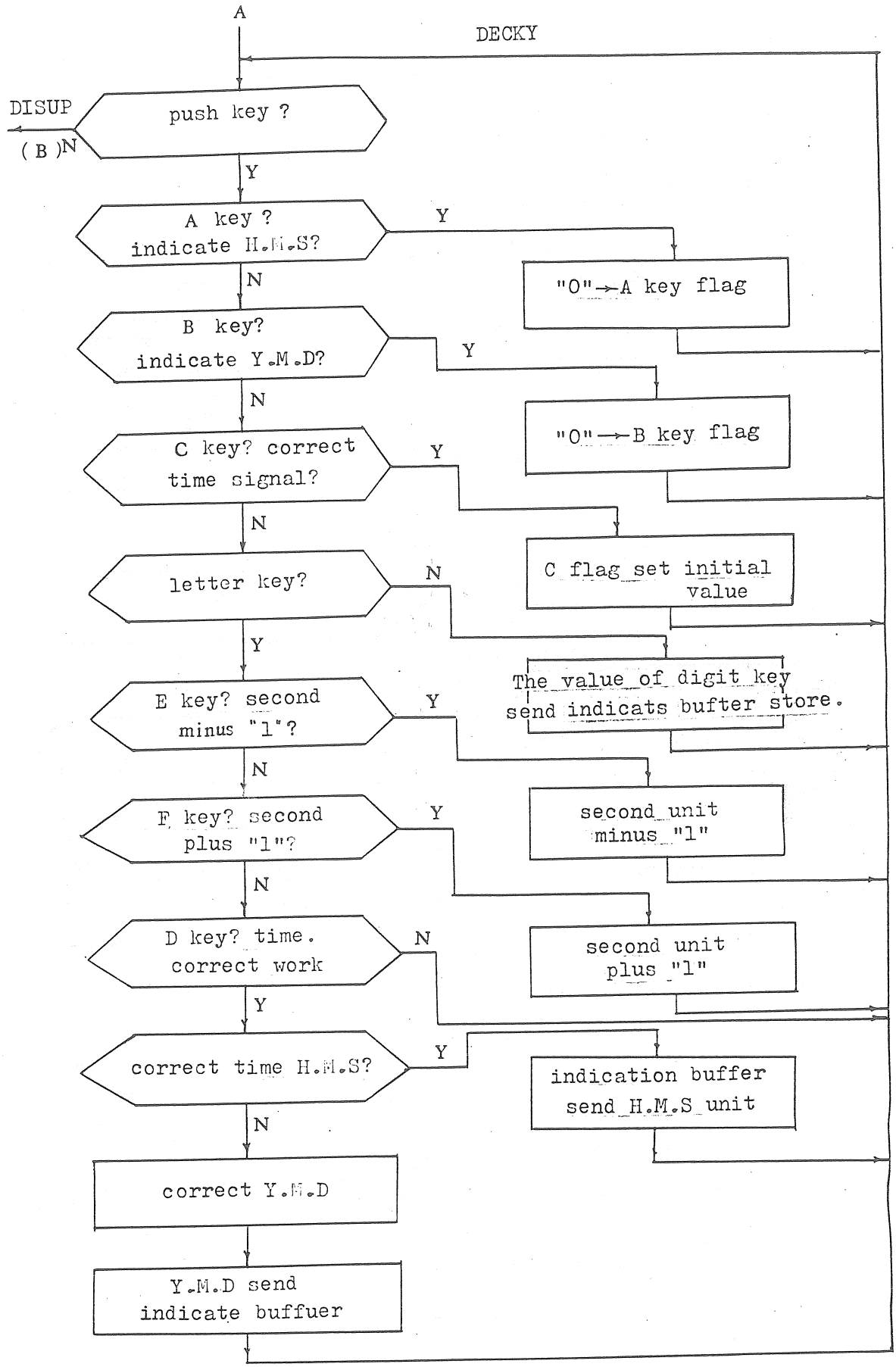

(2)

Flow diagram

DISUP (B)

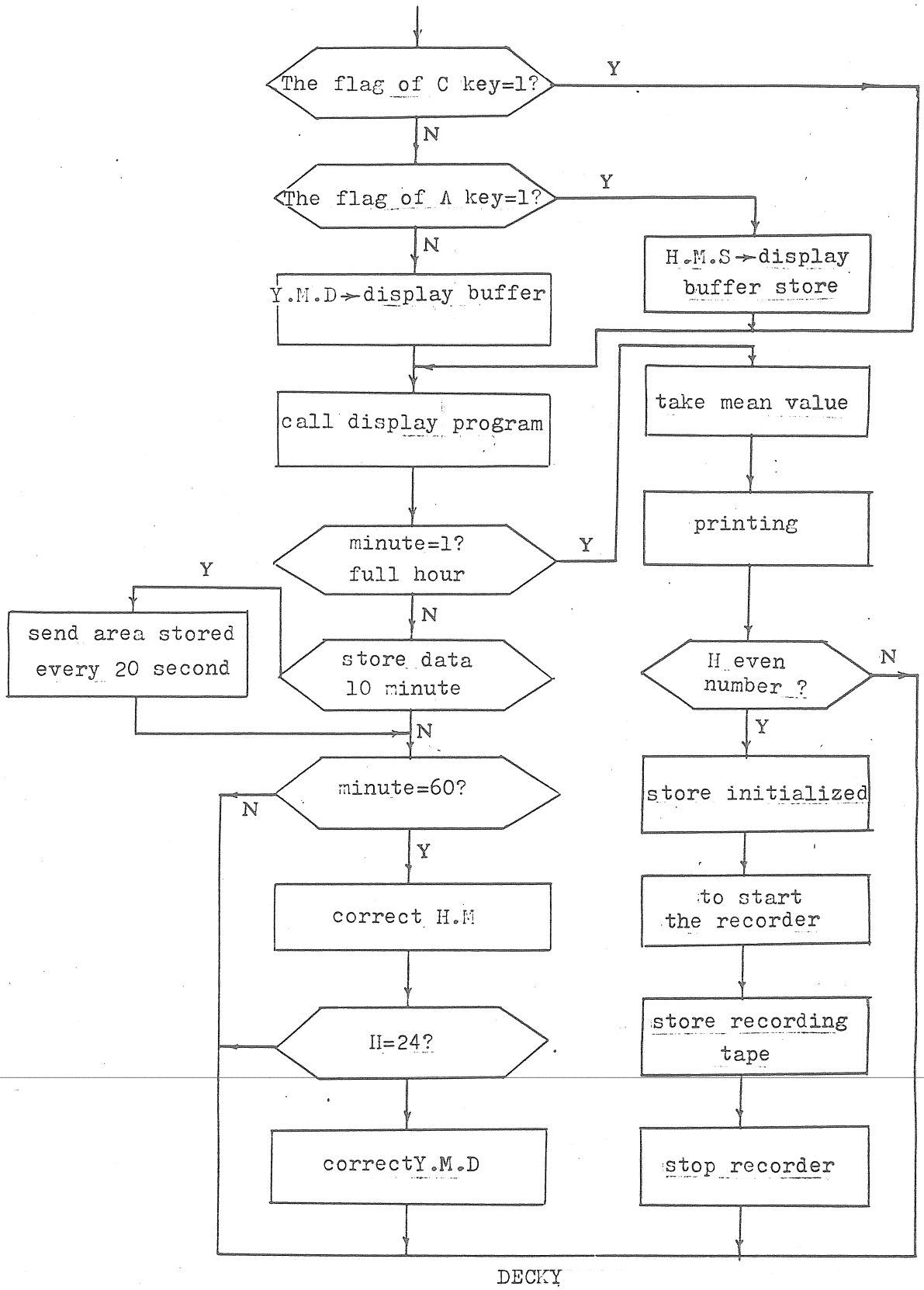

(3)

Flow diagram

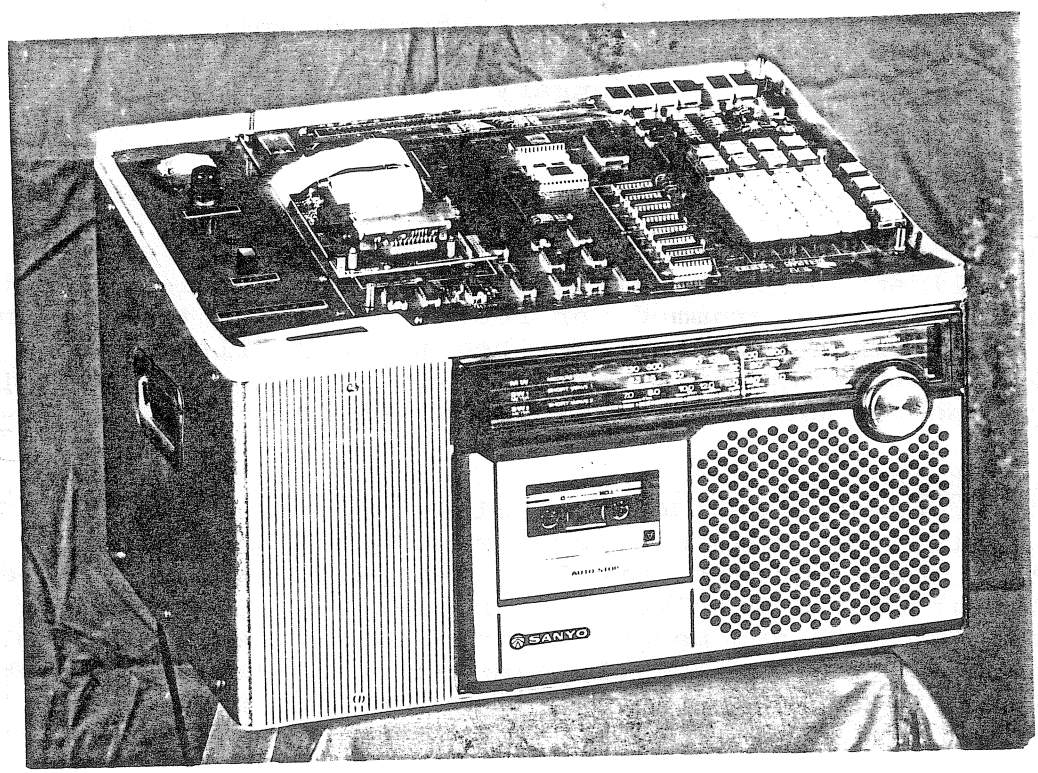

Fig. 4. Photo of the instrument.

AN INTELLIGENT TIDAL SIGNAL RECORDING SYSTEM

Gy. Mentes
Geodetic and Geophysical Research Institute
of Hungarian Academy of Sciences /GGRI/ Sopron,
Hungary

Abstract
The construction and the working principle of an intelligent digital data acquisition system is presented that can be programmed for recording of the tidal signal. A filtering method is described that prefilters the tidal data measured digitally with a high sampling rate and records only the hourly tidal values.

1. Introduction

The properties of the tidal signals /microseismic oscillations, spikes, steps, superposed on the curve and gaps/ cause a lot of problems when digitizing. There are some attempts to solve this problem by applying a high sampling rate and making program systems which are able to preprocess the densely sampled tidal data /Jentzsch, 1981; Plag and Jahr, 1983/. However this method considerably increases the number of data to be stored.

The development of the microprocessor and the microcomputer technique enables the construction of intelligent digital data acquisition systems which combine the advantages of the digital data recording and the manual evaluation of an analog record. Such an intelligent system can prefilter and preprocess the measured tidal data and yields correct hourly tidal data without tiresome manual work and need no large storage capacity for tidal recording.

2. The electric construction of the intelligent digital data acquisition system

Figure 1 shows the block diagram of the data acquisition system. It is controlled by a microprocessor MC 6802 from MOTOROLA. The controller program is stored in the EPROM memory. The RAM memory is used for calculations and temporary storage of data as a buffer memory. When the buffer memory is full, the sampled or preprocessed data can be transferred in blocks into the exchangeable non-volatile semiconductor memory which may be exchanged as a cassette, or into the cassette unit, or the data can be directly transferred via telephone line into a large computer. The exchangeable semiconductor memory is more reliable under conditions of an Earth tide observatory than the cassette unit which contains moving mechanical parts. The storage capacity of the exchangeable semiconductor memory is sufficient for about 15 days to store the prefiltered hourly values of

tidal data measured e.g. by a pair of horizontal pendulums including the records of environmental parameters, too. The digital recorder system has 16 analog input channels, an analog multiplexer and a 12 bits analog to digital converter. The sampling and converting of the analog channels is controlled by the master processor. The exact time is given by the real-time clock which can be synchronized by means of a DCF-77 receiver. The speed of the system can be increased applying a slave processor which can be a high speed arithmetic or an FFT processor depending on the desired filtering algorithm.

The data acquisition system has an keyboard and a display too, for the manual control of its operation and for input and display parameters needed for data sampling and filtering.

3. The description of the filter algorithm

It is the duty of the filter program to remove the undesired signals /self-swingings, steps, spikes/ from the tidal curve, similarly to the manual evaluation of the analog records. The filtering cannot be solved solely by mathematical filters with the desired accuracy, as even if such filters decrease the amplitude of spikes significantly, nevertheless they smudge the spike over the whole curve after the apperance of the spike. By inserting logical decisions into the filter program this problem can be eliminated.

It is assumed in the filtering algorithm described hereafter that the sampling period is less than the half of the eigenperiod of the self-swinging and the hourly time mark is an integral multiple of the sampling period.

Let us suppose that the sampled tidal data are

$$a_1, a_2, a_3, \ldots, a_i, \ldots$$

a_i is an extreme end value, if

$$a_{i-1} < a_i > a_{i+1} \quad \text{or} \quad a_{i-1} > a_i < a_{i+1}$$

then

$$b_j = b_{j+1}$$
$$b_m = a_i \qquad j = 1,2,3,\ldots,m-1,$$

where the nth point of the smoothed curve s(n) will be calculated from m extreme end values:

$$s(n) = \frac{1}{2^{m-1}} \sum_{j=1}^{m} \binom{m-1}{j-1} b_j + C$$

where

C = the value of the step correction calculated at the previous point.

The predicted value for s(n) from the previous p smoothed values is

$$s(n)_p = \sum_{k=1}^{p} \alpha_k \, s(n-k), \qquad k = 1,2,\ldots,p,$$

where

α_k = the linear predictive coefficients

If

$$|s(n)_p - s(n)| > S \ ;$$

where S is a prefixed limit for the presence of a step in the curve and

$$\begin{aligned} C &= C + s(n)_p - s(n) \\ u_1 &= u_{\ell+1} \\ u_r &= s(n)_p \qquad ; \qquad \ell = 1,2,\ldots,r-1 \end{aligned}$$

Otherwise

$$\begin{aligned} u_1 &= u_{\ell+1} \\ u_r &= s(n) \qquad ; \qquad \ell = 1,2,\ldots,r-1 \end{aligned}$$

The tidal value at the hourly time mark is:

$$y = \frac{1}{2^{r-1}} \sum_{\ell=1}^{r} \binom{r-1}{\ell-1} u_\ell \quad ,$$

where the average value is calculated from r smoothed and step-corrected values.

The method gives good results for Earth tide recording even if we use only three values for the Fox-Schuller averaging and only two previous values for the linear prediction.

In this case

$$s(n) = (b_1 + 2b_2 + b_3)/4 \ ; \ y = (u_1 + 2u_2 + u_3)/4$$

and

$$\alpha_1 = 2 \qquad ; \qquad \alpha_2 = -1.$$

It means that the microprocessor can calculate very quickly the averages and the linear prediction by shifting registers instead of multiplication and division algorithms which would require several hundred machine cycles.

Because some parts of the system are still under construction, the filter method was tested on a computer. Figure 2 shows the simulated input signal. The eigenperiod of the "simplified" tidal signal /a sinus wave of one day period/ was 50 s, the spikes and steps had amplitudes half of the signal. The accuracy of the method depends on the quality of the linear prediction, the gain of the system, the sampling rate and the limit

S. Table 1 shows the errors of the method at different parameters. From the Table 1 it can be seen that both sampling rate and the limit S have an optimum at a given gain. The most important point is to chose properly the limit. When the limit is lower or nearly as low as the errors obtained from the A/D conversion and calculations, the error of the filter program will be very high because the program always substitutes the measured value for the predicted value. If the limit is too high the program will not experience the small steps in the input signal.

4. Conclusion

An intelligent digital data acquisition system does not only diminish the manual work for preprocessing of tidal data but also increases the accuracy of the measurement. The method eliminates the subjective errors. The high dynamic range of the analog to digital converter and the properly chosen parameters of the filter program make possible to achieve a higher accuracy than with other recording methods.

References

Jentzsch, G., 1981: Automatic Treatment and Preprocessing of tidal data recorded at 1 min intervals, BIM, 85, 5415-5428.

Plag, H.-P. and Jahr, T., 1983: On processing of Earth Tidal Data, BIM, 89, 5759-5786.

Table 1.

Limit [s]	Gain / Sampling period [s]	Average error of the filtering in percentage of amplitude with RMS error			
		1	5	10	20
0.1	5	1.10 ± 3.60	4.02 ± 4.24	0.29 ± 0.32	0.15 ± 0.16
	10	26.1 ± 28.1	0.36 ± 0.38	0.72 ± 0.75	0.12 ± 0.15
	20	23.9 ± 26.0	1.94 ± 2.14	1.94 ± 2.14	295.0 ±457.0
0.05	5	80.67 ± 97.56	0.30 ± 0.33	0.48 ± 0.51	0.26 ± 0.27
	10	81.20 ± 98.07	0.72 ± 0.76	0.08 ± 0.08	0.13 ± 0.15
	20	2.0 ± 2.1	1.94 ± 2.14	0.33 ± 0.40	295.0 ±457.0
0.02	5	4.0 ± 4.2	0.40 ± 0.40	0.19 ± 0.07	65.5 ± 68.0
	10	0.36 ± 0.40	0.08 ± 0.104	0.07 ± 0.08	65.4 ± 68.0
	20	1.90 ± 2.1	295.0 ± 456.8	0.57 ± 0.63	64.6 ± 67.0
0.01	5	0.8 ± 0.8	0.50 ± 0.52	0.37 ± 0.11	42.0 ± 43.0
	10	1.8 ± 1.8	0.36 ± 0.36	0.25 ± 0.10	42.0 ± 43.0
	20	1.2 ± 1.3	0.68 ± 0.84	0.60 ± 0.42	41.0 ± 43.0

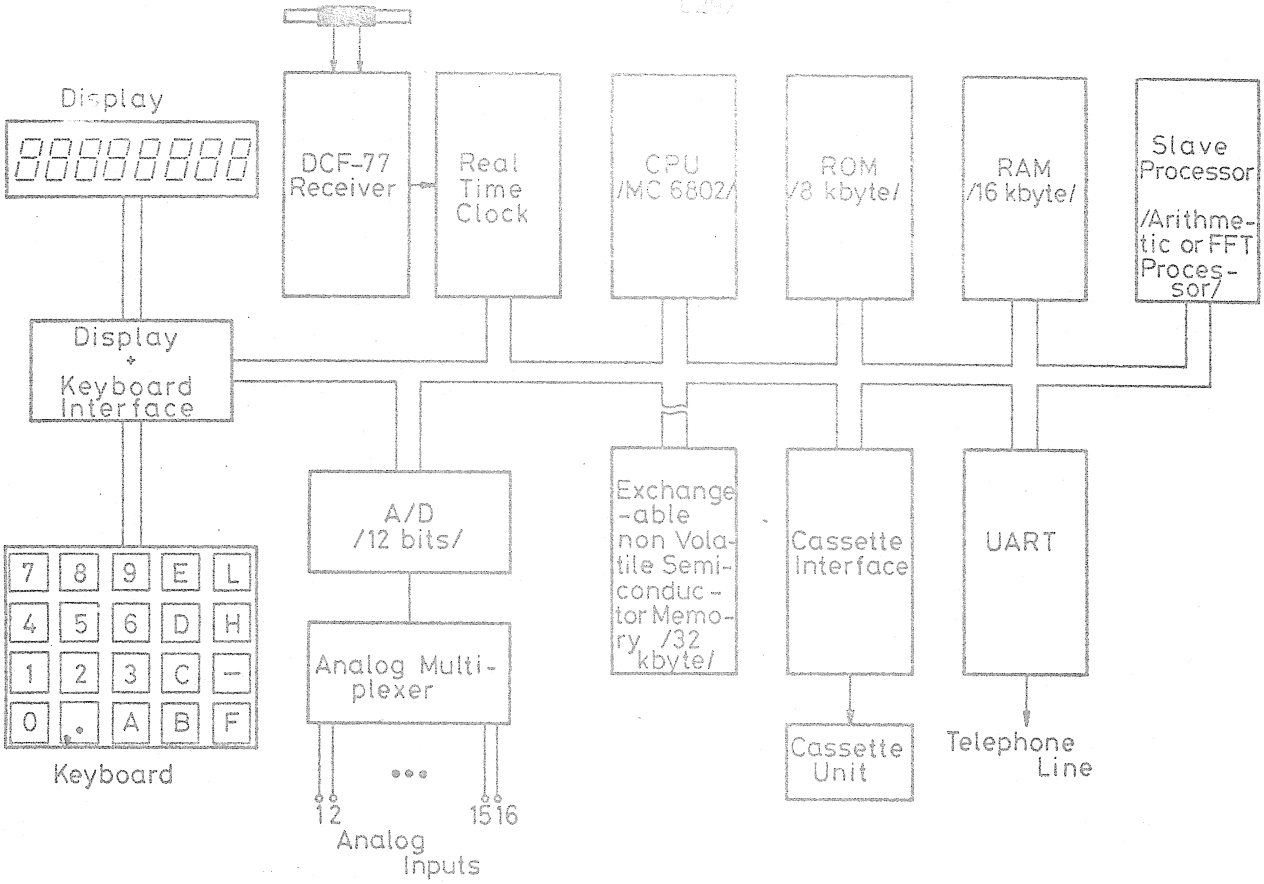

Figure 1.

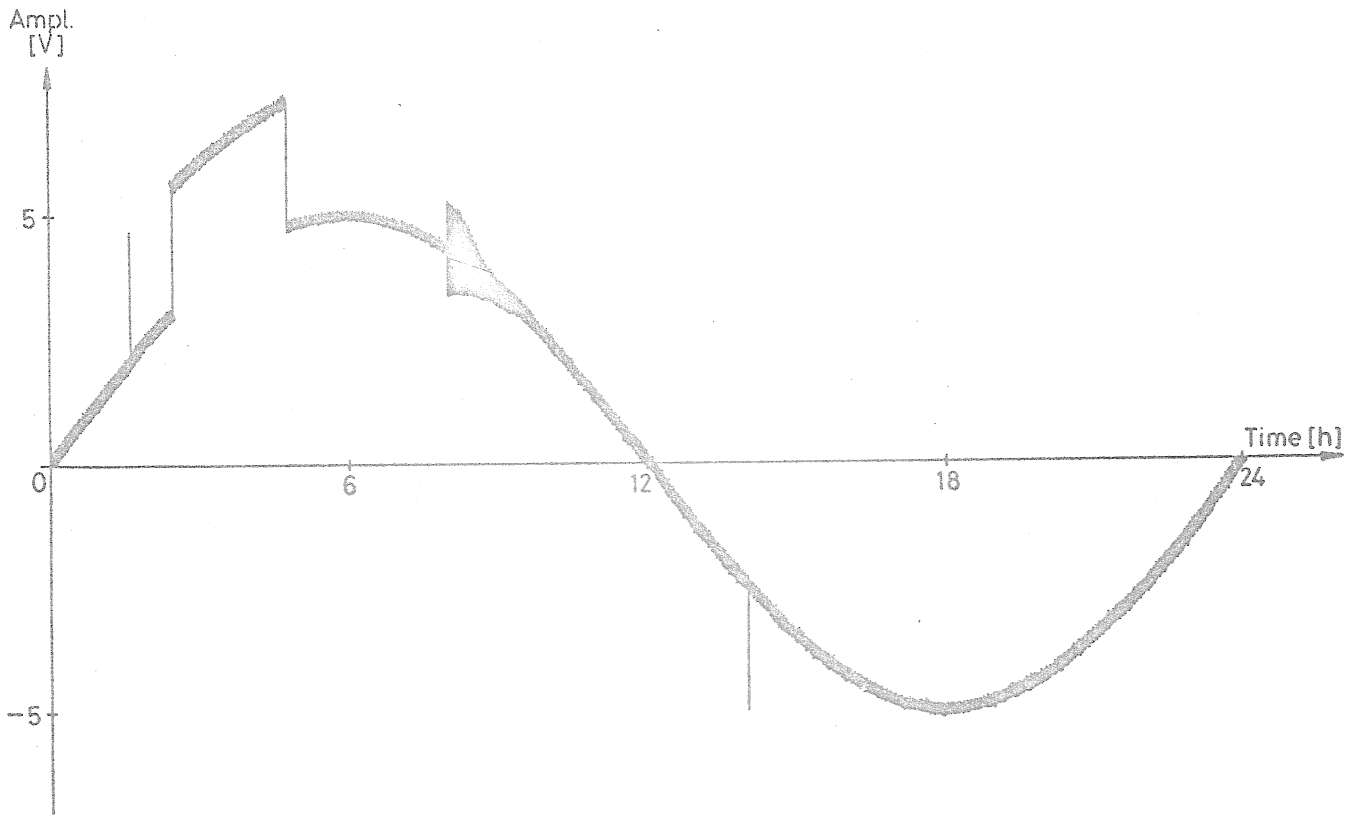

Figure 2.

Digital Data Processing by the Microcomputer System MPS 4944 at the Gravimetric Observatory Potsdam

by

W. Schwahn, J. Neumeyer, H.- J. Dittfeld

Academy of Sciences of the GDR
Central Institute for Physics of the Earth
DDR-1500 Potsdam, Telegrafenberg A17

Abstract

The program for the one-line digital processing of the gravimetric registration by a microcomputer system MPS 4944 may be characterized by a parameter set. These parameters are

(1) the sample size of a running mean value,

(2) the threshold for the difference between the single sample and the running mean (1) to detect anomalous values (events),

(3) the time interval and the number of events for the detection of earthquakes and calibration shifts in the registration on the basis of the occurence of events in (2),

(4) the sample size for an adjustment by a polynomial of second degree to get representative readings,

(5) the sample size for a further adjustment of the adjusted values in (4),

(6) the sample size for the on-line drawing of the adjusted registration.

At present the sampling interval is 10 sec, the running mean sample in (1) is 7, the sample size in (4) amounts 45, i.e. every 7.5 minutes we obtain a representative value for the time points 0.0, 7.5, 15.0, 22.5, 30.0, 37.5, 45.0 and 52.5 min of an hour, the sample size in (6) is 5, i.e. a smoothed curve over the last 37.5 minutes.

For the combination of the reconstructed GS 114/R and the MPS 4944 we gathered for the period Aug. 83 - Dec. 83 about 14000 (fourteen thousand) representative readings. After the rejection of values influenced by earthquakes this data set was the basis for the CHOJNICKI-analysis (A15K, accuracy estimation based on residuals). Here are some results (without corrections) using 12 wave-groups: mean square error m_o

$$m_o = \pm 2.13 \ \mu gal \quad \text{and}$$

$$\delta O_1 = 1.1546 \pm 0.003 \quad \text{and} \quad \delta M_2 = 1.1865 \pm 0.001$$
$$\varkappa O_1 = -0.06 \pm 0.158 \qquad \varkappa M_2 = 1.412 \pm 0.066.$$

1. Introduction

We have the intention to study the gravity variations in the spectral range from a few minutes up to the tidal periods, i.e. the whole spectrum outside of the common seismic and microseismic periods. To avoid other influences like the filtering by the registration device the data aquisition takes place as close as possible at the sensor. Therefore the basic experimental and theoretical prepositions for the further considerations are as follows: We use a weak-filtered signal ((tidal period) signal-to-(short period) noise-ratio 10:1, i.e. a noise level in the range of 10 up to 20 seconds of 10 ... 20 /ugals) and we suppose that the deviations with respect to a smoothed curve in the time interval of 5 ... 10 minutes might be regarded as a white noise. Then a representative gravity variation for this time interval can be determined by the method of least squares using an on-line microprocessor.

Under these prerequisites an algorithm was developed which enables us by the aid of characteristic parameters

- to compute representative readings
- to detect anomalous values and to determine their correction
- to identify seismic events
- to calculate for calibrations the difference between consecutive shifts
- to draw on-line a smoothed curve.

2. Parameters for the detection and correction of anomalous samples

Using such a high noise level anomalous values occure often and the assumtion of a normal distribution means on the other hand that anomalous values must be rejected before the adjustment. Parameters 1 and 2 define an anomalous sample:

Parameter 1: Sample size N for a running mean value

A sample r_i was taken at the time moment t_i. Then at first the difference between this sample and the mean value over N forerunners is computed:

$$(1) \quad d_i = r_i - \frac{1}{N} \sum_{j=i-1}^{i-N} r_j = r_i - \bar{r}_i$$

The sample size N must be smaller than the sample size M used for the adjustment, $N < M$. For the meaning of M see parameter 4.

Parameter 2: Threshold D for the identification of an anomalous sample (event)

If $d_i < D$ normal further processing,

if $d_i \geq D$ special consideration using the parameters 3.

The parameters 3 are designed for the consequences with respect to the further treatment of this event.

Parameters 3a and 3b: Number L of consecutive sampling intervals and number K of events choosed for the detection of earthquakes and calibration shifts, $M/4 < L < M/3$, $K \ll M$

By the aid of the parameters 3 the decision is possible, whether there is an essential new character of the registration or not: If only a little disturbance occurs then the curve should be restored. If there are a lot of new informations then these new samples should be accepted.

The algorithm is very simple: If by the aid of the parameters 1 and 2 an event (the p-th) was found then the time point will be stored. The difference l_p between the running number of the preceeding one and that of the actual event is calculated:

(2) $l_p = t_p - t_{p-1}$.

Case 1: $l_p \geq L$ (single "isolated" anomalous sample, correction necessary)

If the number L, within of it a next event might be expected, is smaller than l_p, then an anomalous single sample is detected. The value is replaced by the mean value $\bar{r}_i$, t_{p-1} is replaced by t_p, and the counting of the value k_L starts from the beginning ($k_L = 1$).

Case 2: $l_p \leq L$ (dense sequence of "anomalous" samples)

If the next event occurs within a distinct time interval (interval number L) then the number of events k_L is increased:

(3) $k_L := k_L + 1$

and the relation k_L and K is proved:

Case 2.1: $l_p \leq L$ and $k_L \leq K$ (disturbance over a few samples, correction necessary)

If $k_L \leq K$, i.e. the actual number of events is smaller than a given number, then a small disturbance is found. The actual value is again replaced by the mean value in (1), the time point t_{p-1} is replaced by t_p, but in contrary to case 1 k_L is not changed ($k_L \neq 1$).

Case 2.2: $l_p \leq L$ and $k_L \geq K$ (earthquake or calibration shift are detected, no correction applied)

The case $k_L \geq K$ means that in a comparatively short time ($l_p \leq L$) a lot of new samples unequal the mean value over the number N of forerunners was gathered. Since such a significant number was reached, this samples are considered as significant also and no rejection takes place.

As a working hypothesis we assumed that the variations during the earthquake have also a normal distribution around the long-term behaviour of a few (5 ... 10) minutes and the same algorithm for the adjustment as for the regular treatment is used. If a calibration shift or a jump occure in the interval used for the adjustment, the adjusted value is not representative and depends on the time point of the shift. Therefore in the caloulation of the difference of the shift for calibration purposes we cancel this first value obtained immediately after the shift in the adjustment (see parameter 5).

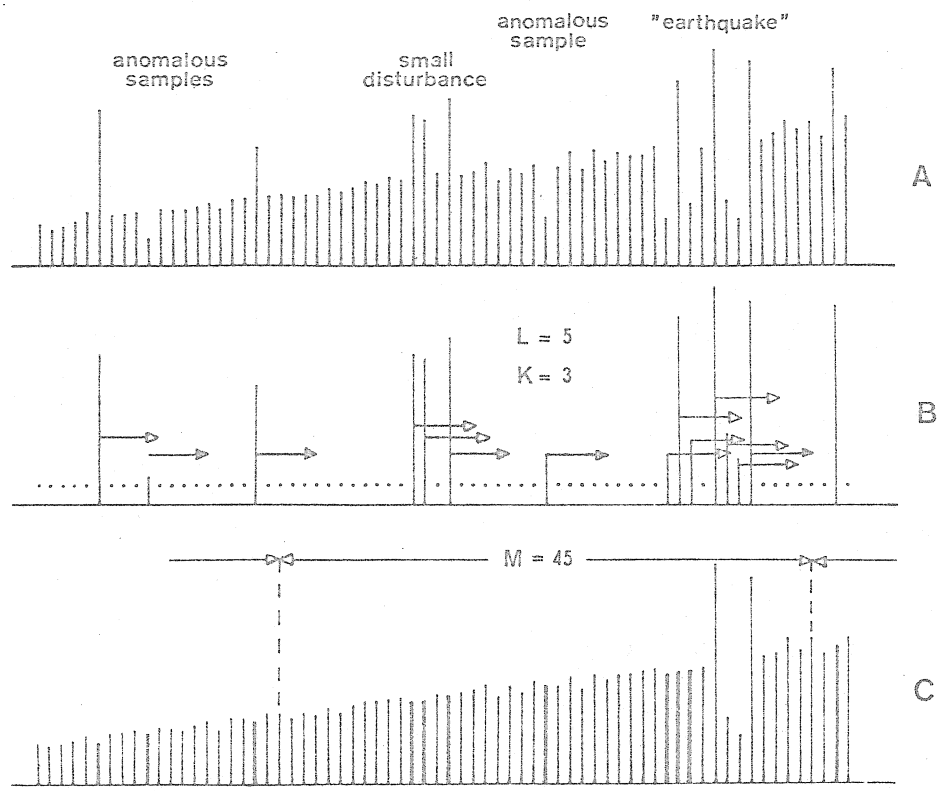

Fig. 1. Explanation for the use of parameters 3: the number L consecutive gravity data (samples) within of it the occurence of a next anomalous sample is checked to count k_L; and the number K of samples for which a correction is applied.

A: Temporal sequence of original samples
B: Principle of the detection and handling of anomalous samples, disturbances and earthquakes or shifts respectively in the series A. The lenth of the arrows demonstrate the number L, the white arrow tips indicate that $l_p < L$, the dark ones that $l_p > L$.
C: The improved sequence of samples. The samples whose values are replaced by the running mean values are marked by thick bars. Note the corrected samples also at the very beginning of the "earthquake" depending on the number K. The sample size M for the adjustment (parameter 4) is M = 45.

3. Parameters for the computing of representative readings

Parameter 4: Sample size M for the first adjustment

To approximate the tidal curve in a sufficient way and to simplify matters we used a polynomial of second degree, choosed an odd number M for the sample size, gathered the data r_i in the range $-M/2 + 0.5 \leq t_i \leq +M/2 - 0.5$ and compute the value R_n of the polynomial for the central point by the expression (ZURMÜHL, R.; Praktische Mathematik, 1965, S.336-342),

$$(4) \quad R_n = \frac{[t^4][r] - [rt^2][t^2]}{[t^4]\,M - [t^2]^2}$$

$[\,]$ means tne summation over i in the above noted range. R_n is allocated to the middle of the interval. By this way also hourly readings in the traditional understanding may be produced by an appropriate starting point.

Parameter 5: Sample size P for the second adjustment

For the determination of the difference between consecutive shifts and data validation we used the same procedure as for the parameter 4, but the input data are now the R_n and the sample size amounts P, in general $P < M$.

Parameter 6: Sample size J for the on-line drawing

As a first instructive information on a graphic recorder (see fig. 2) the values R_n are represented. A smoothed curve is drawn also on-line on the basis of R_n with the aim to obtain a feature like the common tidal registrations which are strongly filtered. For this purpose the three coefficients in the polynomial are determined and the function was extrapolated until the next R_n is computed (see fig. 2).

4. Further data processing and first results

The representative readings R_n and the value of the second adjustment were transferred by a punched tape to a large computer. To get an insight in the data structure we have not applied any filtering or decimation techniques, i.e. we used the dense sequence of all representative readings for the CHOJNICKI analysis.

In the time interval Aug. 83 till the first days of Jan. 84 the first observation campaign of the reconstructed GS 11 No. 114 took place. We collected about 14 000 representative readings (see abstract for further preliminary informations). On this basis we can conclude that the data volume plays the most important role. The selection of time intervals characterized by "good" readings reduces the data volume, reduces the m_o but does not yield a smaller error estimate for the tidal parameters. It means that the application of a dense reading, realized by a microprocessor, improves the validity of the results.

In our example, in which we gathered 8 representative readings per hour, the accuracy grows up by a factor 3 with respect to the use of hourly values only. To sum up it can be said that in a short time we obtained reliable tidal parameters which is important both under scientific and economic aspects.

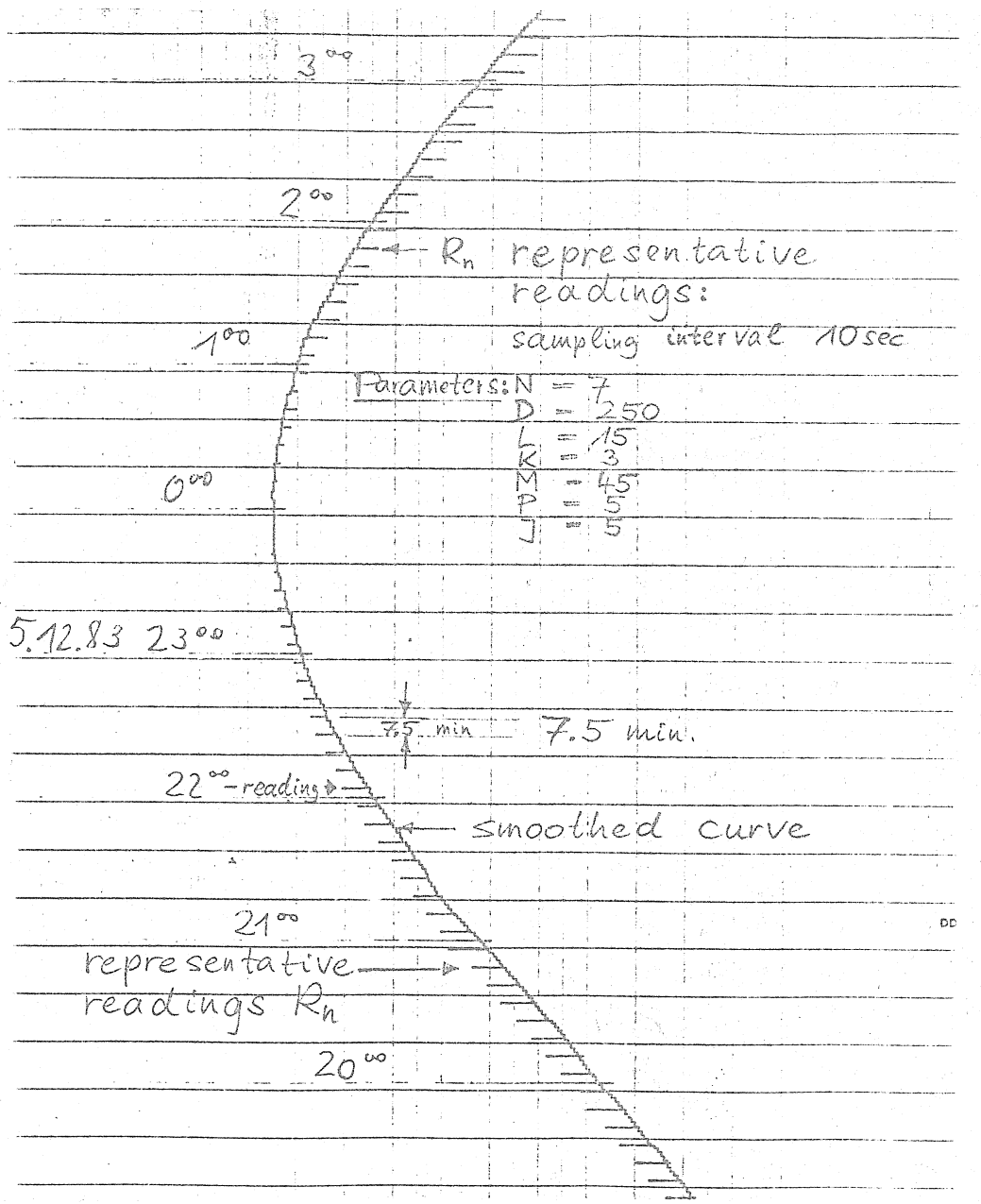

Fig. 2: A section of the gravity registration given by the microprocessor system MPS 4944 combined with the reconstructed (by Neumeyer and Dittfeld) GS 11 No. 114. The computed representative readings R_n are marked by horizontal bars. Since an one-line adjustment over five R_n's (parameter 7, J=5) is used, a phase shift in the smoothed curve is inevitable. D (parameter 2) is given in digits, the gravity difference between the hours 20 and 0 amounts 90 ,ugal.

Acknowledgement

We are indebted to many collegues for their kind assistence: For the implementation of the drawing software Mr. Urban, and for the excellent data transfer Mr. Hirsch, both of the Central Institute for Astrophysics, and last not least for their careful support in the data processing Miss Jurzyk and Mrs. Oppermann.

C H E T S

PROGRAM PACKAGE FOR COMFORTABLE HANDLING OF EARTH-TIDE SERIES

H.-J. Kümpel & C. Milkereit
Institute of Geophysics, University of Kiel, FRG

1. General Information

Design : CHETS is designed to handle comfortably time-series of earth-tidal or tide related data. Time-series have not necessarily to be continuous. Handling includes reading from and writing to data-files, plotting, filtering, linear transformations, spectral-analysis, cross-correlations, and other simple operations on time-series.

CHETS does not perform tidal harmonic analyses or other kinds of regression analyses except simple Fourier-Transformations, nor is CHETS designed for editing time-series.

Restrictions : Time-series that can be handled by CHETS have to meet following conditions :

- Series have to be at hourly rate (or at daily rate, but are then internally extended to hourly rate, e.g. daily averages of signals, or daily rainfall data),
- series have to start at either 0(UT) or 12(UT) and have to end at either 11(UT) or 23(UT),
- series are restricted to a maximum length (capacity dependant),
- series are allowed to have a maximum number of datagaps.

For each time-series CHETS performs book-keeping on its length, its name, its beginning and its final date, on its eventual scale-factor, and on its datagaps.

Command-Structure : Operations on time-series are called actions. Each action consists of a 3-letter-code followed by none, one or two internal names of time-series (up to 5 characters each). For instance,

LIN NAMEX

simply subtracts the linear drift from a time-series that is internally named *NAMEX* .

Internal names may be altered by certain actions, especially those that read time-series from datafiles into working arrays of CHETS. Up to three time-series may be handled simultaneously (if operations on more than three time-series are planned within one run of CHETS, series that are actually not needed may be stored on datafiles meanwhile).

For most actions, CHETS wants to know additional parameters, that describe how an action has to be performed. For instance,

ROT NAMEX NAMEY/ 35.4/

rotates both time-series *NAMEX* and *NAMEY* by 35.4 Degrees, assuming that *NAMEY* is in azimuth perpendicular to *NAMEX* (sense of rotaion is eastwards, if *NAMEY* is a signal component 90 Degrees eastwards of *NAMEX*). Prior to the execution of this action, CHETS automatically checks whether both time-series cover the same interval. The resulting time-series contain eventual datagaps from both original series.

Mode of Dialogue : CHETS allows two modes of entering actions, names of time-series, and additional parameters :

- Interactive Mode, i.e. all dialogue is handled via terminal, or
- Quasi Batch Mode, i.e. the user given part of the dialogue is known in advance and is written on a separate command-file; however, still a minimum interactive dialogue with some plot-actions is necessary for scaling reasons of amplitude axes.

A special service action allows the user to switch between both modes during execution of CHETS. A succession of recurring commands can thus be retrieved from a command-file during a run in Interactive Mode.

Documentation : CHETS echoes completed actions on the terminal and creates a "minutes"-file where characteristic parameters and useful information of completed actions are preserved for documentation and later verification by the user.

Language : CHETS is a FORTRAN-10 (similar to FORTRAN-V or FORTRAN-77) program package of roughly 2500 statements. The FORTRAN experienced user may easily modify existent actions of CHETS or add new actions. Since plot-routines and file-control statements (like "OPEN" and "CLOSE") are sometimes not compatible among various installations, they might have to be rewritten. Because of its volume, CHETS has to be implemented as an overlay structure in many computers.

Availability : To users from scientific institutions, CHETS is available from the authors on delivery of a 9-track magnetic tape. Industrial users will receive a quotation on request. Delivery of the program package includes a manual with detailed description of all actions.

Block-Scheme :

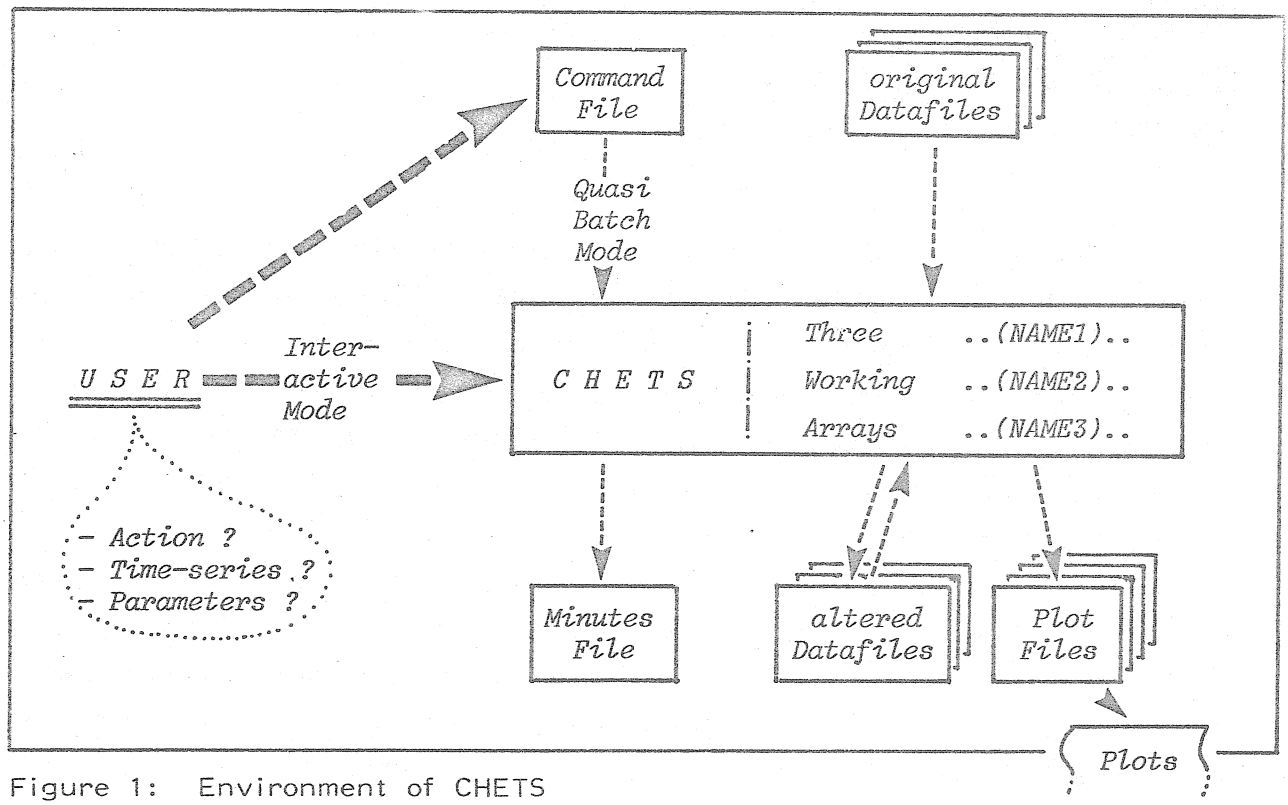

Figure 1: Environment of CHETS

II. Example

Assume a plot of North/South- and East/West- tilt signals with rainfall data is required for a specified interval. Linear drift should be removed from the tilt signals.

Let the tilt signals be written in international format on files *TILTNS* and *TILTEW* for the period "August 1977" to "January 1978". and let the rainfall data reside as daily cumulative values of 6(UT)--measurements on file *RAINFALL* . This file may contain all data from years 1977 and 1978. The interval chosen for the plot, however, might only cover the last 100 days in 1977 (i.e. days 266 to 365).

The following sequence of action-commands may be entered in a command-file for a run of CHETS in Quasi Batch Mode. In Interactive Mode, CHETS asks for those parts of action-commands at a time, that are separated by slashes (/).

```
INP TILTN NAME1/TILTNS/ 266.77, 365.77/
INP TILTE NAME2/TILTEW/ 266.77, 365.77/
INU RAIN  NAME3/RAINFALL/ 2/ 1.77, 265.77, 365.77/ 1/ 6/
LIN TILTN
LIN TILTE
GPH RAIN / 0.3333/ 0, 0/ 1/ 6., 10./ ..(title)../
GPH TILTE/ 0, 0/ 1/ 17., 8./
GPH TILTN/ 0, 0/ 1/ 25.5, 10./
GPH TILTN/ 1, -1/ 6., 31./
FIN
```

The first two actions read hourly data from files *TILTNS* and *TILTEW* into working arrays *NAME1* and *NAME2*, addressing them internally *TILTN* and *TILTE*; however, only the interval chosen for the plot is read from the datafiles. *INU* reads unformated data, that is daily cumulative (indicated by 2. parameter), from file *RAINFALL* into *NAME3* , naming the series now *RAIN*; since the data is not in international format, the date of the first value has to be given as well as the interval required for the plot (3. to 5. parameter); the 6. parameter gives the scale-factor that is used with the data, the last parameter indicates the hour of the daily measurements (since it is not equal to zero, the interval needed from *RAINFALL* starts at day 265 already). Dates in the parameter list may either be given as DDD.YY or as YYMMDDH (YY for year minus

1900, MM for month, DD for day in month, H=0 or 2, if the first value starts at 0 or 12(UT), or if the last value ends at 11 or 23(UT)). The *LIN* -actions subtract the linear drift from *TILTN* and *TILTE* .

The first *GPH* -action initiates a plot for several entries, that are all represented with a plot-reduction-factor of 0.3333; the plot will be overwritten by ..(title).. . First, series *RAIN* is plotted over a range of 10 units above a baseline at 6 units (with respect to the zero-line of the plot), then series *TILTE* over a range of 8 units above a baseline at 17 units, then series *TILTN* over a range of 10 units above a baseline at 25.5 units. The units are centimeters times plot-reduction-factor. In fact, these values for amplitude ranges and baselines are the user's proposals; they are fixed interactively when CHETS offers various amplitude-scales for various proposed ranges. Thus, the user will achieve standardized scales for different series (e.g. same scales for *TILTE* and *TILTN*). The scale of the time-axis is controlled by the plot-reduction-factor. The 2. to 4. parameters of the first *GPH* -action and the 1. to 3. parameters of the two following (i.e. 0, 0, and 1) indicate (a) another entry to this plot will follow, (b) there is no rectangular

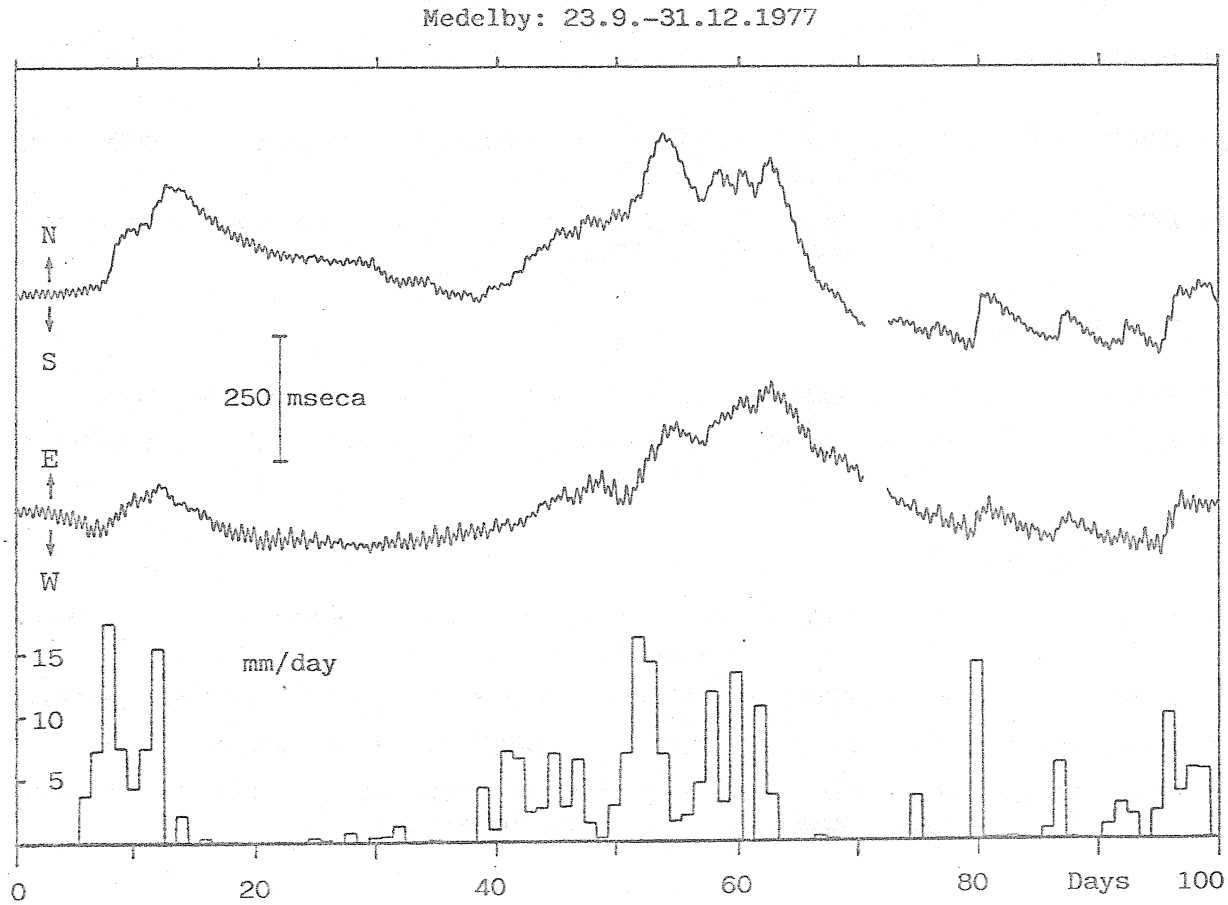

Figure 2: Plot example of CHETS (labelling added by typewriter)

frame wanted around a single series, and (c) the series are plotted at hourly rate. The last *GPH*-action simply closes the plot and adds a rectangular frame of 31 units height beginning at a height of 6 units. The *FIN*-action causes CHETS to close the minutes-file and to stop execution.

The plot generated along with this example is shown in fig. 2 .

III. Table of Actions

The following list is a short (and necessarily uncomplete) description of actually implemented actions. Detailed information is available from the manual.

Time-series with no relations to other series are named *NAMEA* and *NAMEB* in the list; series that are meant to be signal components in perpendicular azimuth (preferably North and East) are referenced as *NAMEX* and *NAMEY*.

Read-Actions :

IND NAMEA NAMEB Reads part of a formated datafile into array *NAMEB* and names it *NAMEA* .

INP NAMEA NAMEB Reads total of formated datafile into array *NAMEB* and names it *NAMEA* .

INU NAMEA NAMEB Reads total or part of an unformated datafile into array *NAMEB* and names it *NAMEA* .

Write--Actions :

OUT NAMEA Writes *NAMEA* in international format on new datafile.

OUU NAMEA Writes *NAMEA* on new datafile, unformated, at arbitrary multiple of hourly rate.

Plot-Actions :

GPH NAMEA Plots *NAMEA* as one of several time-series in a single plot (axes not labelled).

TIS NAMEA Plots *NAMEA* as the only series in a plot (labelled axes).

TRC NAMEX NAMEY Plots trace of *NAMEX* and *NAMEY* (labelled axes).

SPC NAMEA NAMEB Plots amplitude spectrum of *NAMEA* as an option (labelled axes, *NAMEB* used as working array).

Arithmetical Actions :

ANG NAMEX NAMEY	*NAMEX* = ARCTG(*NAMEX* / *NAMEY*), i.e. azimuth for individual values of *NAMEX* and *NAMEY*.
ARI NAMEA	subtracts arithmetic mean from *NAMEA*.
FAD NAMEA	*NAMEA* = $C_1 \cdot$ *NAMEA* + C_2 (C_1, C_2 = constants) .
RAD NAMEX NAMEY	*NAMEX* = SQRT ($NAMEX^2$ + $NAMEY^2$), i.e. distance from origin for individual values of *NAMEX* and *NAMEY*.
ROT NAMEX NAMEY	Rotates *NAMEX* and *NAMEY* to certain azimuth.
SUM NAMEA NAMEB	*NAMEA* = *NAMEA* + $C_1 \cdot$ *NAMEB* , also more sophisticated summation (C_1=constant).
TGS NAMEA NAMEB	*NAMEA* = *NAMEA* / *NAMEB* , i.e. normalization of *NAMEA* - values by *NAMEB*-values.

Filter-Actions :

COS NAMEA	Filters *NAMEA* using cosine-weighted running means.
DIF NAMEA	Computes weighted running differences of *NAMEA*.
FFF NAMEA	Computes Fourier-Transform of *NAMEA* for given frequency.
FSB NAMEA	Subtracts specified sine-wave from *NAMEA*.
FSW NAMEA	Computes tidal variations in *NAMEA* from running window analyses.
LIN NAMEA	Subtracts linear drift from *NAMEA*.
PZV NAMEA	Applies Pertzev-Filter <1> to *NAMEA*.
SMO NAMEA	Smoothes *NAMEA* for wild values by "3RSS"-Algorithm <2>.
WIN NAMEA	Applies Hanning-Window to *NAMEA*.

Time/Length Varying Actions :

COM NAMEA NAMEB	Attaches *NAMEA* to *NAMEB*.
CUT NAMEA	Shortens *NAMEA* to specified interval.
EXT NAMEA	Extends *NAMEA* to specified length by adding a gap.
SFT NAMEA	Performs time-shift of *NAMEA*.

Informative Actions :

COR NAMEA NAMEB	Computes crosscorrelation-function between *NAMEA* and *NAMEB* , also more sophisticated correlations.
MAX NAMEA	Returns minimum and maximum values of *NAMEA*.
SPC NAMEA NAMEB	Computes Fourier-Amplitudes and -Phases of *NAMEA* (*NAMEB* used as working array).
TYP NAMEA	Returns header-information and specified values of *NAMEA*.
VAR NAMEA	Computes variance of *NAMEA*.
VAR NAMEX NAMEY	Computes variance of SQRT($NAMEX^2$ + $NAMEY^2$) .

Service-Actions :

FIN	Terminates execution of CHETS.
GET NAMEA NAMEB	Copies *NAMEB* to *NAMEA*.
HLP	Lists available actions.
NAM	Returns actual internal names of time-series in CHETS.
NGP NAMEA	Interpolates gaps in *NAMEA* linearly.
SWI	Switches from Interactive to Quasi Batch Mode or vice versa.

Generally, Fourier-Transforms are calculated using the Goertzel-Algorithm<3>. The algorithm allows exact Fourier-Transforms for arbitrary frequencies by only one sine- and cosine-computation per frequency. Up to 85% computer time is saved with regard to the straightforward method.

Sine-waves in the time-domain are computed using the Orzechowski-Algorithm <4>. The algorithm needs only two sine- and cosine-computations per frequency.

IV. References

<1> Pertzev, B.B., 1959: Sur la dérive dans les observations de marrées élastiques.- Izv. Acad. Sc. URSS, Sér.Géoph., 4, 547--548.

<2> Kleiner, B. & Graedel, T.E., 1980: Exploratory data analysis in geophysical sciences.- Rev. Geoph. Space Phys., 18, 3, 699-717.

<3> Goertzel, G., 1958: An algorithm for the evaluation of finite trigonometric series.- Am. Math. Month., 65, 34.

<4> Orzechowski, J., 1975: Moyens d'accélération et de l'acroissement de la précision des calcules dans la méthode des analyses des observations des marrées.- Bull. d'Inform. Marrées Terrestres, 72, 4143-4149.

Publ. No. 280 of Institute of Geophysics, University of Kiel, FRG

DETERMINATION OF THE SHAPE OF THE CALIBRATION CURVE

Tadeuz Chojnicki

Space Research Centre, Polish Acad. of Sc., Warsaw

Tidal observations $P_o(t)$ are obtained, as a rule, in a non-tidal measure. Thus it is necessary to obtain a calibration curve C(t) defined at each moment at which an observation was obtained. As is well known, this is the fundamental issue in tidal measurements.

In observation practice, certain standard routine for determining the calibration curve has been elaborated. Discrete values of curve C(t) are determined by means of a direct calibration at some intervals of time different than intervals of observations, and then they are interpolated in different ways for moments within those intervals. Intervals between calibrations are different for different instruments and, in general, they are not shorter than 12^h but frequently are much longer. The reason why longer periods between direct calibrations are chosen are technical difficulties of calibration for a given type of an instrument, lack of automation or the fact that, in some cases, calibration may disturb the process of continuous observations. The consideration given below, refer to studies in which long intervals between calibrations were made.

We can conceive an error of the calibration curve as a sum of two parts : that concerning its general level i.e. reference to the system of measures (tidal and of a recording), and the one concerning its shape. The first part of the error causes the same change of the scale of all determined amplitude factors of tidal waves, and the second part involves a different change of different coefficients. In the present paper we are dealing mostly with the second part of the calibration error.

Assuming that the direct calibration has been done correctly, the error of the shape of the calibration curve results from the inconsistency of results of an adopted way of interpolation with its real course. Of course,

every incidental error of any direct calibration would increase the error of shape even more. That error deforming different waves in different ways makes it impossible to obtain precise results even if in tidal research we restrict ourselves to studies of relations between individual waves, for example when we investigate resonance of the liquid core.

Using the least square method for determining tidal parameters x we adjust observations $P_o(t)$ comparing them with theoretical tides $P_T(t)$ according to the scheme

$$v(t) = P_T(t,x_r) - P_o(t) \cdot C_r(t). \tag{1}$$

If a shape of curve $C_o(t)$ is not consistent with the real state $C_r(t)$, equation (1) will be written as

$$R(t) = P_T(t,x_o) - P_o(t) \cdot C_o(t), \tag{2}$$

where residuum R(t) will contain, beside an accidental error of observation v(t), an information on a real variation of the calibration curve $C_o(t)$.

Denoting a relation of the real and performed calibrations as K(t) we can write

$$K(t) = \frac{C_r(t)}{C_o(t)} = \frac{P_o(t) \cdot C_o(t) - r(t)}{P_o(t) \cdot C_o(t)} + T, \tag{3}$$

where r(t) is residuum without an accidental error, and T deforming function resulting from the fact that the calibration error does not enter exclusively in the residuum but also in parameters of adjustment x, as well as to the fact that during adjustment residuum is minimized according to the least square method.

As is derived from equation (3), the relation of the tide after adjustment to the observed one will be an approximation of coefficient K(t). Neglecting for a while the determination of function T, we have investigated what results may be obtained when deriving K(t) from formula

$$K(t) \cong \frac{P_o(t) \cdot C_o(t) - r(t)}{P_o(t) \cdot C_o(t)} \tag{4}$$

by the method of consecutive iterations.

To realize formula (4) in practice, some way of eliminating the accidental error from residuum should be found. For this purpose, using R(t), K was calculated as a mean of individual K values calculated in the period from t_{-n} to t_n; the value so obtained represented the moment t_o. To increase the precision of calculating K, weights were introduced which were equal to $|P_o(t)|$. Moreover, individual K values were eliminated where their weight was less than

a limiting minimal value P_{min} determined in advance. Finally we have used formula

$$K(t_o) = \frac{1}{\Sigma\,|p(i)|} \sum_{i=t_{-n}}^{t_n} \frac{P_o(i) \cdot C_o(i) - R(i)}{P_o(i) \cdot C_o(i)} \cdot |P(i)|, \qquad (5)$$

$$|P(i)| \geq P_{min}.$$

In preliminar practical realization of the above method the following assumption were used :

- representation moments t_o of calculated values of K correspond to the start of a day, that is increments of function (5) are equal to one day and $n=12^h$.
- limiting minimal value P_{min} is equal to 20 μgal or 2 msec.

In computations model observations were used. Each model contains a period of 2 months of observations of the vertical component at the Warsaw station. Three models A, B and C were prepared. In each model the real calibration curve is a straight line

$$C_r(t) = 1. \qquad (6)$$

Diagrams of "observed" (deformed) calibration curves in individual models are presented in Fig. 1.

All three models were elaborated in eight iterations. Zero iteration denotes the first adjustment of observations obtained for non-corrected calibration curve. In each iteration coefficient K(t) for each day was calculated and was adopted as a corrected calibration curve for the next iteration. Results of individual iterations are shown in Table 1 in which the following elements are given :

1. $\Delta\delta$ - deviations of amplitude factors δ from real values for five waves Q_1, O_1, K_1, M_2 and S_2;
2. $m\delta$ - a mean square error of determining factor δ with weight 1 on the basis of deviations mentioned under 1. Weight of factors were adopted as proportional to wave amplitudes. A weight equal to 1 was adopted for wave K1;
3. the mean square error of observation m_o after adjustment and mean errors in frequency bands : diurnal - m_1, and semi-diurnal - m_2;
4. K - the mean from discrete values of function K(t) for 60 days of the observation period. This value presents a change of a general level of the calibration curve caused by the adopted deformation in the model;
5. m_K - The mean square error of the mean value shown under 4. This error

is the measure of how a determined calibration curve differs from the real one after a given iteration. It should be a straight horizontal line that is its m_K should be equal to zero.

To simplify comparisons of results from individual iterations values given under 1. and 3. (and, consequently, under 2.) were reduced to the real level of calibration i.e. they were divided by value given under 4.

In Fig. 1 the dashed line presents also the calibration curve obtained from the zero iteration. The curve from the last iteration in the scale of the figure is identical with the assumed curve.

From the above results the following conclusions can be drawn :

- the iteration process employed here is convergent and it helps to obtain the real shape of the calibration curve and real values of determined tidal parameters;
- errors of a shape of the calibration curve result in great deformations of relations between factors δ of individual waves and they appear as great differences between mean square errors of observations in main frequency bands of tidal waves;
- already the first iteration essentially corrects calibration errors. Each successive iteration reduces the error of factors δ by a half.

In the presented example the determination of the general level of calibration was easy because we know that the correct value of curve $C_r(t)$ at every moment should be equal to 1. In the case of real observations, it is sufficient to have at least one moment for which a precise value of $C_r(t_i)$ is known. If a shape of this curve is determined by the way given above, it is sufficient to displace it in the reference system so as it coincides with value $C_r(t_i)$ at moment t_i.

To speed up the process of iteration, the first trial of improvement of formula (4) was done. Denoting the real tide as P_r, amplitude factor after adjustment as x_c, deviation of this factor due to the calibration error as Dx, and index of the wave group into which we divide theoretical tides in adjustment as i, then neglecting errors of phase differences we can write

$$P_r = \sum^{i} P_{Ti}(x_{ci} + Dx_i) \quad \text{or} \quad P_r = \sum^{i} P_{Ti}\, x_{ci} + \sum^{i} P_{Ti}\, Dx_i \tag{7}$$

From this the real value of coefficient $K_r(t)$ will be equal to

$$K_r(t) = K(t) + \sum^{i} \frac{P_{Ti}}{P_o(t) \cdot C_o(t)} Dx_i. \tag{8}$$

An approximate value Dx_i is calculated from differences between values of am-

plitude factors obtained in individual iterations. In Table 2 the elements are given identical with those in Table 1 obtained from processing models A, B and C with consecutive iterations according formula (8). It is seen that this way speeds up the process by one iteration.

The determination of calibration variation as outlined here is not finally elaborated. It should also be mentioned that the same approach could be used in investigations of variation of amplitude factors in time, provided we have observations with faultless calibration because variation of amplitude factor and calibration curve are inseparable. If we expect that different factors will change in time differently, individual groups of waves should be separated from observations, for example by filtration, and they ought to be studied independently.

In the last place, results are presented of the discussed way of determining calibration variations as used for real observations. Fig. 2 presents the calibration curve determined as described above for the pendulum and a diagram of azimuth variation for that pendulum for two annual series of clinometric observations of Ksiaz. Because of unperpendicularity of the arms of the instrument base, azimuth changes are correlated with changes of pendulum sensitivity. The presented figure confirms that fact.

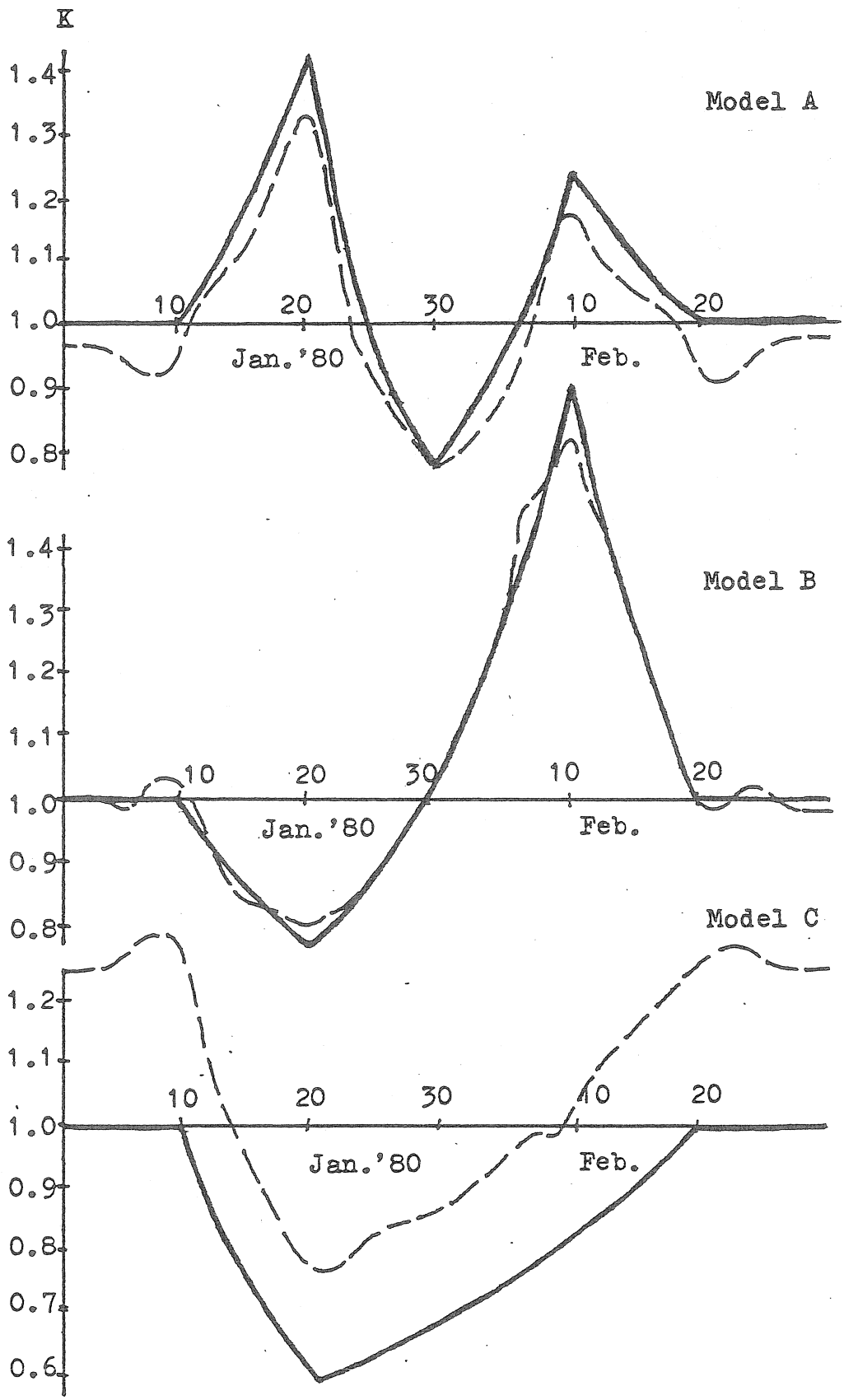

Fig. 1. Deformation of calibration curve in the individual models

Table 1. Determining the calibration curve according to the formula /4/.

Iteration	0	1	2	3	4	5	6	7	8
$\Delta\delta$		Model A							
Q1	+0.1955	+0.0824	+0.0385	+0.0184	+0.0088	+0.0041	+0.0019	+0.0010	+0.0005
O1	−0.0120	−0.0089	−0.0052	−0.0028	−0.0015	−0.0007	−0.0003	−0.0001	0.0000
K1	−0.0030	−0.0003	−0.0001	0.0000	+0.0001	+0.0001	+0.0001	+0.0001	+0.0001
M2	+0.0041	+0.0008	+0.0004	+0.0003	+0.0002	+0.0002	+0.0001	+0.0001	+0.0001
S2	−0.0234	−0.0073	−0.0028	−0.0012	−0.0005	−0.0002	0.0000	0.0000	0.0000
m_δ	±0.0286	±0.0122	±0.0058	±0.0028	±0.0014	±0.0006	±0.0003	±0.0002	±0.0001
m_o	±7.932	±0.784	±0.334	±0.157	±0.077	±0.039	±0.022	±0.015	±0.012
m_1	±34.449	±2.954	±1.173	±0.542	±0.255	±0.121	±0.059	±0.030	±0.018
m_2	±23.515	±2.727	±1.178	±0.529	±0.243	±0.111	±0.051	±0.026	±0.015
K	0.9526	0.9528	0.9534	0.9538	0.9540	0.9541	0.9542	0.9542	0.9542
m_K	±0.0032	±0.0016	±0.0008	±0.0005	±0.0003	±0.0002	±0.0001	±0.0001	±0.0001
$\Delta\delta$		Model B							
Q1	−0.2143	−0.0817	−0.0364	−0.0163	−0.0074	−0.0034	−0.0016	−0.0008	−0.0003
O1	+0.0750	+0.0117	+0.0061	+0.0035	+0.0018	+0.0011	+0.0007	+0.0004	+0.0003
K1	−0.0044	+0.0006	+0.0005	+0.0004	+0.0003	+0.0002	+0.0002	+0.0002	+0.0001
M2	+0.0092	−0.0013	−0.0009	−0.0005	−0.0003	−0.0001	0.0000	0.0000	+0.0001
S2	+0.0272	−0.0019	−0.0023	−0.0016	−0.0010	−0.0006	−0.0003	−0.0001	0.0000
m_δ	±0.0324	±0.0123	±0.0056	±0.0026	±0.0013	±0.0006	±0.0004	±0.0002	±0.0001
m_o	±8.954	±0.575	±0.260	±0.129	±0.068	±0.039	±0.025	±0.017	±0.013
m_1	±38.524	±2.226	±0.978	±0.476	±0.244	±0.132	±0.075	±0.043	±0.027
m_2	±27.170	±1.987	±0.905	±0.437	±0.223	±0.118	±0.065	±0.038	±0.022
K	1.0001	0.9987	0.9981	0.9978	0.9977	0.9976	0.9976	0.9975	0.9975
m_K	±0.0027	±0.0014	±0.0008	±0.0005	±0.0003	±0.0002	±0.0002	±0.0002	±0.0001
$\Delta\delta$		Model C							
Q1	−0.1991	−0.0736	−0.0323	−0.0145	−0.0064	−0.0029	−0.0013	−0.0006	−0.0003
O1	+0.0148	+0.0053	+0.0030	+0.0016	+0.0009	+0.0006	+0.0004	+0.0003	+0.0002
K1	−0.0043	+0.0001	+0.0002	+0.0002	+0.0002	+0.0001	+0.0001	+0.0001	+0.0001
M2	+0.0067	−0.0002	−0.0003	−0.0002	−0.0001	0.0000	0.0000	+0.0001	+0.0001
S2	+0.0077	+0.0026	+0.0005	+0.0001	0.0000	0.0000	0.0000	0.0000	+0.0001
m_δ	±0.0289	±0.0106	±0.0047	±0.0026	±0.0010	±0.0005	±0.0002	±0.0001	±0.0001
m_o	±9.193	±0.353	±0.157	±0.076	±0.038	±0.021	±0.013	±0.010	±0.008
m_1	±38.703	±1.325	±0.571	±0.273	±0.133	±0.067	±0.036	±0.021	±0.013
m_2	±28.739	±1.226	±0.540	±0.250	±0.117	±0.057	±0.029	±0.017	±0.010
K	1.2588	1.2585	1.2582	1.2580	1.2579	1.2579	1.2579	1.2579	1.2579
m_K	±0.0021	±0.0011	±0.0006	±0.0003	±0.0002	±0.0001	±0.0001	0.0000	0.0000

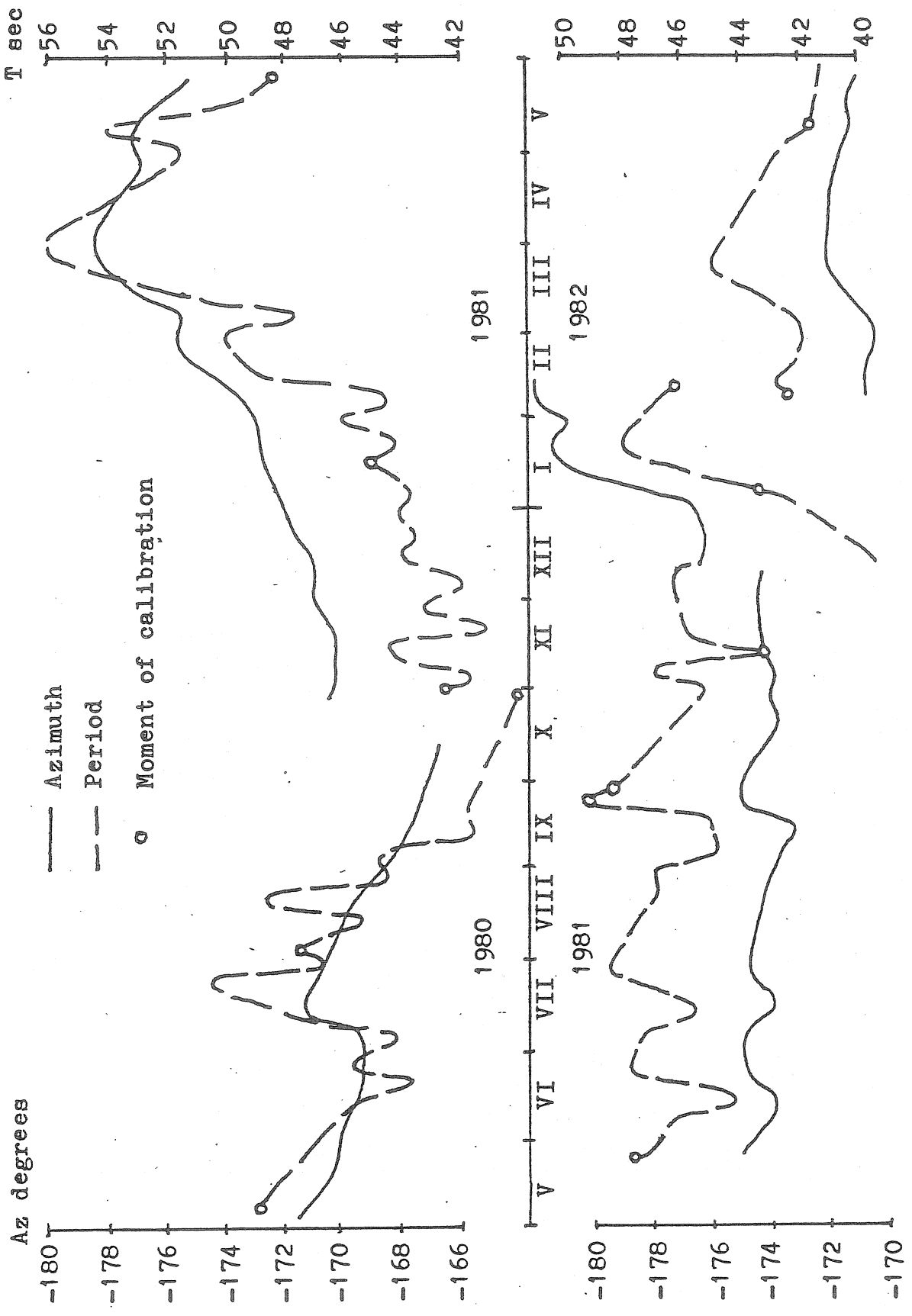

Fig.2. Correlation between azimuth and period for the pendulum H-74 at Książ

Table 2. Determining the calibration curve according to the formula /8/.

Iteration	0	1	2	3	4	5	6	7	8
$\Delta\delta$		Model A							
Q1	+0.1955	+0.0430	+0.0071	−0.0085	−0.0090	−0.0041	+0.0001	+0.0016	+0.0012
O1	−0.0120	−0.0070	−0.0033	−0.0006	+0.0004	+0.0004	+0.0002	+0.0001	0.0000
K1	−0.0030	−0.0003	0.0000	0.0000	+0.0001	+0.0001	+0.0001	+0.0001	+0.0001
M2	+0.0041	+0.0008	+0.0004	+0.0002	+0.0001	+0.0001	+0.0001	+0.0001	+0.0001
S2	−0.0234	−0.0049	−0.0009	+0.0006	+0.0008	+0.0005	+0.0002	+0.0001	0.0000
m_δ	±0.0286	±0.0067	±0.0016	±0.0012	±0.0013	±0.0006	±0.0001	±0.0002	±0.0002
m_o	±7.932	±0.656	±0.252	±0.112	±0.059	±0.027	±0.013	±0.011	±0.010
m_1	±34.449	±2.646	±0.970	±0.450	±0.236	±0.101	±0.026	±0.026	±0.021
m_2	±23.515	±2.378	±0.902	±0.358	±0.182	±0.082	±0.026	±0.030	±0.021
K	0.9526	0.9523	0.9517	0.9509	0.9500	0.9488	0.9476	0.9465	0.9453
m_K	±0.0032	±0.0014	±0.0006	±0.0003	±0.0002	±0.0001	±0.0001	±0.0001	0.0000
$\Delta\delta$		Model B							
Q1	−0.2143	−0.0338	+0.0023	+0.0141	+0.0103	+0.0031	−0.0013	−0.0021	−0.0013
O1	+0.0250	+0.0080	+0.0031	+0.0004	−0.0003	−0.0002	+0.0001	+0.0003	+0.0002
K1	−0.0044	+0.0010	+0.0006	+0.0003	+0.0002	+0.0001	+0.0001	+0.0002	+0.0001
M2	+0.0092	−0.0020	−0.0012	−0.0004	−0.0001	0.0000	+0.0001	+0.0001	+0.0001
S2	+0.0272	−0.0085	−0.0065	−0.0039	−0.0020	−0.0009	−0.0002	+0.0001	+0.0001
m_δ	±0.0324	±0.0059	±0.0020	±0.0022	±0.0015	±0.0004	±0.0002	±0.0003	±0.0002
m_o	±8.954	±0.487	±0.228	±0.130	±0.076	±0.035	±0.018	±0.015	±0.011
m_1	±38.524	±1.856	±0.810	±0.451	±0.254	±0.106	±0.051	±0.043	±0.027
m_2	±27.170	±1.713	±0.829	±0.465	±0.261	±0.110	±0.045	±0.037	±0.023
K	1.0001	0.9990	0.9992	0.9999	1.0008	1.0019	1.0030	1.0041	1.0051
m_K	±0.0027	±0.0012	±0.0007	±0.0004	±0.0002	±0.0002	±0.0001	±0.0001	±0.0001
$\Delta\delta$		Model C							
Q1	−0.1991	−0.0271	+0.0048	+0.0134	+0.0088	+0.0022	−0.0014	−0.0019	−0.0010
O1	+0.0148	+0.0028	+0.0008	−0.0002	−0.0003	0.0000	+0.0002	+0.0002	+0.0002
K1	−0.0043	+0.0003	+0.0002	+0.0002	+0.0001	+0.0001	+0.0001	+0.0001	+0.0001
M2	+0.0067	−0.0004	−0.0002	−0.0001	0.0000	+0.0001	+0.0001	+0.0001	+0.0001
S2	+0.0077	−0.0005	−0.0016	−0.0014	−0.0008	−0.0002	+0.0001	+0.0001	+0.0001
m_δ	±0.0289	±0.0040	±0.0008	±0.0019	±0.0013	±0.0003	±0.0002	±0.0003	±0.0002
m_o	±9.193	±0.173	±0.060	±0.067	±0.043	±0.014	±0.010	±0.011	±0.009
m_1	±38.703	±0.665	±0.236	±0.257	±0.159	±0.045	±0.030	±0.035	±0.021
m_2	±28.739	±0.574	±0.176	±0.220	±0.142	±0.042	±0.025	±0.030	±0.017
K	1.2588	1.2585	1.2586	1.2589	1.2592	1.2597	1.2602	1.2606	1.2610
m_K	±0.0021	±0.0005	±0.0002	±0.0002	±0.0001	0.0000	0.0000	0.0000	0.0000

TIME VARIATIONS IN TIDAL ADMITTANCE - INVESTIGATIONS AT THE CHARLEVOIX OBSERVATORY, QUEBEC.

John Peters

Oceanography Department
Dalhousie University, Halifax, Canada.

Paper presented at the Working Group on Earth Tides : Data Acquisition and Analysis, University of Bonn, October, 1984.

ABSTRACT

Tilt observations from two boreholes located in the Charlevoix seismic zone in Quebec are analysed in conjunction with data from tide gauges in the adjacent St. Lawrence estuary. Time variations in the tilt admittance for the M_2 constituent are found to be related to variations in the marine tide admittance through tidal loading. A baseline for the detection of time variant crustal response anomalies, after accounting for the loading input variations, is established at the 2-3% level for M_2.

INTRODUCTION

In general, analyses of consecutive short (30-60 day) series of tidal data indicate that the tidal admittance estimated from observations is not constant [Schuller, 1977; Baker and Alcock, 1983; Peters and Beaumont, 1984]. Although we normally regard the tidal forcing function as a stationary process, measurements influenced by a strong marine tidal load

will be affected by the instability of the marine tide. Baker and Alcock [1983] have described seasonal variations in the M_2 tide recorded in tide gauges around the British Isles and reflected in near-coastal tilt measurements. They attribute the cause of some of the variations to modulation by the non-linear interactions MKS_2 and MSK_2. In some areas, non-tidal energy associated with meteorological influences may contribute strongly to the total energy in the tidal bands, inducing apparent modification of the tidal response. In any case, a time varying marine tide represents a time varying input to the tilt measurement system and therefore must be accounted for before the crustal tidal response can be described.

In this brief account of the Charlevoix tidal tilt experiment, we discuss the time variant analysis of parallel recordings of tilt data from two boreholes at the Charlevoix Observatory. The relationship between the marine tidal loading from the nearby St. Lawrence river and the tilt admittance variations is examined, and a baseline for the detection of crustal response anomalies established. Such anomalies are expected to be generated in seismic zones as a result of elastic property changes associated with high tectonic stresses [Beaumont and Berger, 1974; Beaumont, 1978].

The Charlevoix seismic zone is situated about 150Km north-east of Quebec City and is one of the most active areas in eastern North America. The observatory site is located on the north shore of the St. Lawrence river in the centre of the Ordovician age Charlevoix impact crater which overlaps the zone of seismicity. The data considered in this study were recorded during 1983 by two borehole tiltmeters [Peters and Beaumont, 1984], and by two tide gauges near the site, St. Joseph de la Rive and Tadoussac. The 47m deep boreholes are 80m apart and instrumented with Bodenseewerk borehole pendulums. A separate analysis of tide gauge data recorded during 1972 to 1974 at eight stations distributed over the estuary was also made.

DATA ANALYSIS

The time variant analysis was made using the HYCON tidal analysis programme of Schuller [1977]. While the basic algorithm is similar to that of other standard methods (for example, Chojnicki, [1973]), the programme is set up to automatically perform a sequential analysis of overlapping data subsets from which a time varying admittance can be determined. Two important features are: the application of the Hanning window to the data subsets in order to eliminate spectral leakage from unmodelled constituents in neighbouring tidal groups, and the calculation of errors for each of the subsets on the basis of the residual variance in each of the tidal bands.

In our use of the programme we have reduced the number of astronomical constituents from 505 to 73 which can be detected above the noise. These are separated into 11 groups in which the admittance is assumed to be the same for each member constituent. In addition to the astronomical frequencies, 9 non-linear constituents known to be prominent in the marine loading tide were included. A basic interval for the data subsets of 1440 hours was chosen with a step size of 240 hours for the overlapping sequence. In combination with the Hanning data window, this arrangement ensured that there would be no interaction between high energy levels in adjacent tidal groups.

RESULTS OF THE TIME VARIANT ANALYSIS

Figures 1 and 2 show the M_2 amplitude and phase variations, respectively, determined from HYCON sequential analysis of the south and east components of tilt from boreholes 1 and 2, and from tide gauges St. Joseph de la Rive and Tadoussac in the St. Lawrence river near the site. The range of the tilt amplitude variations is 8-10% and is clearly well correlated between boreholes and between component directions.

There is a marked difference in the absolute and fractional ranges between the two tide gauge M_2 amplitude series and also in comparison with the tilt. Nevertheless, the pattern of the variations is strongly correlated among all the series. The phase variations shown in figure 2 are well correlated among the two components of tilt, but there appears to be no agreement between the tilt and the tide gauge variations or, indeed, between the two tide gauges. The range of the phase variations is approximately 5 degrees for all series.

Since the results from the two borehole measurements are in agreement, we expect that the observed variations are regional. The agreement between the two component directions is expected if the source of the variations is marine since both components are strongly affected by loading. It is apparent that since the phase variations are different for each of the tide gauges and the tilt, the loading induced variations cannot be estimated from observations made by a single gauge.

A separate study of marine data from eight tide gauges recording concurrently during 1972 to 1974, and distributed over the whole of the estuary, confirmed the coherent M_2 amplitude variations in the part of the estuary near the observatory. Also confirmed were the spatially incoherent M_2 phase variations. By comparison, the diurnal constituent amplitude and phase variations were each strongly coherent over the whole estuary. It appears that the driving mechanism for the M_2 variations is locally generated in comparison with the obviously large-scale diurnal effect. It is possible that timing errors may be significantly affecting the M_2 results.

Since the amplitude and phase parts of the admittance variations seem to be physically unrelated, it is worthwhile to investigate separately the tilt amplitude variations after eliminating the time varying input based on the loading. The correlation coefficient between each of the tilt amplitude series and the tide gauge at St. Joseph de la Rive exceeds 0.9. We can therefore explain most of the tilt amplitude variations in terms of the tide gauge variations. Figure 3 shows the residual tilt amplitude variations derived from the linear regression of the tide gauge and tilt amplitude series. Apart from the prominent excursion in the south

component beginning near day 240, the variations are confined within a range of 2-3% in both directions. The abovementioined excursion is artificial and is due to a poor interpolation model used in filling a gap in the tide gauge data.

DISCUSSION AND CONCLUSIONS

The typical 95% error associated with each of the 1440 hour tilt M_2 estimates has a range of 3% indicating that the observed admittance variations are significant. Furthermore, the residual amplitude variations shown in figure 3 are strongly coherent between the redundant measurements at a level well below the least squares error range. Clearly, the errors are not, as assumed, random but contain as yet unmodelled regional signal components. This may not have been recognized had we not made parallel observations in two installations. Again, the importance of performing redundant measurements is confirmed.

Although the connection between the marine tides and the time varying tilt admittance is established, the mechanism which produces 10% variations in tilt amplitude, while the sampled tide gauge amplitudes vary between 2 and 5%, is unclear and needs to be investigated.

Parallel tidal tilt measurements have been made in two boreholes located at the Charlevoix Observatory. Time variant analysis of the tilt and nearby tide gauge observations indicates that variations in the marine tide are largely responsible for the behaviour of the tilt. The amplitude baseline after removal of the first order marine tide regression model was reduced to the 2-3% level for M_2. This is consistent with the variability established for strain at the Pinon Flat Observatory which is located in a locally aseismic region of southern California [Agnew, 1979].

ACKNOWLEDGEMENTS

This work was supported by the Air Force Geophysics Laboratory, Hanscom AFB (under contract F19628-83-K-0023). The Earth Physics Branch provided facilties at the Charlevoix Observatory.

REFERENCES

Agnew, D.C.,Strain tides at Pinon Flat: Analysis and interpretation, unpub. Ph.D. thesis, Univ. of California, San Diego, 1979.

Baker, T.F., and G.A. Alcock, On the Time Variation of Ocean Tides, Proceedings of the Ninth Int. Symp. on Earth Tides, J.T. Kuo ed., E. Schweizerbart'sche Verlagsbuchhandlung, 1983.

Beaumont, C., Linear and nonlinear interactions between the earth tide and a tectonically stressed earth, in: Applications of Geodesy to Geodynamics, I. Mueller, ed., Ohio State University Press, 313-318, 1987.

Beaumont, C., and J. Berger, Earthquake prediction: modification of the earth tide tilts and strains by dilatancy, Geophys. J. R. ast. Soc., 39, 111-121, 1974.

Chojnicki, T., Ein Verfahren zur Erdgezeitenanalyse in Anlehnung an das Prinzip der kleinsten Quadrate, Mitt. aus dem Inst. f. Theo. Geod. der Univ. Bonn, 15, Bonn, 1973.

Peters, J., and C. Beaumont, Borehole tilt measurements from Charlevoix, Quebec, submitted to J. Geophys. Res., 1984.

Schuller, K., Tidal Analysis by the Hybrid Least Squares Frequency Domain Convolution Method, M. Bonatz and P. Melchior eds., Institut fur Theoretische Geodesie Der Univ. Bonn, Fed. Rep. Germany, 1977.

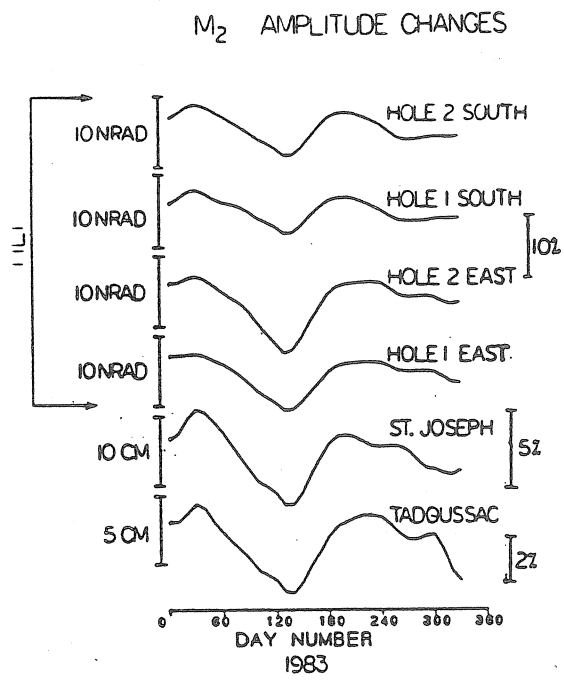

Figure I. Plots versus time of the changes in M_2 amplitude for the south and east components of tilt in boreholes I and 2 and the tide gauges at St. Joseph de la Rive and Tadoussac. The percentage scales represent fractions of the mean amplitude.

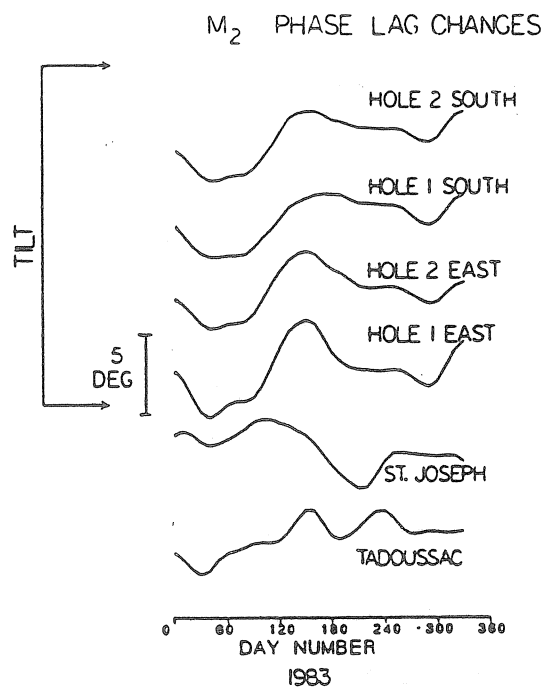

Figure 2. Plots versus time of the changes in M_2 phase lag for the south and east components of tilt in boreholes I and 2 and the tide gauges at St. Joseph de la Rive and Tadoussac.

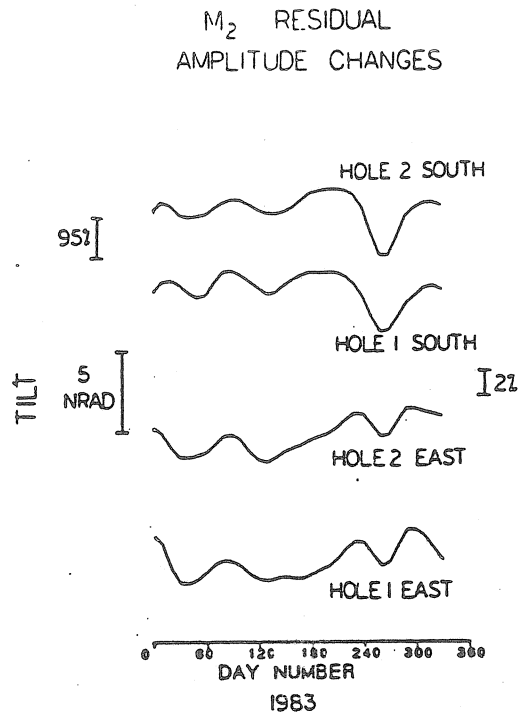

Figure 3. Plots versus time of the residual changes in M_2 amplitude for the south and east components of tilt in boreholes I and 2. The 2% scale represents the fraction of the mean amplitude. The 95% scale represents twice the typical 95% error associated with each of the overlapping amplitude estimates.

HIGH FREQUENCIES AND THEIR INTERPRETATION IN THE TIDAL TILT SIGNAL

G. Bartha
Geodetic and Geophysical Research Institute
of Hungarian Academy of Sciences /GGRI/ Sopron,
Hungary

SUMMARY

A horizontal pendulum with capacitive transducer was used to detect the Earth free oscillation after Earth quakes. The electric signal was analogously recorded and sampled in each 23 sec. The power spectra of the time series were computed by FFT, and some peaks of them were identified as free oscillation modes.

INTRODUCTION

A Zöllner type, metal fibred horizontal pendulum with capacitive transducer was developped in the Geodetic and Geophysical Research Institute, Sopron /Mentes, 1981/. The electric output provides a possibility for an almost arbitrary dense sampling therefore a chance is given to investigate the frequencies which are higher than the tidal ones.

Partly this possibility, partly some earlier works inspired us to try the detectation of the free oscillations of the Earth. In 1962 Bolt and Marussi reported the observation of this phenomenon with horizontal pendulum after the big Chilean quake. In 1971 Drattler and Block published results about the observation of the normal modes by means of a vertical pendulum and the magnitude of the monitored quakes were 7.1 and 6.3, respectively. The last information confirmed our hope that the free modes could be observed not only after the infrequent large quakes but after smaller ones, too.

We monitored two quakes with the home-made horizontal pendulum in 1983 and the first treatment of the records was reported in the UGGI meeting, Hamburg /Bartha, Czompó, 1984/. In the present paper a more detailed investigation of the power spectra is given. The theoretical and instrumental background has been discussed in earlier papers /Bartha and Czompó, 1984; Bartha, 1984/ therefore only a short summary is given here in this sense.

OBSERVATION OF FREE OSCILLATION WITH HORIZONTAL PENDULUM

In the classical physics this phenomenon can be described by the motion equation of the elastic bodies in absence of the external forces further by the Poisson equation to take the gravity into consideration:

$$\zeta \ddot{\underline{s}} = \zeta \underline{F} + \zeta \nabla V + \nabla \underline{\underline{T}}_{ik} \qquad /1/$$

$$\nabla^2 V = -4\pi G \nabla (\zeta \underline{s}) \qquad /2/$$

where ζ means the density, s the displacements, F_g the force from the selfgravitation, T_{ik} the elasticity tensor, ∇ the gradient operator, G the gravitional constant.

The solution in the Cartesian system for a non rotating, homogeneous, elastic sphere in absence of the selfgravitation was given by Lamb in 1882. It consists of two groups of oscillations which are the so called "spheroidal" oscillations /denoted by ${}_n S_l^m$/ and the "torsional" ones /denoted by ${}_n T_l^m$/. The notations /proposed by Mac Donald and Ness, 1961/ describes the pattern of the nodal lines in latitude /subscript l/ and in longitude /subscript m/ further the radial nodal surfaces /subscript n/. The simplest modes are shown in Fig. 1.

The solution of Eq.1. and Eq.2. in spherical coordinates for a non rotating, stratified, elastic, spherical model was given by Alterman, Jarosch and Pekeris in 1959. The rotating model was discussed by Backus and Gilbert in 1961 and later by Dahlen /1969/ who involved the ellipticity into the problem. Later Dahlen /1976/ investigated the effect of the lateral inhomogenity, too. Recently Shen and Manshina /1976/ and Wahr /1981/ discussed the mentioned model with an embedded fluid core.

The horizontal pendulum is influenced by the free oscillation effect in two senses. At first it reacts as a simple accelerometer to the torsional vibrations in the horizontal plane /accelerometer mode/, at second it gives a response as tiltmeter to the tilt produced by the spheroidal modes /tiltmeter mode/. The response functions in these two modes are shown in Fig. 2. They were computed from the solution of the motion equation of the pendulum. In the tilt mode the response function $Q(1/f)$ is given as Φ/φ where is the beam response to the tilt described by $\varphi = \varphi_o \sin 2\pi f t$. In the accelerometer mode the response function $Q(1/f)$ is given as X/x where X denotes the displacement of the beam at the sensor with respect to the frame, and $x = x_o \sin 2\pi f t$ is the motion of the frame in the horizontal plane due to the torsional oscillations.

From Fig. 2. we can conclude that first of all the detectation of the spherical modes can be expected and the torsional ones would only appear at "large" motions /i.e. after bigger quake/.

SPECTRA OF TIDAL TILT SIGNAL OBSERVED AFTER QUAKES

In 1983 two quakes were monitored with horizontal pendulum. The data of the observed quakes are summarized in Table 1.

The analogous signals were sampled in each 23 seconds and the data series were processed by an FFT program. The computational work was carried out by Mr. J. Czompó by means of the HP 1000 computer of the GGRI. The computed spectra are shown in Fig. 3. and the identified /or those assumed as identified, respectively/ peaks are detailed in Table 2. The periods of normal modes were taken for the identification from Mendiguren, 1973. In connection with the spectra it must be mentioned that some instrumental noise /IN/ of a frequency of 1/1200 - probably due to the clock system - was superposed to the recorded signal. Unfortunately it makes distorsions in the spectra at period of 1200 and at its overtones /i.e. 600, 400, 300, 250 etc. sec./.

REFERENCES

Alterman at al, Oscillation of the Earth, Proc. Roy. Soc. London A 252, 80, 1959.

Bartha, G. and Czompó, J., High frequencies in tidal records before and after Earthquakes, 19th IUGG General Ass. Hamburg, Vol 1. p. 104-124, 1983.

Bartha, G., High frequencies in tidal tilt records, 5th International Symp., Geodesy and Physics of the Earth, Magdeburg, 1984.

Bolt and Marussi, Eigenvibrations of the Earth observed at Trieste, GJ, 6, 299, 1962.

Dahlen, The normal modes of a rotations, elliptical Earth, JGR, astr. Soc. 18, 397, 1969.

Dahlen, Models of the lateral homogenity of the Earth consistent with eigen frequency splitting data, JGR, astr. Soc. 27, 337, 1972.

Drattler and Block, A wide Band Horizontal Accelerometer ...., JGR, 27, 337, 1971.

Mac Donald and Ness, A study of the free oscillation of the Earth, JGR, 66, 1865, 1961.

Mendiguren, Identification of free oscillation spectral peaks, JGR, 33, 281, 1973.

Mentes, Gy., Horizontal pendulum with capacitive transducer, Acta Geod. Geoph. et Mont. Hung., 16/1981/, 269-280, 1981.

Shen and Manshina, Oscillation, nutation and ...., JGR, 46, 467, 1976.

Wahr, A normal mode expansion for the forced response of a rotating earth, JGR, 64, 651, 1981.

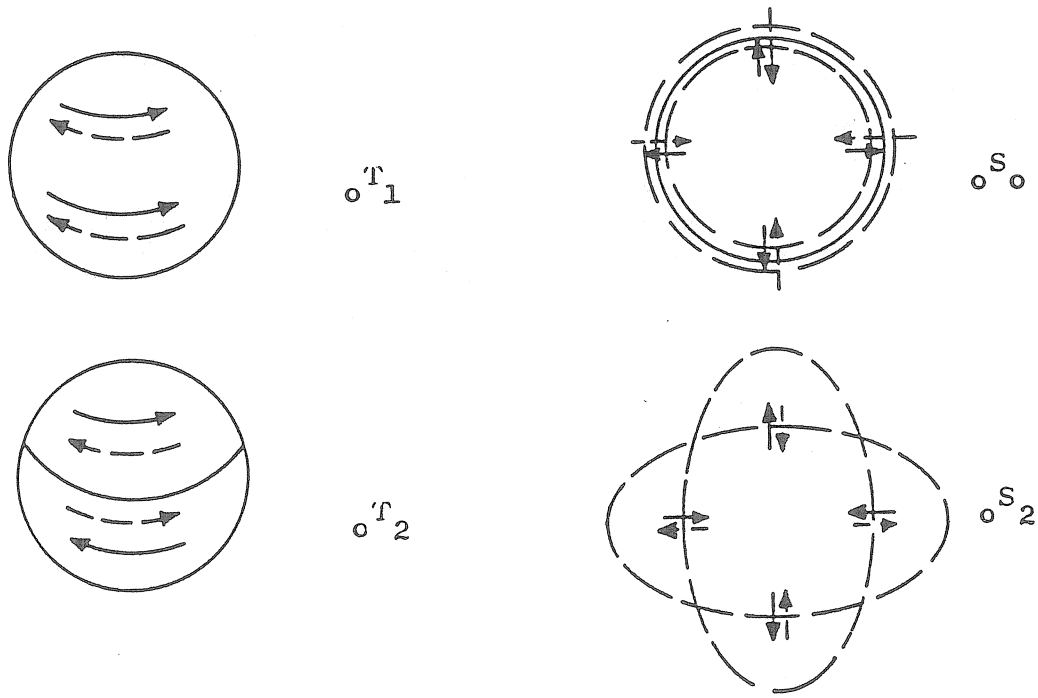

Figure 1.
The simplest normal modes

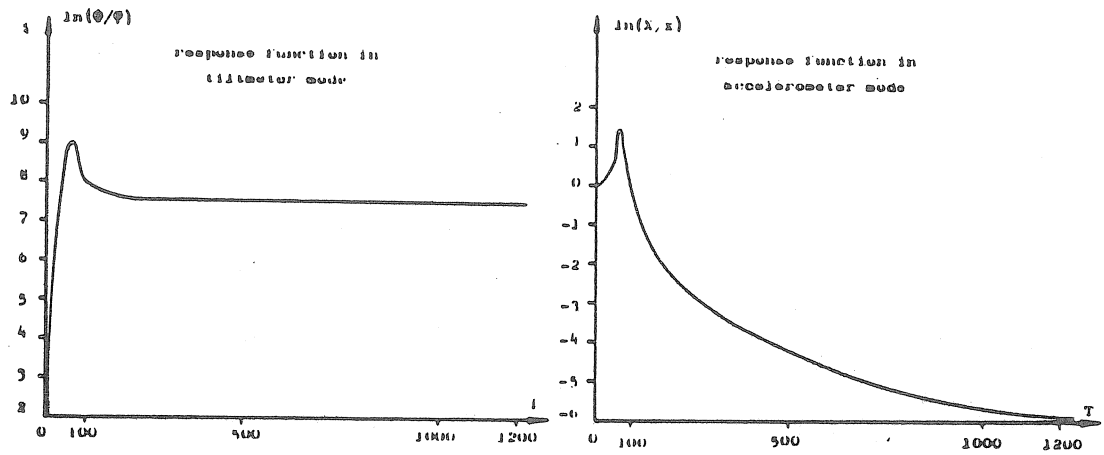

Figure 2.
Responses of the horizontal pendulum

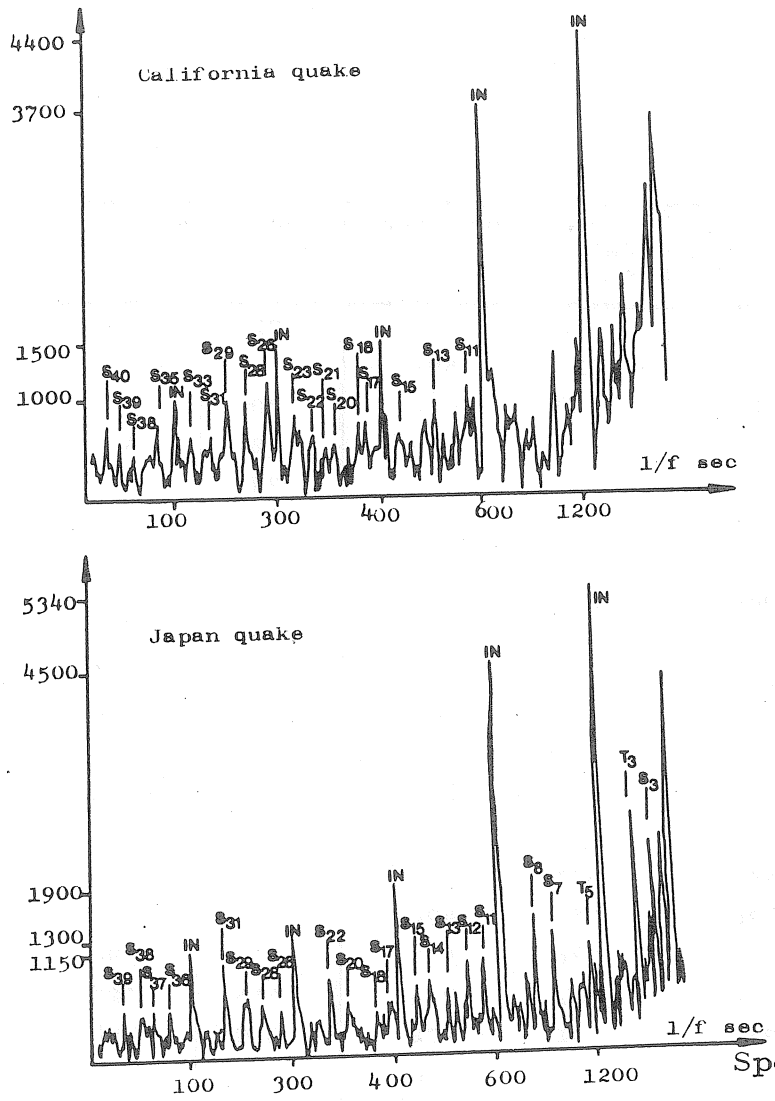

Figure 3.
Spectra of monitored quakes

Name	California	Japan
event	earth quake	earth quake
date	02.05.83.	26.05.83.
origin time GMT	$23^h42^m37.9^s$	$03^h00^m0.6^s$
epicenter	φ = 36.242 N λ = 120.301 W	φ = 40.370 N λ = 139.153 E
depht km	12 km	normal
magnitude M_B	6.2	6.8
M_S	6.5	7.7
distance	87.977^o	78.609^o
arrival time GMT	$23^h55^m29^s$	$03^h12^m00^s$
real motion	15.9	520.8
recording periods		
before event	08^h12^m Cal.1.	
after event	16^h32^m Cal.2.	11^h35^m Japan

Table 1.
The observed quakes

modes	period from Mendiguren, 1973 [sec]	period Cali-fornia	amplitude	period Japan [sec]	amplitude
S_{40}	212	212	721	212	570
S_{39}	216	217	592		
S_{38}	220	222	452	220	542
S_{37}	224			224	574
S_{36}	229			230	546
S_{35}	235	235	357		
IN overtone		240	989	240	1156
S_{33}	245	247	632		
S_{31}	256	257	616	257	1030
S_{29}	268	266	1003	269	669
S_{28}	275	278	951	278	598
S_{26}	290	292	1138	289	526
IN overtone		300	1500	300	1326
S_{23}	315	316	682		
S_{22}	325	327	609	327	841
S_{21}	336	336	494		
S_{20}	347	346	531	343	590
S_{18}	374	372	716	355	325
S_{17}	389	392	472	390	598
IN overtone		401	1516	401	1922
S_{15}	426	430	517	425	732
S_{14}	448			443	816
S_{13_x}	473	482	916	476	705
S_{12_x}	504			517	1013
S_{11}	537	553	1053	553	1040
IN overtone		599	3716	599	4452
IN normal mode		1189	4398		
$S_{8_x}^{x}$	707			721	1515
S_{7_x}	812			802	1318
T_{5}^{x}	1059			1049	1185
IN normal mode				1209	5337
$T_{3_x}^{x}$	1718			1784	2672
S_{3}^{x}	2133			2162	1520

[x] from Chilean and Alaskan earthquakes /in Int. Dictionary of Geophysics ed by Run corn/

Table 2.

The identified peaks of the spectra

PRELIMINARY INVESTIGATION ABOUT A QUALITY FACTOR OF TIDAL GRAVITY STATIONS

R. Chueca*, B. Ducarme**, P. Melchior**

* Université Polytechnique de Madrid

** Observatoire Royal de Belgique.

We have now the possibility to use the Tidal Gravity Data Bank constructed by B. Ducarme (1983) to make systematic investigations about the geographical distribution of residue vectors called $\vec{X}$ (see Melchior et al.).

It immediately appears that, with more than 200 stations, it is absolutely necessary to define in an impersonal way a "quality factor" for each series of measurements. As a preliminary search we have constructed two different quality factors as follows :

$$Q_1 = \frac{10\,R}{\sqrt{\varepsilon_1\ \varepsilon_2}}\ (1 + P)$$

$$Q_2 = \frac{R}{\sqrt{\varepsilon(O_1)\ .\ \varepsilon(M_2)}}$$

where :

R : station's efficiency (number of readings/24 x number of days)

* ε_1 : standard deviation in the diurnal band

* ε_2 : standard deviation in the semi-diurnal band

$\varepsilon(O_1)$: mean square error on O_1 wave observed amplitude

$\varepsilon(M_2)$: mean square error on M_2 wave observed amplitude

P : Weighing of the series i.e. : P = 0 in case of no separation of the diurnal group $P_1\ S_1\ K_1$; P = 1 in case of a successful separation of P_1 from K_1; P = 2 in case of a successful separation of ψ_1.

In doing this, our objective is to introduce to some extent the external errors and not only the internal errors given by the analysis.

As an example the station's efficiency R depends on the interruptions due to failures and also on the number of rejected data during computation.

---

* In case the standard deviations are not available, we use the following approximate relations

$$\varepsilon_1 = 4\ \varepsilon(O_1)\ \sqrt{n}$$

$$\varepsilon_2 = 4\ \varepsilon(M_2)\ \sqrt{n}$$

n : number of observations equations.

The weighing factor P reflects the perturbations in the diurnal band which mainly spoil the waves in the K_1 group.

In the least squares analysis the error on the parameters decreases as the square root of the number of observations. Q_2 is thus increasing according to this law but not Q_1 which increases stepwise with the length of the series (P can be equal to 1 only if the recording length exceeds 6 months and equal to 2 only if it exceeds 1 year). However, as most of the analysed records are comprised between six months and one year the two factors give similar results.

We systematically applied these two definitions to 455 series of data analysed at ICET, by the same Venedikov method. These data come from the 215 stations presently included in the bank.

This application was made according to the instrumental type and gave the following results.

Instrumental type	Number of series at Bruxelles	Number of series at Elsewhere	Q_1 Bruxelles	Q_1 Elsewhere	Q_2 Bruxelles	Q_2 Elsewhere
Askania 11, 12	4	33	1.1	0.9	3.3	3.2
Askania 15, BN	8	86	2.6	4.2	4.8	9.4
Geodynamics	25	90	4.0	6.2	8.7	10.2
LaCoste Romberg G, D	34	134	2.9	3.6	4.7	6.5
LaCoste Romberg ET	—	36	—	13.1	—	22.1
Superconducting	1	4	60.0	106.2	98.0	200.0

It must be noted that, for a large number of series, the Q factors are lower at Bruxelles because the instruments were submitted to experiences in view of improvements in that fundamental station which results in many interruptions. Also the Superconducting gravimeter is disturbed by the trafic on a nearby railway line and will be transferred elsewhere.

We provisionally conclude that the instruments can be roughly rated as follows :

Instrument	Series	Quality
Askania 11, 12	37	1
LCR mod. G/D	168	3
Askania 15 + BN	94	4
Geodynamics	115	6
LCR mod. ET	36	12
Superconducting	5	100

As defined, the quality factors Q_1 and Q_2 are inversely proportional to the standard deviations of the measurements in the diurnal and semi diurnal bands. The contributions to these standard deviations come from several error sources; some of them are directly proportional to the amplitude of the signal as the non linearity and the calibration errors. Others are characteristic of the type of instrument as the resolution, the noise level and the sensitivity to external perturbations (e.g. pressure and temperature). Finally the quality of the station itself will influence the quality of the results through the sensitivity of the instrument to the external sources of perturbations that will perturb either the instrumental stability (e.g. effects of tilt on the sensitivity of astaticized gravimeters) either the recorded tidal signal (e.g. diurnal perturbations).

The old Askania GS11 equipped with photoelectric recording is poorly thermostatized and exhibits an unstable calibration as well as a low signal to noise ratio.

The GS15 type and the BN transformed Askania instruments have a much better signal to noise ratio and a very stable calibration. However the thermostatisation is not improved.

The LaCoste & Romberg G and D meters (LCR) are well thermostatized but, being highly astaticized instruments, show large changes of sensitivity in perturbed stations. It is why sensitivity smoothing procedures improve so much the internal errors. These instruments also require the use of a rheological model to correct the instrumental phase lags.

As the GS15 and BN gravimeters were installed in the best conditions, at middle latitude stations, they benefit of sligthly better quality factors than the LCR meters engaged in tropical and equatorial zones of the Trans World Tidal Gravity Profiles.

The Geodynamics (GEO) instruments are very well thermostatized and less astatized than the LCR. The instrumental stability is better, even in difficult conditions.

The zero method instruments show higher standards. The Tidal LaCoste (ET) are generally better than the electrostatically fedback LCR (Harrison-Sato method). This is mainly due to the improved thermostatisation with a dubble thermostat system.

At high latitudes the amplitude of the tidal signal decreases very much and the contribution of the errors due to fluctuations of sensitivity becomes negligible compared with the instrumental noise level. It follows that

the quality factors of the astaticized gravity meters becomes higher in these areas.

The quality factors, as defined, could be correlated with the latitude or with the distance to the nearby sea and even with the economic development of the country (through the quality of the electric network). This is now under investigation; results will be presented at the Madrid Symposium.

x x x

We think that a responsibility of the working group is also to urge the people to send their data to ICET for comparative analysis, quality evaluation and inclusion in the data bank (when requested, such data can be kept "classified" for a time and not distributed without permission). The collection of data in World Data Centers is a principle of international cooperation set up at the time of the IGY.

We do think that isolate data about local tidal parameters are without real value if they are not intercompared with other stations on a regional or continental basis.

THE SUPERCONDUCTING GRAVIMETER OF THE ROYAL OBSERVATORY OF BELGIUM

B. Ducarme*, M. Van Ruymbeke**, C. Poitevin **

A superconducting gravimeter is operating at Brussels since the end of april 1982.

Except for a few days last due to a failure of a power supply there is no gap in the records.

As the instrument is not calibrated we had to normalize its data in order to get the accepted value for $\delta\ (O_1)$ in Brussels (Ducarme, 1975) i.e.

$$\delta\ (O_1) = 1.161$$

From a preliminary analysis (Ducarme, 1983) we concluded that the apparent sensitivity is

$$S = 0.2922\ \mu gal\ mm^{-1}$$

An important problem is to determine the transfer function of the barometric effects. As a first step, we determined a constant coefficient

$$C = -0.35\ \mu gal\ mbar^{-1}$$

by minimizing the standard deviation in the diurnal band.

Later on F. De Meyer applied its MISO method (1982) to our data and found that, in the time domain, the correction on the hourly readings can be represented by the expression :

$$C(t) = -0.2628\ p\ (t) - 0.0779\ p\ (t-1) - 0.0167\ p\ (t-2)$$

where c is expressed in µgal and p in mbar.

Correcting the raw observations by this algorithm we obtained the analysis results given in table 1. They are of course excellent and confirm the preliminary publication (Ducarme, 1983).

* Chercheur qualifié FNRS,
Observatoire Royal de Belgique.

** Centre de Géophysique Interne,
Observatoire Royal de Belgique.

However the standard deviations are higher than those obtained in Frankfurt with a similar instrument (Richter, 1985). This is obviously due to the high level of industrial noise at the site and especially to a railway line located at less than one kilometer from the Royal Observatory.

It is of course interesting to consider also the very long term behaviour of the instrument.

For that purpose we subtracted from the hourly readings a synthetic tide computed by using the observed (δ factors and phase differences in the diurnal, semidiurnal and terdiurnal bands and a theoretical δ value (1.16) for the long period waves.

A daily value of the drift was then obtained applying the Pertsev filter. The obtained curve is shown on figure 1. During the first six months the setting of the instrument produced an exponential drift followed by a very long period oscillation.

However no conclusion can be drawn so far as there is still a very important instrumental correction to apply.

Due to a slight helium leak inside of the gravimeter the heating power of the thermostat is continuously increasing. After six months operation the voltage reaches its maximum allowed value (10V) and it becomes necessary to extract the helium gaz from the inner container by means of a "getter". This getter is a ceramic cristal trapping the helium at very low temperature; it is introduced inside of the dewar and connected with the inner container through a vacuum line. In less than one hour the operation is completed and the voltage of the thermostat drops back to its minimum value (4V). This operation has to be done every six months and produces an instantaneous drift of the gravimeter by an amount of 3 μgal V^{-1}. We can assume that a similar drift occurs when the voltage of the thermostat slowly increases during the next six months.

This hypothesis is supported by the aspect of some parts of the drift as shown by the figure 2. One sees also that the voltage increase is irregular as it is modulated by the helium level in the dewar. When it drops below fifty per cent the increase stops and below forty per cent we can even see a decrease. This lag is recovered at the next helium filling.

As the 20 μgal decrease produced by the getter is removed directly from the observations by the smoothing of the data, we should observe , after the initial setting of the gravimeter, a more or less monotonous positive drift of the order of 0.1 μgal day^{-1}.

After correction of the influence of the voltage of the thermostat on the readings we fitted an exponential to the data to compute the installation

drift under the form

$$d = d_o e^{-t/T_o}$$

and obtained

$$d_o = 100 \text{ µgal}$$
$$T_o = 150 \text{ days}$$

The remaining drift appears in figure 3.

We then apply a last correction to take into account the changes of centrifugal force due to the latitude variation of the station and get the final drift behaviour depicted in figure 4.

One clearly sees an yearly variation of gravity with a total amplitude of 10 µgal.

REFERENCES

De Meyer, F., 1982. A multi Input-Single Output Model for Earth Tides data. Bull. Inf. Marées Terr., 88 : 5628-5675.

Ducarme, B., 1975. A fundamental station for Trans World Tidal Gravity Profiles. Phys. Earth and Planet. Interiors, 11 : 119-127.

Ducarme, B., 1983. Tidal Gravity parameters at Brussels reconfirmed by a superconducting gravimeter. Phys. Earth and Planet. Interiors, 32 : 1-3.

Richter, B., 1985. Three years of registration with the Superconducting Gravimeter. Bull. Inf. Marées Terrestres, 24 :

TABLE 1.

TRANS WORLD PROFILES BRUSSELS FUNDAMENTAL STATION

STATION 0201 BRUXELLES-UCCLE COMPOSANTE VERTICALE BELGIQUE
50 47 55 N 04 21 29 E H 101 M P 4M D 90KM 981 117 301
BASSIN EOCENE DE BRUXELLES SUR LE CAMBRIEN DU MASSIF DU BRABANT.
SABLES LUTETIENS.
OBSERVATOIRE ROYAL DE BELGIQUE DEPT.1 P.MELCHIOR
GRAVIMETRE A SUPRACONDUCTIVITE
ENREGISTREUP POTENTIOMETRIQUE
CORRECTION DE PRESSION -.26277*P(T)-.07785*P(T-1)-.01669*P(T-2)
CALIBRATION BRUXELLES - STATION FONDAMENTALE
INSTALLATION R.WARBURTON,M.VAN RUYMBEKE,B.DUCARME
MAINTENANCE B.DUCARME,M.VAN RUYMBEKE,R.LAURENT,F.RENDERS

LEAST SQUARE ANALYSIS / VENEDIKOV FILTERS ON 48 HOURS / PROGRAMMING B.DUCARME
POTENTIAL CARTWRIGHT-TAYLER-EDDEN / COMPLETE DEVELOPMENT
COMPUTING CENTER INTERNATIONAL CENTER FOR EARTH TIDES/FAGS/ BRUSSELS
COMPUTER SPERRY-UNIVAC 1100/81 PROCESSED ON 85/ 4/22

INERTIAL CORRECTION PROPORTIONAL TO THE SQUARE OF ANGULAR SPEEDS

G777 82 422/82 524 82 6 3/83 823

TIME INTERVAL 490.0 DAYS 11568 READINGS 2 BLOKS

WAVE GROUP ARGUMENT	N	WAVE	ESTIMATED AMPL.	R.M.S.	AMPL. FACTOR	R.M.S.	PHASE DIFF.	R.M.S.	RESIDUE AMPL.	RESIDUE PHASE
115.-11X.	11	SIGMQ1	.27	.01	1.2061	.0468	1.940	2.222	.01	41.8
124.-126.	10	ZQ1	.90	.01	1.1673	.0143	-1.862	.704	.03	-79.4
127.-129.	11	SIGMA1	1.07	.01	1.1521	.0126	-.922	.625	.02	-112.4
133.-136.	20	Q1	6.79	.01	1.1638	.0019	-.282	.094	.04	-53.3
137.-139.	10	RO1	1.27	.01	1.1464	.0102	-.353	.508	.02	-151.7
143.-145.	16	O1	35.35	.01	1.1610	.0004	-.092	.018	.07	-49.1
146.-149.	10	TAU1	.45	.01	1.1383	.0294	-.037	1.479	.01	-178.0
152.-155.	15	NO1	2.81	.02	1.1745	.0085	-.177	.414	.04	-12.9
156.-158.	7	KI1	.54	.01	1.1838	.0241	1.566	1.164	.02	52.5
161.-162.	3	PI1	.96	.01	1.1566	.0137	.179	.677	.00	69.7
163.-163.	7	P1	16.45	.01	1.1610	.0006	.085	.040	.11	13.2
164.-164.	3	S1	.46	.02	1.3761	.0481	-.712	2.031	.08	-4.3
165.-165.	11	K1	49.15	.01	1.1477	.0003	.156	.013	.45	17.2
166.-166.	2	PSI1	.41	.01	1.2123	.0337	4.532	1.593	.03	108.7
167.-168.	7	PHI1	.72	.01	1.1794	.0188	-.641	.912	.01	-69.2
172.-174.	8	TETA1	.52	.01	1.1442	.0249	-.124	1.246	.01	-171.9
175.-177.	14	J1	2.79	.01	1.1643	.0041	.311	.202	.02	64.7
181.-183.	7	SO1	.46	.01	1.1627	.0284	-.198	1.399	.00	-63.4
184.-186.	11	OO1	1.52	.01	1.1598	.0098	-.704	.486	.02	-93.6
191.-195.	14	NU1	.29	.01	1.1378	.0451	1.706	2.269	.01	124.3
215.-22X.	19	EPS2	.25	.01	1.1486	.0241	2.243	1.200	.01	105.2
233.-236.	10	2N2	.88	.01	1.1543	.0074	1.978	.368	.03	99.3
237.-23X.	10	MU2	1.09	.01	1.1358	.0071	3.721	.340	.07	73.2
243.-245.	13	N2	6.76	.01	1.1763	.0010	2.644	.050	.32	74.6
246.-248.	11	NU2	1.28	.01	1.1734	.0058	2.929	.263	.07	78.9
252.-258.	26	M2	35.71	.01	1.1894	.0002	2.448	.010	1.75	60.9
262.-264.	5	LAMB2	.24	.01	1.0943	.0280	4.854	1.462	.03	127.0
265.-265.	9	L2	1.01	.01	1.1870	.0110	4.870	.529	.09	77.3
267.-272.	5	T2	.99	.01	1.2040	.0076	-.162	.361	.04	-4.0
273.-273.	4	S2	16.61	.01	1.2038	.0004	.861	.021	.66	22.6
274.-277.	12	K2	4.57	.01	1.2025	.0016	1.086	.078	.18	28.4
282.-285.	15	ETA2	.25	.00	1.1864	.0230	-1.333	1.109	.01	-46.7
292.-295.	11	2K2	.07	.01	1.2084	.1248	-2.423	5.895	.00	-47.2
335.-347.	5	MO3	.11	.00	1.1016	.0341	1.000	1.762	.00	29.4
353.-375.	11	M3	.39	.00	1.0510	.0095	.250	.515	.01	164.3

STANDARD DEVIATION D .76 SD .42 TD .23 MICROGAL
O1/K1 1.0115 1-O1/1-K1 1.0894 M2/O1 1.0246

LONG PERIOD WAVES

0 62-077.55 MF	5.88	.08	1.1441	.0162	- .434	.831	.09	28.4

STANDARD DEVIATION LP 5.69

FIGURE 1: Daily drift (microgal)

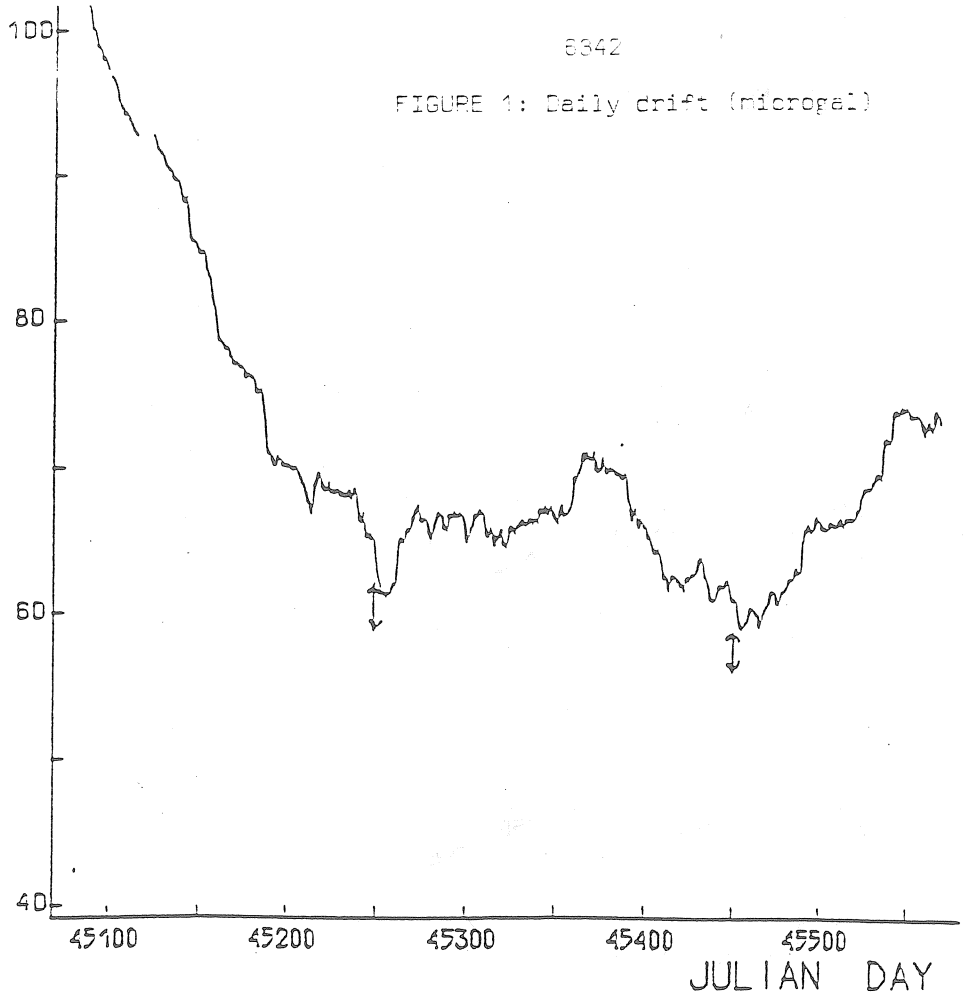

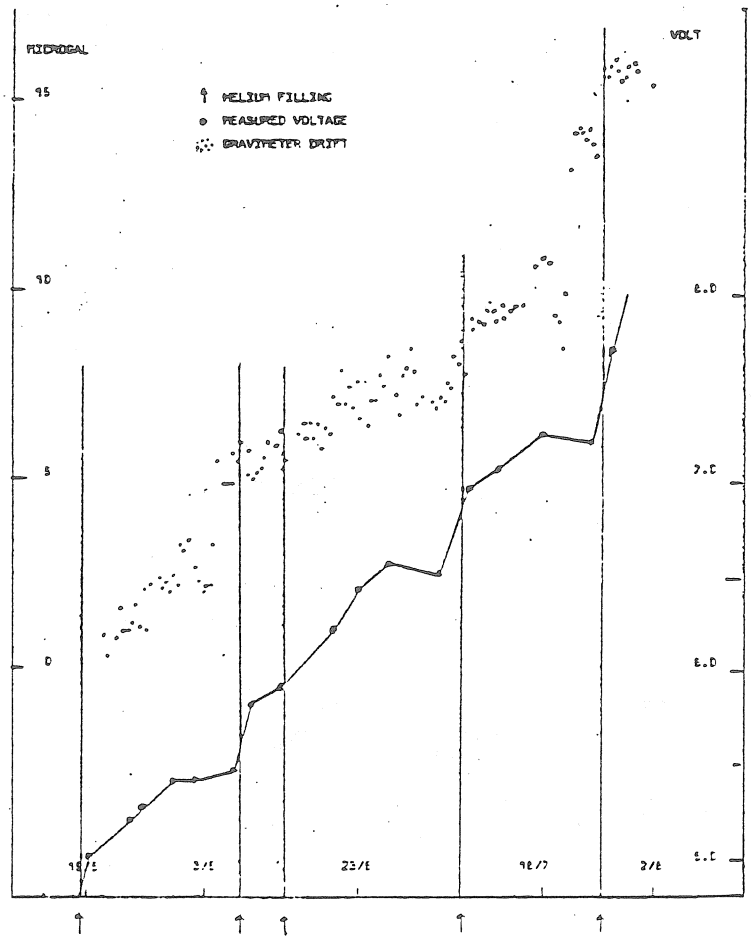

FIGURE 2: Relation between Thermostat voltage and drift. The actual drift rate of 0.04 V day^{-1} corresponds to 3.5 µgal V^{-1}.

FIGURE 3: Corrected drift (microgal)

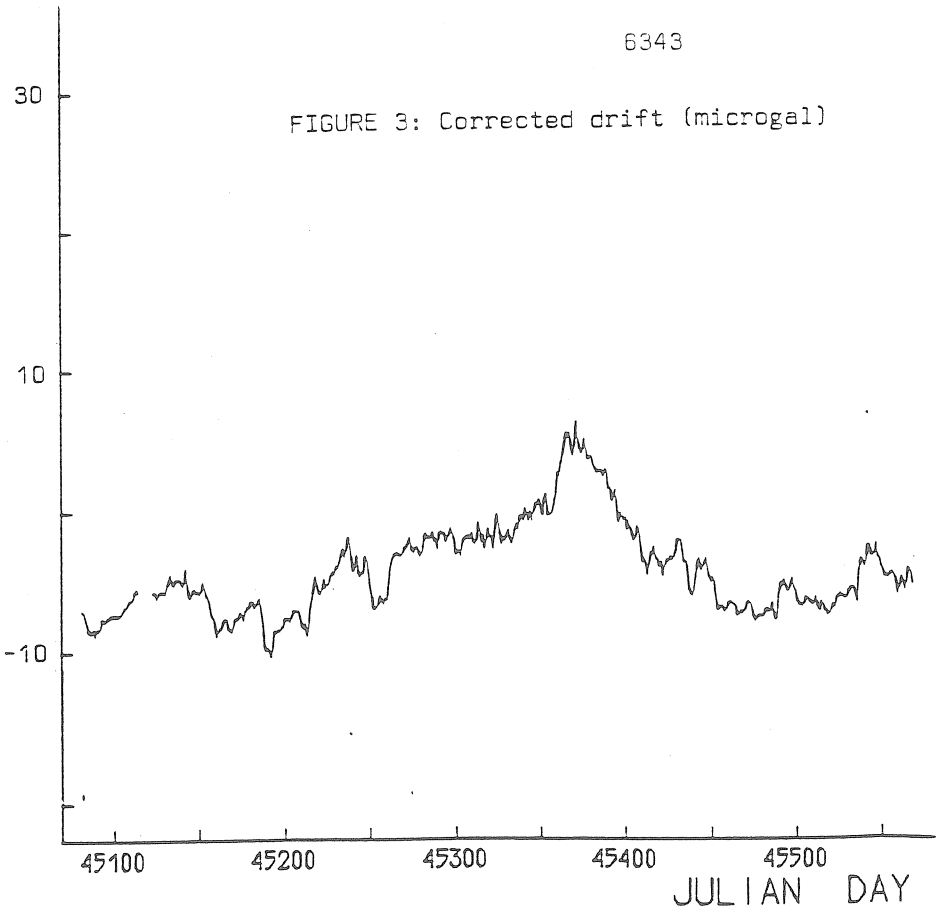

EPOQUE INITIALE 82 4 22

FIGURE 4: Residual drift after subtraction
of the variations of the centrifugal force.

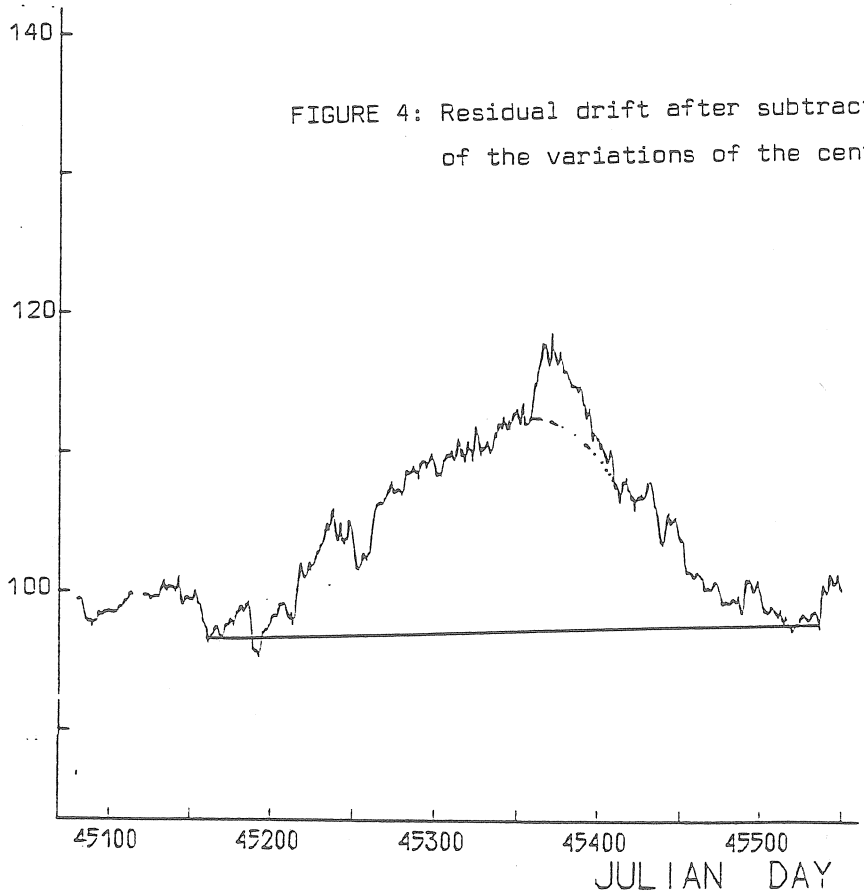

EPOQUE INITIALE 82 4 21

THREE YEARS OF REGISTRATION WITH THE SUPERCONDUCTING GRAVIMETER

Bernd Richter
Mitteilung aus dem Institut für Angewandte Geodäsie
Richard-Strauss-Allee 11
D-6000 Frankfurt 70

1. INTRODUCTION

The GWR-Superconducting gravimeter TT 40 no. 217 has been registering continuously at the observation station of the Institut fuer Angewandte Geodaesie (IfAG) at the castle in Bad Homburg near Frankfurt (φ = 50.2285, λ = 8.6113, h = 190m) from may 1981 till may 1984.

Then the instrument has to warm up due to an icing problem in the dewar, so that up to now no continuously registration is possible.

In principle, the mechanical spring of the usual gravimeter is replaced in the Superconducting system by a magnetic field, generated by the persitent current flowing in two superconducting coils, which floats a spherical mass. The position of the sphere between the coils is measured by a capacitance bridge. To avoid nonlinearities the position is held fixed by a magnetic feedback system /GWR manual 1981/.

An additional cooling compressor system reduces the gas flow rate of the 210 l Dewar, so that the whole system can operate for more than one year without interruption to supply liquid helium /Richter 1982/.

Since the beginning of the registration three years of hourly data have been collected /Richter 1983/.

The observation from the first three month have been neglected on account of irregular drift behaviour resulting from subsidence of the pier and instrument.

2. CALIBRATION

The calibration factor of the company was improved by the parallel registration with two modified LCR-gravimeters /Brein 1965/. The LCR-gravimeters were calibrated 1973 by field measurements on the European Calibrationline.

The comparison of the results of the analysis of these three instruments show no systematic effect in the amplitude- or phase relation.

Beginning in december 1983 there was another half-year parallel-registration with the well calibrated ET-15 gravimeter of the Institute of Oceanographic Sciences, Bidston. The preliminary results in tab. 1 show a small phase-lag, which coincide with the results determined in Brussels.

wave	δ S.C.	δ E.T.15	$\Delta\delta$	$\varkappa$ S.C.	$\varkappa$ E.T.15	$\Delta\varkappa$
Q1	1.140 5	1.134 7	-6	-0.31 25	0.42 37	0.73
O1	1.143 1	1.145 1	2	-0.08 5	0.02 6	0.10
M1	1.145 18	1.147 14	2	0.85 85	-0.79 73	-1.64
K1	1.133 1	1.135 1	2	0.14 3	0.37 6	0.23
N2	1.170 2	1.163 2	-7	2.01 11	3.04 11	1.03
M2	1.184 1	1.188 1	4	1.65 2	1.99 2	0.34
S2	1.188 1	1.192 1	3	0.55 5	0.81 4	0.26
M3	1.056 23	1.076 28	20	-0.72 1.38	-0.82 91	0.10

tab. 1 results of the analysis of a half year parallel registration (S.C. - E.T.15)

The error bounds of the S.C.-gravimeter are in the same range like the errors of the ET-15 gravimeter, because the data are used without any filterprocedure or driftelimination.

To get a rough information of the timedependance of the calibration factor the three years data set is subdivided in three parts and analysed. The results are compared with the global analysis in tab. 2.

period wave	1.8.81-1.5.82 δ	1.8.81-1.5.82 ϰ	2.5.82-1.5.83 δ	2.5.82-1.5.83 ϰ	2.5.83-1.5.84 δ	2.5.83-1.5.84 ϰ	1.8.81-1.5.84 δ	1.8.81-1.5.84 ϰ
O1	1.1450 5	-0.07 3	1.1450 8	-0.08 4	1.1449 4	-0.06 2	1.1453 5	-0.08 3
P1	1.1459 10	0.10 7	1.1445 26	0.05 13	1.1470 15	0.05 8	1.1467 15	0.03 8
K1	1.1329 5	0.12 2	1.1333 9	0.10 4	1.1330 7	0.10 3	1.1328 6	0.09 3
M2	1.1833 2	1.64 1	1.1836 6	1.65 3	1.1837 4	1.65 2	1.1835 4	1.66 2
S2	1.1861 7	0.24 3	1.1855 12	0.25 6	1.1854 9	0.12 4	1.1856 8	0.24 4
M3	1.0640 120	0.18 0.66	1.0550 300	-0.12 1.62	1.0720 230	0.25 0.92	1.0610 200	-0.09 0.87

tab. 2 comparison of annual analysis with the global analysis

In table 2 no significant chance in the calibration factor can be observed. A more detailed investigation to detected short variations in the calibration factor will follow.

3. LONGPERIOD GRAVITY VARIATION

For the investigation in the long period range the short period tidal waves (diurnal and higher) were subtracted and the drift of the instrument (fig. 1) in the range of 50 µgal/3 years is cancelled out by a polynomial fit. Till now there is no suitable explination for this drift behavior.

The change of the rotational axis of the earth (polar motion) introduces a variation of the centralfugal force, which is direct seen in the gravity signal (fig. 2). To reduce the data the theoretical influence of polar motion is calculated with the polar coordinates published by the U.S. naval observatory and taken into account.

After these two reductions the longperiod tidal waves are analysed by a harmonic least square procedure /Schüller 1976/.

The MF and MM waves are corrected by the indirect effect of the ocean loading.

wave	theo.tide (Wahr model)	estim. parameter δ	estim. parameter $\varkappa$	corr. parameter (ocean loading)	
SA	0.424	4.060 250	-67.4 1.8		
SSA	2.668	1.095 40	- 1.3 2.3		
MM	3.029	1.125 40	0.2 1.9	1.166	-0.4
MF	5.735	1.148 20	0.2 1.0	1.176	-0.5

tab. 3 δ- and x-factors of some longperiod waves

After subtracting the quadratic drift term, the influence of the polar motion and the tidal model from the registered data the residuals are in the range of +/- 2 µgal. The power spectrum of these residuals is demonstrated in figure 3.

4. CONCLUSIONS

The analysis of the three years uninterrupted registration with the S.C. gravimeter demonstrated the high quality and stability of the instrument. Besides the investigations in the short period range the data offers the possibility for studies in the longperiod part of the tidal spectrum as well as the influence of the polar motion. To use the full information of the instrument an absolute calibration with high accuracy is necessary.

5. REFERENCES

Brein, R.: Ergebnisse der Schwereregistrierung mit Verwendung einer elektrischen Feder (1962-1964). Dt. Geod. Komm., R. B, Heft 116 (Mitt. Inst. f. Angew. Geodäsie Nr. 74), Frankfurt 1965.

GWR-manual: Technical description GWR-company, San Diego 1981.

Richter, B., Brein, R., Reinhart, E., Wolf, P.: First results with Superconducting registration at the earth tide station Bad Homburg. Proceedings of the General meeting of the IAG, Tokio 1982.

Richter, B.: The long-period tides in the tidal spectrum. Proceedings of the XVIII General Assembly of the IAG, Hamburg 1983.

Schüller, K.: Ein Beitrag zur Auswertung von Erdgezeitenbeobachtungen. Dt. Geod. Komm., R. C, Heft 227, München 1976.

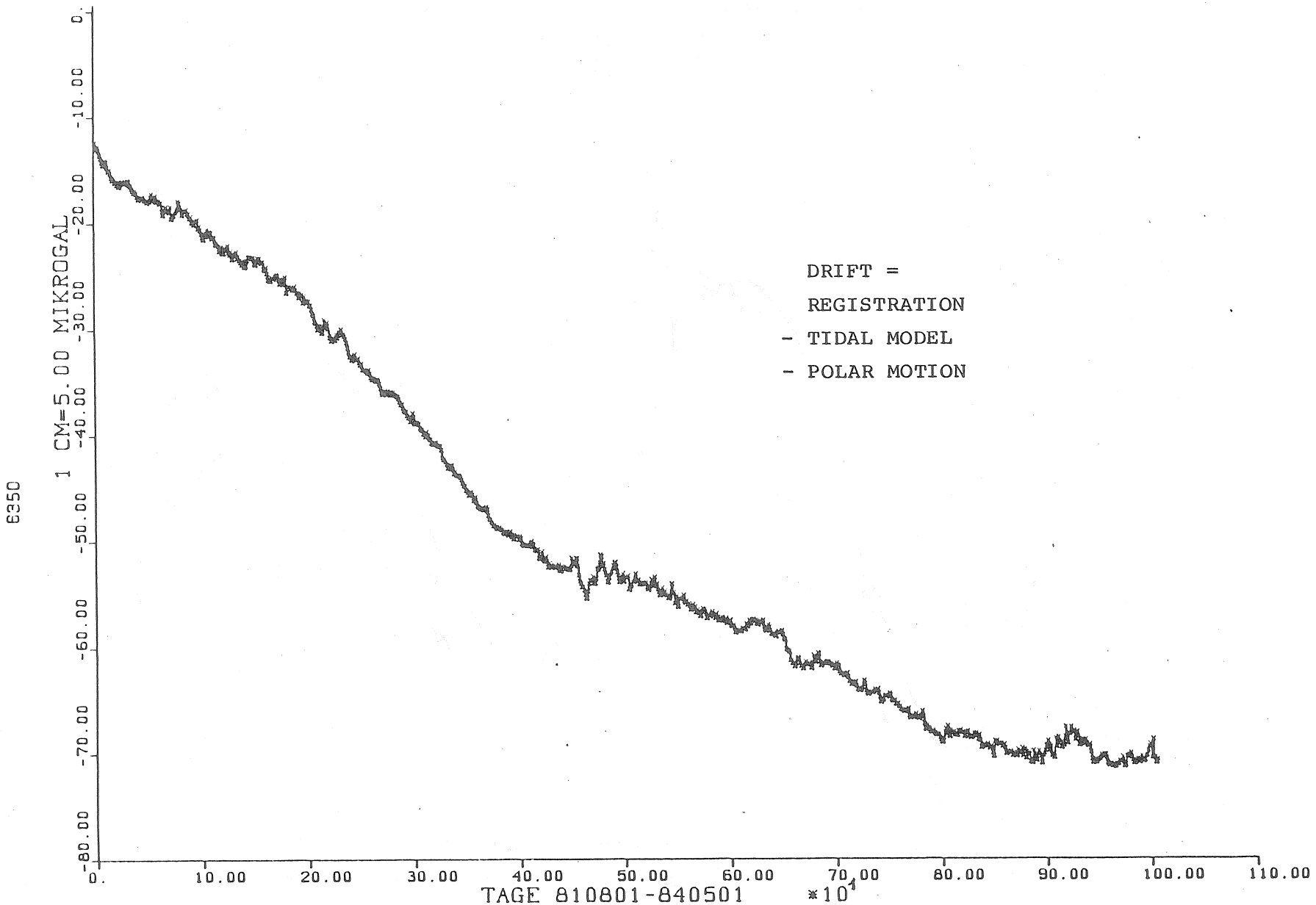

Fig. 1 Drift of the S.C. gravimeter over three years

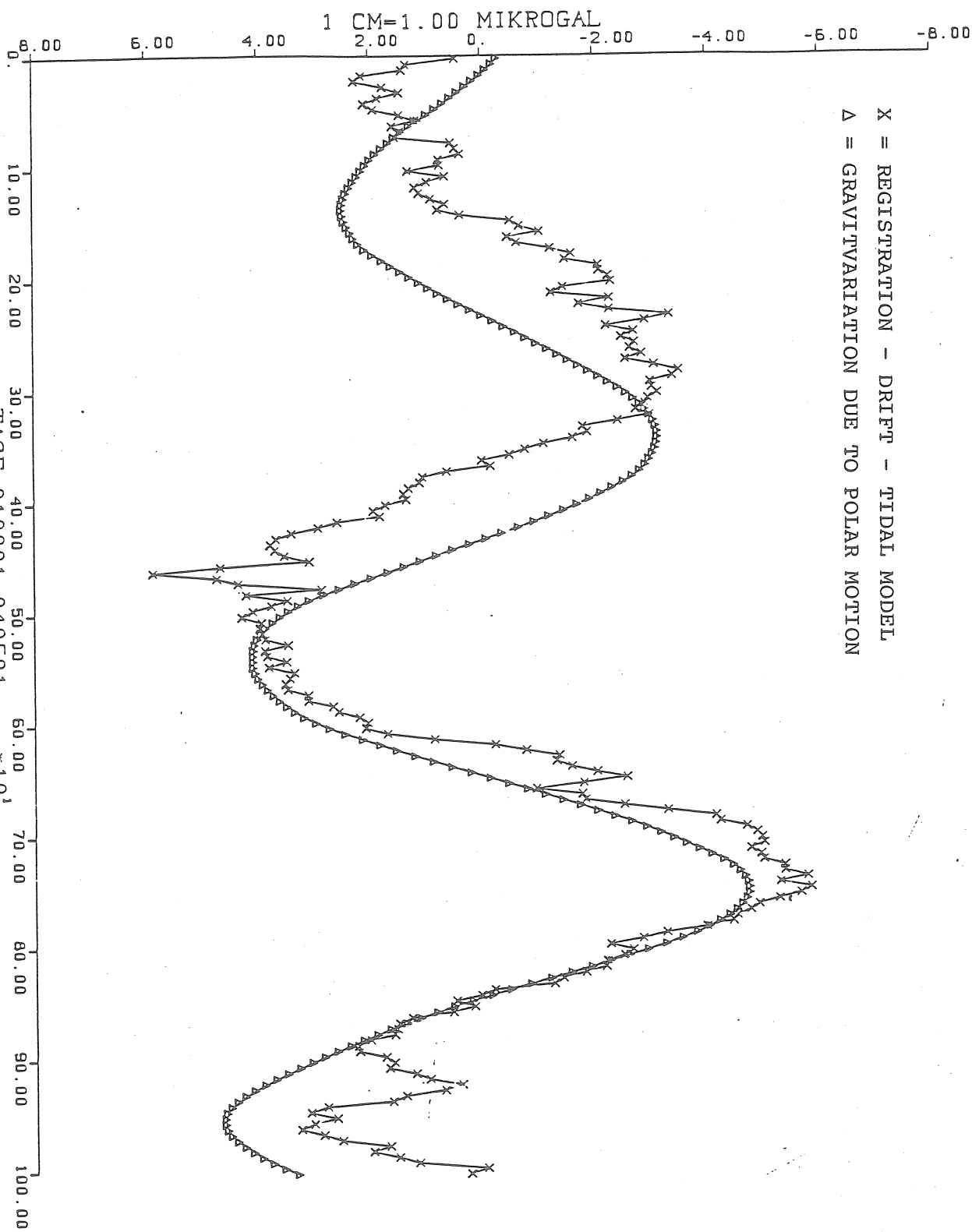

Fig. 2 INFLUENCE of the polar motion

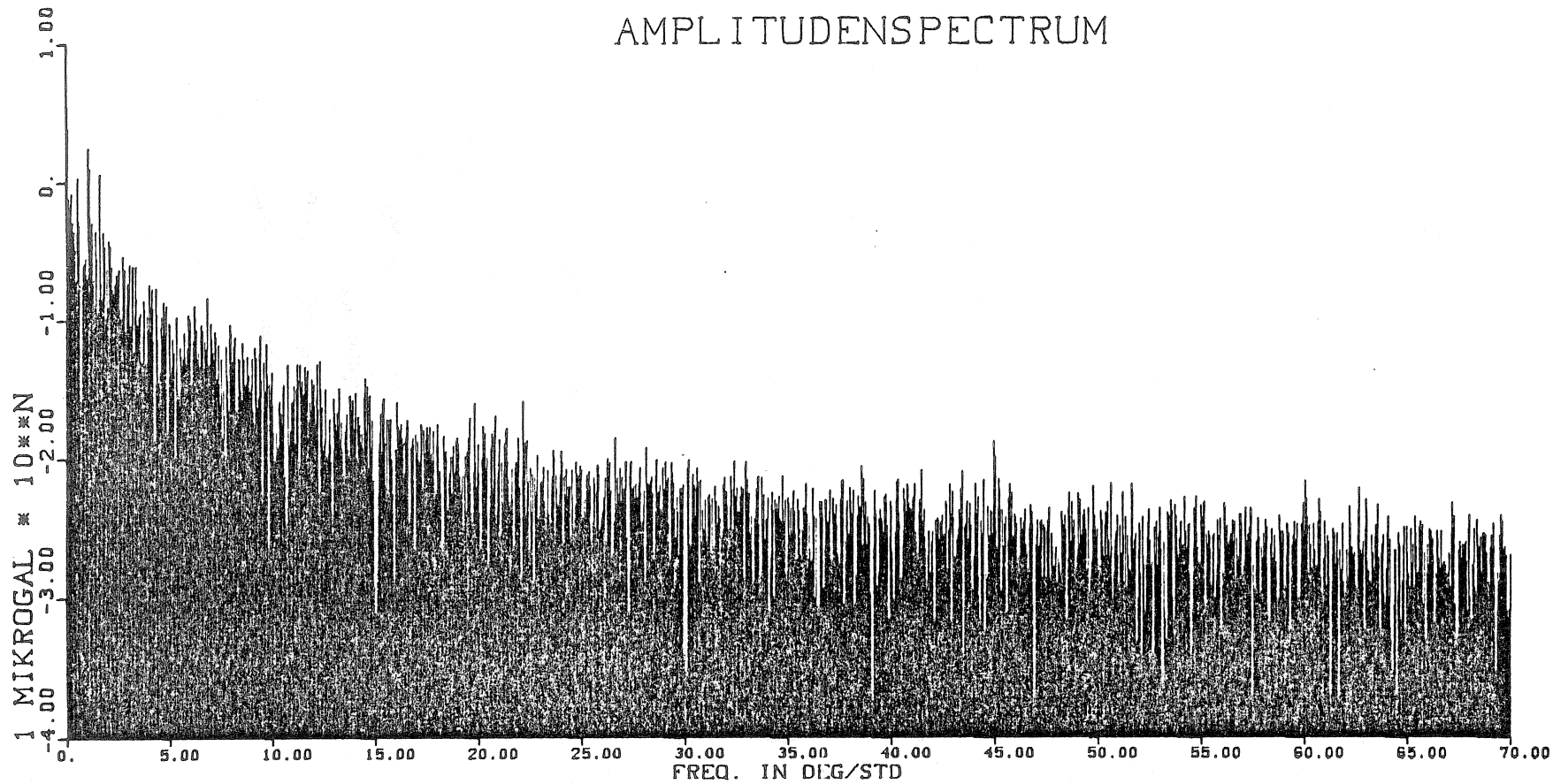

Fig. 3 SPECTRUM OF THE RESIDUALS

The Determination of Earth Tidal Parameters Through Geometric Levelling

by

Ole Remmer

Geodetic Institute
Copenhagen
1984

1. Introduction

The fact that the plumb line deviates from some zero-position has, within precise levelling, been recognized some forty years (see [2]).

And since all levelling instruments measure with respect to this plumb line this has given rise to Jensen's well-known formulae which are normally called Astronomical Correction but which more correctly should be called (earth-) tidal correction, tc , to levelling.

There is however, (as with every other correction) a fundamental ambiguity in applying the tidal correction in levelling. Let the tidal correction be called tc, then tc will equal some sum of theoretical tidal constituents:

$$tc = \sum_{i=1}^{h} R_i \cos \Phi_{it} \qquad (1)$$

where R_i and Φ_{it} are the amplitude and phases of the theoretical earth tide (i.e. some model tide).

In Jensen's application then this correction was applied so to say on "the left-hand side" of the observation equation of precise levelling:

$$z - tc + v = x_i - x_{i-1} + (\Sigma s^2 \Delta z)\eta \qquad (2)$$

Here η is a parameter which determines the refraction ($\Sigma s^2 \Delta z$ is a known coefficient, see [6] and [7] for details), while x_i and x_{i-1} are the height of the points P_i and P_{i-1} in some suitable vertical system while z is the measured height difference between P_i and P_{i-1} and v the residual. In (2) we suppose as already said that we know (or can compute accurately enough) tc (and $\Sigma s^2 \Delta z$ but that is another story), while x_i, x_{i-1} and η are parameters which are determined by a Least Squares Adjustment.

The fact that some of our colleagues actually measure tc (or other functions of earth tide) has of course made those of us working with levelling aware that model computations were just not good enough.

As Melchior [3] has already suggested some years ago this problem could be (in principle) solved by having a tilt-meter accompanying the levelling instrument throughout the levelling campagne.

Although one must agree with Melchior's suggestion there are certain formidable practical difficulties (there simply does not exist as far as the author is informed,

a tiltmeter which can be moved every 5 minutes or less and measuring in between).

Therefore we shall suggest another solution which may be formulated the following way: Let the levelling observations themselves monitor the earth tides.

This we may also say even simpler namely: move tc in (2) from the left hand-side to the right-hand side!

2. The New Observation Equation in Geometric Levelling when Earth Tides are taken into Account.

In geometric levelling we usually measure the same height-difference twice, one forward and one reverse, that is we have between two benchmarks P_i and P_{i-1} two height-differences:

z_{i_f} observed at time t_f

z_{i_r} observed at time t_r

For each of these we can write down (2) (with tc moved to the right-hand side of the equation):

$$z_{i_f} + v_f = x_i - x_{i-1} + (\Sigma s^2 \Delta z)\eta + tc_{t_f} \tag{3}$$

$$z_{i_r} + v_r = x_i - x_{i-1} + (\Sigma s^2 \Delta z)\eta + tc_{t_r} \tag{4}$$

Subtracting (4) from (3) we get

$$\Delta z_i + v_i = tc_{t_f} - tc_{t_r} \tag{5}$$

And calling $\Delta tc = tc_{t_f} - tc_{t_r}$

we get from (5):

$$\Delta z_i + v_i = \Delta tc \tag{6}$$

Now we don't write Δtc according to (1), when we perform measurements to monitor earth tides.

Instead we write (inspired by Chojnicki [1]).

$$\Delta tc = \sum_{i=1}^{h} R_i \gamma_i \cos(\Phi_{it} + \Delta\varphi_i) \tag{7}$$

so that (6) becomes

$$\boxed{\Delta z_i + v_i = \sum_{i=1}^{h} R_i \gamma_i \cos(\varphi_{it} + \Delta\varphi_i)} \tag{8}$$

(8) is then our new observation equation for determining earth tidal parameters through geometric levelling.

In (8) R_i and Φ_{it} are still the theoretical values of amplitude and phase while γ_i is the amplitude coefficient and $\Delta\varphi_i$ is the phase shift both being in principle different for each tidal constituent.

Through (8) we can by a Least Squares Adjustment find

$$\Delta\varphi_1, \Delta\varphi_2, \ldots\ldots\ldots \Delta\varphi_h \quad \text{and} \quad \gamma_1, \ldots\ldots\ldots\ldots \gamma_h .$$

This is of course in reality only possible if

$$\sum_{i=1}^{h} R_i \gamma_i \cos(\varphi_{it} + \Delta\varphi_i)$$

regarded as signal can be seen through the noise of our levelling observations Δz_i.

We shall discuss this problem in our next section.

3. Signal to Noise Considerations when Monitoring Earth Tides with Geometric Levelling

In Melchior's first book [3] on earth tides (p. 291) he mentions that the deviations of the vertical have an amplitude of 0".04. From the context it seems really

that it is the distance from "top to bottom" on the registration paper, so that the amplitude of the vertical deviations may be put to

$$\sim 0''.02$$

This is then the signal which we shall try to convert into a linear displacement of the levelled height difference over the distance of 1 km. In radians 0".02 is of course

$$\frac{0.02}{3600} \cdot \frac{\pi}{180} \text{ radians}$$

For a distance of 1 km this corresponds to a vertical displacement of

$$\frac{0.02}{3600} \frac{\pi}{180} 10^3 \text{ m}$$

And in mm we find that the vertical displacement is

$$s = \frac{0.02}{3600} \frac{\pi}{180} 10^3 \, 10^3 \text{ mm} = 0.1 \text{ mm/km}$$

This is then our signal.

Let us now look on the noise in our height-difference-difference Δz_i. In a good precise levelling the standard error of the height-difference-difference will be (see [5])

$$\sigma\{\Delta z_i\} = \sigma\{z_{i_f} - z_{i_r}\} = 0.6 \text{ mm}/\sqrt{\text{km}}$$

For a levelling line of L km's length we have correspondingly that the signal is

$$s(L) = L \times 0.1 \text{ mm}$$

while the standard error is

$$\sigma(L) = \sqrt{L} \times 0.6 \text{ mm}$$

In order to have conventional significance we must have $s(L) > 1.96\, \sigma(L)$ i.e.

$L \times 0.1 > 1.96 \times \sqrt{L} \times 0.6$ or

$\sqrt{L} > \frac{1.96 \times 0.6}{0.1}$ that is

$\sqrt{L} > 11.76$ and finally

$L > 138.3$ km

That is for a levelling network which comprises more than 140 km double-measured levelling we should be able to compute tidal parameters from the levelling observations themselves.

However, after 140 km we are just able to "see" the total tidal signal. Let us now try to find out how large a levelling network we need in order to see the five principal waves K_1, O_1, N_2, M_2, and S_2:

We have (Melchior [3] p. 76-77) that the amplitudes for these five waves in Western Europe (assumed to be lying between latitude 40^o and 70^o) are:

East-West		Mean	× 0.7
K_1	0".005-0".008	0".0065	0".0046
O_1	0".0035-0".005	0".0047	0".00329
N_2	0".002-0".001	0".0015	0".00105
M_2	0".012-0".005	0".0085	0".0060
S_2	0".005-0".0025	0".0038	0".00266
North-South			
K_1	-0".004-0".005	0".00225	0".0016
O_1	-0".002-0".004	0".0015	0".0010
N_2	0".001-0".001	0".001	0".0007
M_2	0".007-0".005	0".006	0".0042
S_2	0".003-0".002	0".0025	0".00175

And supposing (which is completely realistic) that the levelling lines are evenly distributed in Azimuth we may as amplitude for a levelling line take the mean of the amplitudes of the East-West and North-South components respectively, giving the following mean amplitudes for our principal waves which we then convert into mm/km according to our prior deliberations:

$$K_1 \quad 0''.0031 \sim \frac{0.031}{0.02} \times 0.1 = 0.0155 \text{ mm/km}$$

$$O_1 \quad 0''.0021 \sim \frac{0.0021}{0.02} \times 0.1 = 0.0105 \text{ mm/km}$$

$$N_2 \quad 0''.0009 \sim \frac{0.0009}{0.02} \times 0.1 = 0.0045 \text{ mm/km}$$

$$M_2 \quad 0''.0051 \sim \frac{0.0051}{0.02} \times 0.1 = 0.0255 \text{ mm/km}$$

$$S_2 \quad 0''.0022 \sim \frac{0.0022}{0.02} \times 0.1 = 0.0110 \text{ mm/km}$$

We now make for each wave in decreasing order of magnitude the same computation as we did before for the total tidal signal. That is we ask when the signal of this particular wave rises above the noise of our levelling observations.

We find

M_2:

$$L \times 0.0255 > 1.96\sqrt{L} \times 0.6$$

$$\sqrt{L} > 46$$

$$L > 2116 \text{ km}$$

i.e. after roughly 2000 km's precise levelling we should be able to see the largest wave M_2.

K_1:

$$L \times 0.0155 > 1.96\sqrt{L} \times 0.6$$

$$\sqrt{L} > 76$$

$$L > 5776 \text{ km}$$

i.e. after roughly 6000 km's precise levelling we should be able to see the wave K_1.

O_1 and S_2:

$$L \times 0.0105 > 1.96\sqrt{L} \times 0.6$$

$$\sqrt{L} > 112$$

$$L > 12544$$

i.e. after roughly 12500 km's precise levelling we should be able to see O_1 and S_2.

N_2:

$$L \times 0.0045 > 1.96 \times \sqrt{L} \times 0.6$$

$$\sqrt{L} > 261$$

$$L > 68121 \text{ km}$$

i.e. after roughly 68000 km's precise levelling we should be able to see the wave N_2.

Looking on the last number of 68000 km by which we should be able to discriminate the five principal tidal waves K_1, O_1, N_2, M_2, S_2, we observe that the so-called United European Levelling Network (The U.E.L.N.) which covers Western Europe, is 77.000 km's! We should in other words be able to compute γ - and $\Delta\varphi$ - values for K_1, O_1, N_2, M_2, and S_2 and these tidal parameters will of course be really integrated over the whole of Western Europe and we should thus most emphatically get rid of "local" effects which otherwise plague tilt observations.

4. An Example from the Second Precise Levelling of Denmark.

As we have said above we can not for shorter distances of levelling network hope to see the different waves of the tidal signal but we should fairly soon be able to see the total tidal signal.

Putting in (8) $\Delta\varphi_1 = \Delta\varphi_2 = \ldots\ldots\ldots \Delta\varphi_n = 0$

and $\gamma_o = \gamma_1 \ldots\ldots\ldots = \gamma_n$ we may rewrite (8)

$$\Delta z_j + v_j = \gamma_o \sum^{h} R_i \cos \varphi_{it} \qquad (9)$$

And calling the model tidal signal Δtc_o we get:

$$\Delta tc_o = \sum^{h} R_i \cos \varphi_{it} \qquad (10)$$

Combining (9) and (10) we find

$$\Delta z_j + v_j = \gamma_o \, \Delta tc_o \qquad (11)$$

It is this equation (11) which has been used in a primitive regression analysis of 100 Danish height-difference-differences. As Δtc_o has been used Jensen's old so-called "astronomical" (i.e. real = tidal) corrections, not multiplied by 0.8.

The question that was asked was very simply: can we see the tidal signal in these few levelling observations? The result was somewhat surprising:

We found for increasing levelling distance L:

L km	γ_o dimensionless	$s\{\gamma_o\}$ dimensionless	degree of freedom	level of significance %
5	5.54	3.87	17	92
10	6.38	2.83	28	98
15	5.34	3.10	34	95
20	4.68	3.06	41	93
25	5.19	2.98	48	96
30	4.38	2.81	59	93
35	4.78	2.41	73	97
40	4.83	2.34	82	98
45	4.21	2.16	95	97
47	4.23	2.14	99	97

Table 1

The same figures are depicted in Fig. 1. The bars are 95% error bars.

We can see several things. First from L = 35 and onward we are beyond the conventional significance level (95%), but we also note that the tidal signal really is there already from the 5 km-level and this is of course surprising.

We also see that γ_o is much larger than 1! That means that we are in a situation with so-called indirect effects (see Melchior [3] pp. 189-201). We note that the final γ_o-value from our little analysis is

$$\gamma_o = 4.23$$

In Melchior [3] p. 196 is mentioned a $\gamma_o \sim 5$ so that we seem to have stumbled accidentally into a situation with very large indirect effects too in this small analysis.

It is interesting to compare our findings with those of Zschau [9].

Although no number is given for the size of the indirect effects in N-S direction ([9] p. 581), Zschau's remarks seem to indicate that he has found indirect effects in the North-South direction which are in the same order of magnitude as given by our γ_o above.

The interesting thing is that practically all the levelling observations in our little analysis above lie in the North-South direction very close to the east coast of Jutland going 47 km north from the city of Fredericia, i.e. they are lying in the same distance from both the North Sea and the Baltic as are Zschau's borehole tiltmeters. And we seem to be able to reproduce Zschau's effect in the N-S direction over a much longer distance (i.e. 47km).

To us this indicates that the reason for these large indirect effect in Denmark and Schleswig-Holstein in the N-S direction still represent an open question.

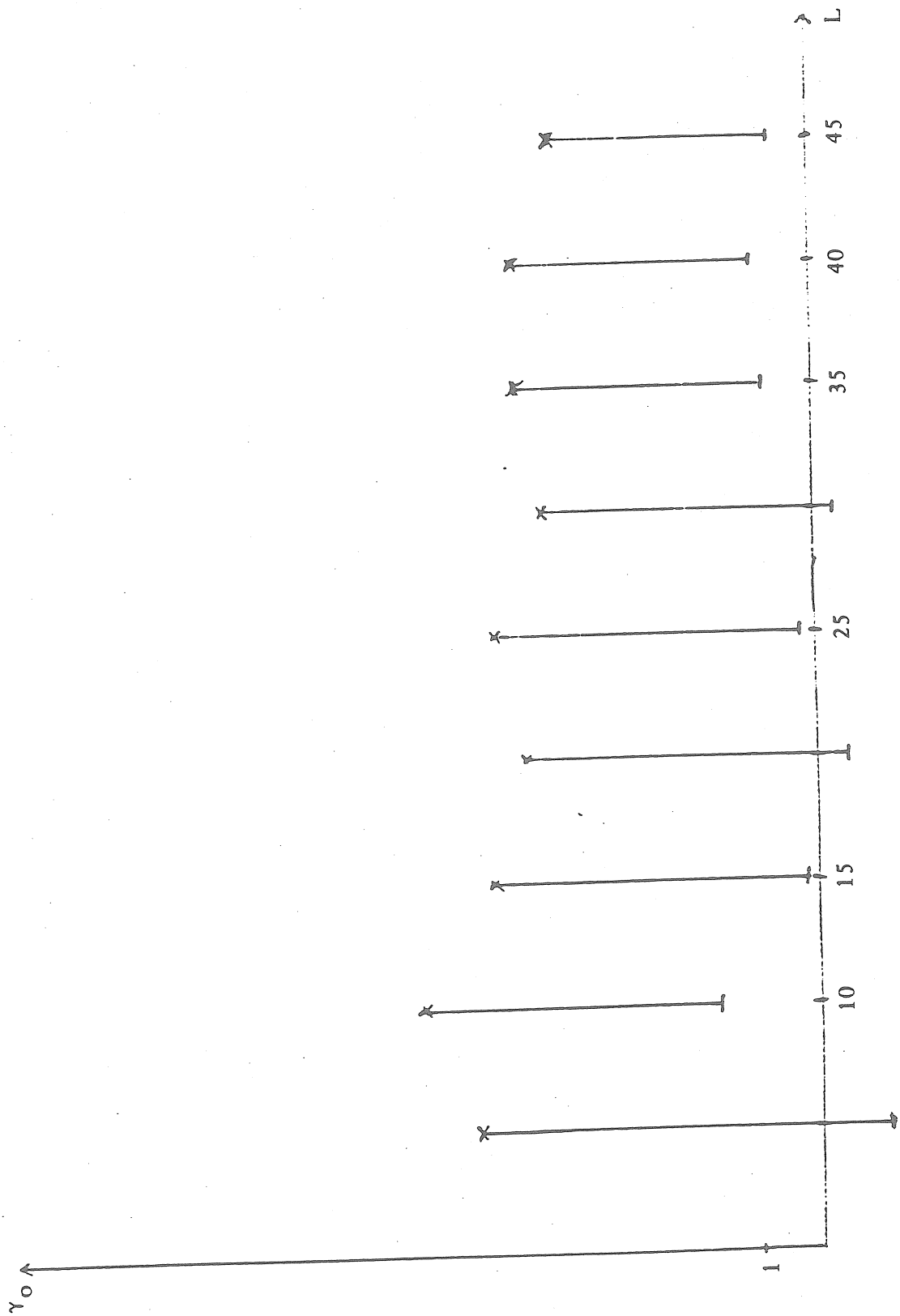
L
45
40
35
25
15
10
1
γ_o

Literature

[1] Chojnicki, T.: Ein Verfahren zur Erdgezeiten Analyse in Anlehnung an das Prinzip der kleinsten Quadrate Mitt. aus den Inst. f. Theor. Geod. Bonn 1973.

[2] Jensen, H.: Formulas for the Astronomical Correction to the Precise Levelling. Geod. Inst. Medd. No. 23, København 1949.

[3] Melchior, P.: The Earth Tides. Oxford 1966.

[4] Melchior, P.: The Tides of the Planet Earth. Oxford 1978.

[5] Remmer, O.: Levelling Errors in Statu Nascendi. Geod. Inst. Medd. No. 51. København 1975.

[6] Remmer, O.: The Direct Experimental Detection of the Systematic Refraction Error of Precise Levelling. Geod. Inst. Medd. No. 52. København 1977.

[7] Remmer, O.: Refraction in Levelling. Geod. Inst. Medd. No. 54. København 1980.

[8] Simonsen, O.: Report on the Astronomical Correction in The New Danish Precise Level Network. Bull. Geod. No. 18. 1950.

[9] Zschau, J.: Tidal Sea Local Tilt of the Crust, and its Application for the study of Crustal and Upper Mantle Structure. Geophys. J.R. Astr. Soc. (1976) pp. 577-593.

METHODS OF TIDAL LOADING COMPUTATION

T.F. Baker
Institute of Oceanographic Sciences
Bidston Observatory
Birkenhead, Merseyside L43 7RA, UK.

SUMMARY

A general review is given of the various methods that have been used for tidal loading computations. An expansion of the ocean tide distribution into surface spherical harmonics and then a summation with an appropriate combination of load Love numbers is useful when only the lowest degree terms are involved, as for example in calculating the tidal perturbations of artificial satellites or the loading response due to the oceans at distances greater than about 1500 km. For load calculations at any distance from the coast, methods have been developed which involve calculating the response of the Earth to loads that are uniform over a limited area or cell. These cells can be either polygons, templates or discs. These should all give equivalent results provided that care is taken in choosing the size of the cells, particularly for the nearest sea area where the Earth's response, the marine tide (and the coastal geometry) are all varying rapidly with distance. If a cell has dimensions of order 2α, then the load response of the Earth at distances greater than 10α from the cell becomes the same as the response due to an equivalent point mass load acting at the centre of the cell. Thus, if the cell size relative to the distance from the observation site is suitably chosen, then the computation reduces to the summation of the effects due to a set of point mass loads. The overall accuracy of a tidal loading computation is mainly determined by the uncertainties in the shelf and ocean tide models used (including that arising from the mass conservation problem).

INTRODUCTION

Since this is the first time that the Working Group has discussed algorithms for ocean tide loading computation, this paper is intended to give a general review of the various methods that have been used for tidal loading computation. The methods that are discussed are normally called :- (1) the spherical harmonic expansion method; (2) the polygon method; (3) the template (or sector) method; (4) the spherical disc (or cap) method; and (5) the point load or Green's function method. In methods (2) to (4) the oceans are divided into a grid of cells of the appropriate geometry and the ocean tide is assumed to be uniform over an individual cell or area. The response of the Earth due to a uniform load over a cell is calculated as a function of distance away from the cell. For any particular point on the Earth's surface, the total load

can then be found from a summation of the effects due to all the individual cells covering the oceans.

In method (5) the individual cells are replaced by point masses at the centre of each cell. The masses are calculated from the area of each cell, the height of the ocean tide in that cell and the density of sea water, ρ_w. The response of the Earth to a point mass load as a function of the distance away from the point load is called the loading Green's function. If the loading Green's function, $\hat{G}$, of the Earth is known, then the loading response $L(\underline{r})$ at an observation point on the Earth's surface with position vector $\underline{r}$ is given by a convolution integral of the form

$$L(\underline{r}) = \rho_w \iint_{\text{oceans}} \hat{G}(|\underline{r} - \underline{r}'|)\ \zeta(\underline{r}')\ dA \qquad (1)$$

where $\zeta(\underline{r}')$ is the height of the ocean tide over the surface area dA at position vector $\underline{r}'$. In method (5) the evaluation of the integral is reduced to a summation of the individual responses due to a set of point masses.

In equation (1), it can be seen that the assumption has been made that the response of the Earth depends only upon the distance between the point mass and the observation point. This is only true on a spherically symmetric layered Earth. At observation sites where lateral changes of structure are important, the finite element method must be used for loading calculations (Beaumont 1978, Asch & Jentzsch 1981). Fortunately, the effects of a lateral change of structure are only important up to distances of a few times the depth of the structural change, so that layered models are sufficient for most loading calculations.

1. THE SPHERICAL HARMONIC EXPANSION METHOD

The spatial distribution of the ocean tide for a particular tidal harmonic can be expanded in surface spherical harmonics

$$\zeta(\theta,\lambda) = \sum_n \zeta_n(\theta,\lambda)$$

$$\text{where } \zeta_n(\theta,\lambda) = \sum_{m=0}^{n} (a_{nm}\cos m\lambda + b_{nm}\sin m\lambda) P_n^m(\cos\theta) \qquad (2).$$

θ and λ are the co-latitude and east longitude. Since ζ is periodic, a_{nm} and b_{nm} are complex coefficients. The gravitational potential at a point (θ,λ) due to the nth degree surface spherical harmonic mass layer is given by

$$W_n'(r,\theta,\lambda) = \frac{4\pi G \rho_w a}{(2n+1)} \left(\frac{a}{r}\right)^{n+1} \zeta_n(\theta,\lambda) \qquad (3a)$$

outside the Earth

and $$W'_n(r,\theta,\lambda) = \frac{4\pi G \rho_w a}{(2n+1)} \left(\frac{r}{a}\right)^n \zeta_n(\theta,\lambda) \qquad (3b)$$

inside the Earth

G is Newton's Gravitational constant, a is the radius of the Earth and r is the distance from the centre of the Earth. Farrell (1972) solved the equations of motion for a spherical, layered, self gravitating, elastic Earth that is loaded by an nth degree surface mass layer. The surface displacements are given by the loading Love numbers h'_n and l'_n and the potential change by the loading Love number k'_n. Farrell evaluated these loading Love numbers up to degree n = 10,000. The tidal loading surface displacements, potential change, gravity, tilt and strain are all given by certain combinations of these three load Love numbers and W'_n or its derivatives.

Pertsev (1970) and Groten & Brennecke (1973) used spherical harmonic expansions of numerical ocean tide models up to degrees n = 32 and n = 35, respectively, together with load Love numbers to evaluate the tidal gravity loading at various tidal gravity stations. Pertsev (1970) showed that for stations greater than 1500 km from the ocean the spherical harmonic expansion method gave results that were very close to the results from the spherical disc method (section 4). The truncation at finite n leads to a remaining spurious tide even in the centre of a continent (Merriam 1980). This is particularly important for the evaluation of the Newtonian gravitational attraction term (Merriam 1980, Pekeris 1978) and Pertsev (1970) found that it was necessary to evaluate this attraction term directly using a numerical integration over the oceans.

For stations nearer to the coast than 1500 km a much higher degree spherical harmonic expansion is required and for this reason the various methods described in the following sections were developed. The spherical harmonic expansion method is most suitable when only the low degree terms are important as for example in calculating the effects of ocean tides on the orbits of artificial satellites using equation (3a). However, Fang, Hsu, Chen and Yang (1983) have developed a computational method which uses a convolution integral (equation 1) in the near region and the spherical harmonic expansion in the far region and which is particularly efficient in computer time.

2. THE POLYGON METHOD

This method was first developed by Bower (1970). The intersections of the co-amplitude and co-phase lines on a co-tidal map form a natural grid of polygons and triangles. Within each figure the tidal amplitude and phase is assumed to be constant and the spherical polygon is replaced by a plane polygon. Bower then

calculates the gravitational potential and the components of the gravitational attraction at the observation site due to each polygon. The Green's function is then integrated across each polygon using the first two terms of a Taylor series. The required accuracy is achieved by ensuring that the dimensions of the polygons are much less than their distance from the observation point. The method clearly has advantages when the ocean tide data is only available in map form. In addition, the digitization of the tidal map has to be done once only and it then can be used for any observation site. The method has been extensively used for loading calculations in N. America (e.g. Beaumont and Lambert 1972). Melchior, Moens and Ducarme (1980) also divide ocean tide maps into spherical polygons and triangles in their ocean loading computations.

3. THE TEMPLATE METHOD

In this method the observation site P is chosen as origin and the oceans are divided up into 'templates' using a polar grid i.e. azimuth lines radiating from P and circles centred on P (see figure 1). The ocean tide is assumed to be uniform within each template. The use of this polar grid leads to some simplification since the integration over azimuth for a single template is trivial and the problem reduces to the integration of the Green's function over distance. One disadvantage of the template method is that a new grid is required for each observation point, although this can be largely overcome by automatic generation of the grid. This method was used by Lambert (1970), Moens (1976) and Zschau (1976) for load calculations in E. Canada, Spitsbergen and N. Germany respectively. Lambert (1970) pointed out the importance of calculating the extra component of tidal gravity due to the vertical component of the Newtonian attraction of the nearby sea due to the height of the gravimeter above sea level. This can be several microgals for elevated sites near the coast and it is approximately proportional to the height above sea level and decreases approximately as the inverse cube of the distance from the load. Thus, it is important to include this height effect in all the various methods outlined in this paper.

In the above papers, the loading response of the Earth due to a template with a uniform mass load was found by numerically integrating a Green's function across the template. An alternative method of calculating the response due to a template is to use the load Love numbers directly in an infinite series (Goad 1980). In figure 1, let $\theta = 0$ be the observation point P and consider a template of width $\Delta\alpha'$ in azimuth and bounded by arcs at geocentric angles θ_1 and θ_2. The nth degree gravitational potential at P due to a uniform tide of height ζ covering the template is

$$W_n'(\theta_1, \theta_2, \Delta\alpha') = \frac{G \rho_w a^2 \zeta \Delta\alpha' a^n}{n(n+1)\, r^{n+1}} \left[\sin\theta_2 P_n^1(\cos\theta_2) - \sin\theta_1 P_n^1(\cos\theta_1) \right] \quad (4)$$

where $P_n^1(\cos\theta)$ is the associated Legendre polynomial of order 1. A summation over n using the appropriate combination of the load Love numbers h_n' and k_n' together with W_n' from equation (4) was used by Goad to obtain the tidal gravity loading due to a template. The Newtonian attraction was found directly by integrating over the template.

Beavan (1974) calculated the loading strain in Britain using templates. He found that if the size of the polar grid relative to the distance from the observation point is correctly chosen, then the computation can be reduced to a summation of the effects due to point masses at the centre of each template.

4. THE SPHERICAL DISC METHOD

Pertsev (1970, 1976) used the response of the Earth to a spherical disc (or cap) with a uniform mass load to calculate the gravity and tilt loading at various stations in Asia, Europe and N. America. In figure 1, a latitude and longitude cell is replaced by an equal area disc D in which the ocean tide has a uniform height ζ. The spherical disc subtends an angle of 2α at the centre of the Earth and the load response is required at an observation point P at a geocentric angle θ away from the centre of the disc. The nth degree gravitational potential at P due to the disc is

$$W_n'(\theta, \alpha) = \frac{4\pi G \rho_w a}{(2n+1)} \left(\frac{a}{r}\right)^{n+1} \frac{\zeta}{2} \left[P_{n-1}(\cos\alpha) - P_{n+1}(\cos\alpha) \right] P_n(\cos\theta) \quad (5)$$

$$\left[W_o' = 4\pi G \rho_w \frac{a^2}{r} \frac{\zeta}{2} (1 - \cos\alpha) \right]$$

A summation over n using the appropriate combination of the load numbers h_n' and k_n' together with W_n' from equation (5) was used by Pertsev to obtain the tidal gravity and tilt loading due to a disc. The Newtonian attraction gravity and tilt were calculated directly rather than using a series summation. Pertsev calculated the loading response as a function of distance from the centre of various discs ranging from a radius of few thousandths of a degree for local loads up to a radius of 2.8° for distant loads. He found that provided that the distance from the centre of the disc is at least 5 times the disc radius then the replacement of a latitude and longitude cell by an equal area disc caused negligible error. It can be seen that the use of equation (5) for a spherical disc is analogous to the use of equation (4) for a template. Due to the axial symmetry of the disc, only the zero order Legendre polynomials are involved. One advantage of the disc method is that a different grid is not required for every observation site.

Farrell (1973) also calculated the response of the Earth to a disc load by integrating a Green's function across the disc using Simpson's rule. By calculating the response of the Earth to discs of various radii at several distances, he was able to construct a table of disc factors which could be used for speeding up global convolution integrals. Thus a numerical ocean tide model in which the results are given on a latitude and longitude finite difference grid can be replaced by a set of disc loads. Farrell's disc calculations also show that at distances away from the centre of a disc of greater than 10 times its radius, the response is within 1% of the response due to an equivalent point load acting at the centre of the disc. Thus once again it can be seen that if the grid size relative to the distance from the observation point is correctly chosen, then the computation reduces to a summation of the effects due to a set of point masses.

Farrell also pointed out that many of the ocean tide models do not conserve mass and that this has important effects particularly on tidal gravity load calculations. Farrell suggested two methods for forcing mass conservation - removing the P_o term in the Green's function or removing a uniform tide from all the oceans. Goad (1980) followed the first procedure but overall the second procedure has been more widely used. However, Pertsev (1976) and Melchior, Moens and Ducarme (1980) have also introduced corrections proportional to the local amplitude of the ocean tide. Clearly, there is no unique method of conserving tidal mass since the non-conservation is essentially a reflection of the inability of the ocean tide models to correctly resolve the smaller scale hydrodynamics and to model the dissipation mechanisms. However, Agnew (1983) pointed out that removal of the P_o term from the Green's function is incorrect since this procedure does not, in fact, conserve mass.

5. THE POINT LOAD METHOD

The polygon, template and disc methods should all give equivalent results provided that care is taken in choosing the grid size relative to the distance from the observing station. This is particularly important for the nearest sea areas where the Green's function, the tidal amplitude and phase, and the coastal geometry are all varying rapidly with distance. It has also been seen that the grid size can be chosen such that these methods can all be reduced to a summation of the responses due to a set of point mass loads. When the ocean tide model is given in the form of a latitude and longitude finite difference grid, each cell can be replaced by the equivalent point mass acting at the centre of the cell. The nearest cells to the observation site can readily be subdivided in order to check the accuracy of the loading computation and to fit the geometry of the coastline. With the availability of faster computers several papers using this method have been published over the

past few years.

The Green's functions can be calculated using equation (5) for a disc load and taking the limit as the disc radius α goes to zero. In practice, the Green's functions are calculated using a disc load of finite radius, but with the distance from the centre of the disc always being $>$ 10 times the disc radius (Farrell 1972). One advantage of the use of Green's functions is that they give a physical insight into the dependence of the response at various distances on the parameters at various depths within the Earth. This is particularly useful for loading tilt or loading strain (see e.g. Farrell 1972, Beaumont and Lambert 1972, Baker 1980).

REFERENCES

Agnew, D.C., 1983, Conservation of mass in tidal loading computations, Geophysical Journal Royal Astronomical Society, 72, 321-325.

Asch G. and Jentzsch G., 1981, Finite element studies on tidal loading, Earth Evolution Sciences, 1, 87-88.

Baker, T.F., 1980, Tidal tilt at Llanrwst, North Wales : tidal loading and Earth structure, Geophysical Journal Royal Astronomical Society, 62, 269-290.

Beaumont, C., 1978, Tidal loading : crustal structure of Nova Scotia and the M_2 tide in the northwest Atlantic from tilt and gravity observations, Geophysical Journal Royal Astronomical Society, 53, 27-53.

Beaumont, C., and Lambert A., 1972, Crustal structure from surface load tilts, using a finite element model, Geophysical Journal Royal Astronomical Society, 29, 203-226.

Beavan, R.J., 1974, Some calculations of ocean loading strain tides in Great Britain, Geophysical Journal Royal Astronomical Society, 38, 63-82.

Bower, D.R., 1970, Some numerical results in the determination of the indirect effect, pp. 106-112, in Proceedings of 6th International Symposium on Earth Tides, Strasbourg 1969, Communications Observatoire Royal de Belgique, A9(96).

Fang T., Hsu H.T., Chen Z. and Yang H.B., 1983, Effect of ocean tides on gravity observations, in Proceedings of 9th Int. Symposium on Earth Tides, New York 1981, Schweizerbart, Stuttgart, 179-186.

Farrell, W.E., 1972, Deformation of the Earth by surface loads, Reviews of Geophysics and Space Physics, 10(3), 761-797.

Farrell, W.E., 1973, Earth tides, ocean tides and tidal loading, Philosophical Transactions of the Royal Society London, A274, 253-259.

Goad, C.C., 1980, Gravimetric tidal loading computed from integrated Green's functions, Journal of Geophysical Research, 85(B5), 2679-2683.

Groten, E. and Brennecke J., 1973, Global interaction between Earth and sea tides, Journal of Geophysical Research, 78(B5), 8519-8526.

Lambert, A., 1970, The response of the Earth to loading by the ocean tides around Nova Scotia, Geophysical Journal Royal Astronomical Society, 19, 449-477.

Melchior, P., Moens M, and Ducarme, B., 1980, Computations of tidal gravity loading and attraction effects, Bulletin d'Observations des Marees Terrestres, IV(5), 95-133.

Merriam, J.B., 1980, The series computation of the gravational perturbation due to an ocean tide, Physics of the Earth and Planetary Interiors, 23, 81-86.

Moens, M., 1976, Solid Earth tide and Arctic oceanic loading tide at Longyearbyen (Spitsbergen), Physics of the Earth and Planetary Interiors, 13, 197-211.

Pekeris, C.L., 1978, The bodily tide and the yielding of the Earth due to tidal loading, Geophysical Journal Royal Astronomical Society, 52, 471-478.

Pertsev, B.P., 1970, The effect of ocean tides upon Earth tide observations, pp. 113-115, in Proceedings of 6th International Symposium on Earth tides, Strasbourg 1969, Communications Observatoire Royal de Belgique, A9(96).

Pertsev, B.P., 1976, The influence of ocean tides in near zones on Earth tide observations, Izvestiya, Earth Physics, 12(1), 7-11.

Zschau, J., 1976, Tidal sea load tilt of the crust and its application to the study of crustal and upper mantle structure, Geophysical Journal Royal Astronomical Society, 44, 577-593.

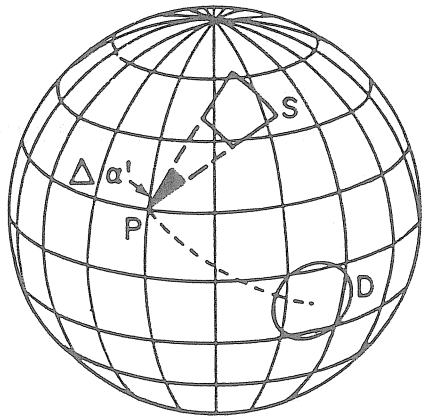

FIGURE 1. Computing the loading response of the Earth at position P due to a uniform tide over a template (sector) S or a disc (cap) D on the surface of the sphere. The template subtends an azimuth angle $\Delta\alpha'$ at P and is bounded by geocentric angles θ_1 and θ_2 with respect to P. The disc D subtends an angle of 2α at the centre of the Earth and its centre is at a geocentric angle θ away from P.

OCEANIC LOADING CORRECTION TO TIDAL STRAIN OBSERVATIONS

H.T. Hsu

Institute of Geodesy and Geophysics, Academia Sinica

ABSTRACT

In this paper we split the loading strain convolutions into two parts, the effects of adjacent ocean zone and of remote region. For the former, convolution integrals are carried out as usual. As to the latter, we have derived a set of working formulas based on the coordinate transformation of the spherical harmonic expansion of tide height, so that it can be directly estimated from the expansion coefficients and the computation work will be decreased greatly.

In practical evaluation, loading strain model consists of superposition of the effects of four main waves, M_2, S_2, O_1 and K_1, and Schwiderski's global cotidal maps associated with the local maps along the coast of China sea are used.

The effect of oceanic loading to strain observations on the earth's surface can be expressed as follows: [1]

$$\vec{\vec{T}} = \begin{pmatrix} \sum_p t_{xx}^p \cos(\omega_p t + \chi_p - \delta_{xx}^p), & \sum_p t_{xy}^p \cos(\omega_p t + \chi_p - \delta_{xy}^p) \\ \sum_p t_{xy}^p \cos(\omega_p t + \chi_p - \delta_{xy}^p), & \sum_p t_{yy}^p \cos(\omega_p t + \chi_p - \delta_{yy}^p) \end{pmatrix} \qquad (1)$$

T is loading strain tensor on the earth's surface, x, y, z are the coordinates of loading point in local horizontal coordinate system (in which, the origin located at observation station and x, y, z are taken positives towards the east, the north and upside respectively) t_{xx}^p, t_{xy}^p, t_{yy}^p and δ_{xx}^p, δ_{xy}^p, δ_{yy}^p are components of loading strain amplitudes and of phase lags caused by tide wave p, and ω_p, χ_p are the angular frequency and astronomical argument of wave p, t is universal time. Generally, it is necessary to consider the effects of eight Schwiderski's global

cotidal maps, namely M_2, S_2, N_2, K_2, O_1, K_1, P_1 and Q_1, associated with four local maps (M_2, S_2, O_1, K_1) along the coast of China sea.

From [1], all the components in (1) can be expressed in the form of following convolution integrals

$$\left.\begin{aligned}
t^p_{xx}\cos\delta^p_{xx} &= \int \mu H^p_c(\varphi,\lambda)(\sin^2\alpha E_{\psi\psi}+\cos^2\alpha E_{\lambda\lambda})\,ds\\
t^p_{xx}\sin\delta^p_{xx} &= \int \mu H^p_s(\varphi,\lambda)(\sin^2\alpha E_{\psi\psi}+\cos^2\alpha E_{\lambda\lambda})\,ds\\
t^p_{xy}\cos\delta^p_{xy} &= \int \mu H^p_c(\varphi,\lambda)(E_{\psi\psi}-E_{\lambda\lambda})\sin\alpha\cos\alpha\,ds\\
t^p_{xy}\sin\delta^p_{xy} &= \int \mu H^p_s(\varphi,\lambda)(E_{\psi\psi}-E_{\lambda\lambda})\sin\alpha\cos\alpha\,ds\\
t^p_{yy}\cos\delta^p_{yy} &= \int \mu H^p_c(\varphi,\lambda)(\cos^2\alpha E_{\psi\psi}+\sin^2\alpha E_{\lambda\lambda})\,ds\\
t^p_{yy}\sin\delta^p_{yy} &= \int \mu H^p_s(\varphi,\lambda)(\cos^2\alpha E_{\psi\psi}+\sin^2\alpha E_{\lambda\lambda})\,ds
\end{aligned}\right\} \qquad (2)$$

where

$$H^p_c=\xi^p\cos\delta^p, \qquad H^p_s=\xi^p\sin\delta^p \qquad (3)$$

ξ^p and δ^p are tide height amplitude and Greenwich phase of wave p, taken from the corresponding cotidal maps; μ density of sea water, equals to 1.03; ds differentiable spherical element; $E_{\psi\psi}$, E_{11} the strain Green functions, both are the functions of polar distant ψ (the spherical distance from mobile element to observation station as shown in fig. 1), and for different ψ, its values can be obtained from various earth interior models:

$$\left.\begin{aligned}
E_{\psi\psi} &= \frac{1}{m}\sum_{n=0}^{\infty} h_n' P_n(\cos\psi)+\frac{1}{m}\sum_{n=0}^{\infty} l_n'\frac{\partial^2 P_n(\cos\psi)}{\partial\psi^2}\\
E_{\lambda\lambda} &= \frac{1}{m}\sum_{n=0}^{\infty} h_n' P_n(\cos\psi)+\frac{1}{m}\operatorname{ctg}\psi\sum_{n=0}^{\infty} l_n'\frac{\partial^2 P_n(\cos\psi)}{\partial\psi^2}
\end{aligned}\right\} \qquad (4)$$

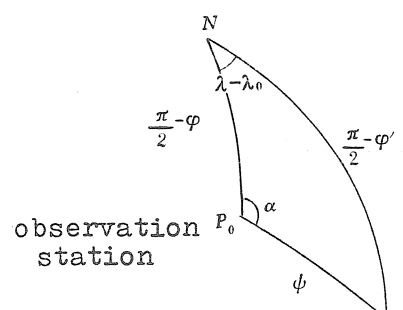

Fig. 1 System of Geographical Coordinate

h'_n, ℓ'_n are the loading Love numbers, m the mass of the earth. The normalized strain Green functions $E_{\psi\psi}$, E_{11} are calculated based on Gutenberg-Bullen and 1066A models shown in fig.2, the computation method can be easily found in [3] [4]

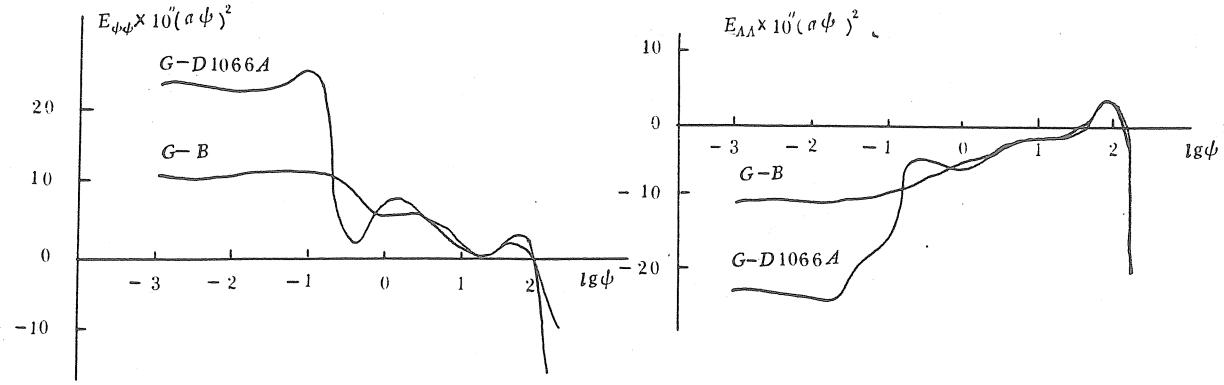

Fig.2 Strain Green Fuction a=6371 km Unit : C.G.S

Therefore, for each tide component, we need to do convolution integral six times, then substituting it in (1), the loading strain tensor is obtained, finally, the linear strain of arbitrary direction can be evaluated too. As convolution (2) needs to carry out numerical integral in global scope, the computation work is rather arduous. However, analysing the properties of Green functions $E_{\psi\psi}$, E_{11}, it is easy to find that their values attenuate rapidly with the increase of ψ. Hence, following the idea given in [5], we can divide the whole convolution into two parts (adjacent zone and remote region) by a spherical cap ψ_0, for example

$$\bar{t}_{xx}\cos\delta_{xx} = t_{xx}\cos\delta_{xx,\mathrm{I}} + t_{xx}\cos\delta_{xx,\mathrm{II}} = \int_0^{\psi_0} + \int_{\psi_0}^{\pi}$$

Here, for convenience, we omit the upper indices in preceding formulas and use lower indices I or II to represent the effect of adjacent zone or remote region respectively. For the former, obviously conventional numerical integral technique can be adopted, so here we put the emphasis on the calculation of the effect coming from remote region.

For this reason, let's expand the tide height (3) into the series of spherical harmonic function:

$$\left.\begin{aligned} H_c(\varphi,\lambda) &= \sum_{n=0}^{\infty} H_{cn}(\varphi,\lambda) = \sum_{n=0}^{\infty}\sum_{m=0}^{n}(a_{nm}\cos m\lambda + b_{nm}\sin m\lambda)P_{nm}(\sin\varphi) \\ H_s(\varphi,\lambda) &= \sum_{n=0}^{\infty} H_{sn}(\varphi,\lambda) = \sum_{n=0}^{\infty}\sum_{m=0}^{n}(a'_{nm}\cos m\lambda + b'_{nm}\sin m\lambda)P_{nm}(\sin\varphi) \end{aligned}\right\} \quad (5)$$

H_{cn}, H_{sn} are the expansions of n-order Laplace's spherical function for the cosine, sine components of the tide height.

The expansions (5) are expressed in terms of geographic coordinates, but on the contrary, in convolution (2) the integral variables (ψ, α) used are coordinates in a polar coordinate system with the origin at observation station. Thus, it is more convenient to develop the tide height into the following spherical harmonics:

$$\left.\begin{aligned} H_c &= \sum_{n=0}^{\infty}\sum_{k=0}^{n}(A_{nk}\cos k\alpha + B_{nk}\sin k\alpha)P_{nk}(\cos\psi) \\ H_s &= \sum_{n=0}^{\infty}\sum_{k=0}^{n}(A'_{nk}\cos k\alpha + B'_{nk}\sin k\alpha)P_{nk}(\cos\psi) \end{aligned}\right\} \qquad (6)$$

The relationship between two sets of coefficients, a_{nm}, b_{nm}, a'_{nm}, b'_{nm} and A_{nk}, B_{nk}, A'_{nk}, B'_{nk} and their transformation have been discussed in detail in [6, 7]. From [6] we have

$$\left.\begin{aligned} A_{nk} &= \sum_{m=0}^{n} a^{k}_{nm}\cdot(a_{nm}\cos m\lambda_0 + b_{nm}\sin m\lambda_0) \\ B_{nk} &= \sum_{m=0}^{n} b^{k}_{nm}\cdot(b_{nm}\cos m\lambda_0 - a_{nm}\sin m\lambda_0) \end{aligned}\right\} \qquad (7)$$

for application, it is deeply concerned in values when k=0 and k=2. From [6], we have

$$\left.\begin{aligned} a^{0}_{nm} &= P_{nm}(\cos\theta_0) \\ a^{2}_{nm} &= \frac{2}{(n-1)(n+2)}P_{nm}(\cos\theta_0) + \frac{4}{(n-1)n(n+1)(n+2)}\frac{d^2P_{nm}(\cos\theta_0)}{d\theta^2} \\ b^{2}_{nm} &= \frac{4m\csc\theta_0}{(n-1)n(n+1)(n+2)}\left\{\operatorname{ctg}\theta_0\cdot P_{nm}(\cos\theta_0) - \frac{dP_{nm}(\cos\theta_0)}{d\theta}\right\} \end{aligned}\right\} \qquad (8)$$

where $\phi_0 = 90° - \phi_0$ is the colatitude of station. Substituting (8) into (7) we obtain

$$\left.\begin{aligned} A_{no} &= H_{cn}(\theta_0,\lambda_0) \\ A_{n2} &= +\frac{2}{(n-1)(n+2)}H_{cn}(\theta_0,\lambda_0) + \frac{4}{(n-1)n(n+1)(n+2)}\frac{\partial^2 H_{cn}(\theta_0,\lambda_0)}{\partial\theta^2} \\ B_{n2} &= \frac{4\operatorname{ctg}\theta_0}{(n-1)n(n+1)(n+2)}\frac{\partial H_{cn}(\theta_0,\lambda_0)}{\sin\theta_0\,\partial\lambda} - \frac{4}{(n-1)n(n+1)(n+2)}\frac{\partial^2 H_{cn}(\theta_0,\lambda_0)}{\sin\theta_0\,\partial\theta\partial\lambda} \end{aligned}\right\} \qquad (9)$$

We have the same expressions for A'_{no}, A'_{n2}, and B'_{n2} but H_{sn} instead of H_{cn}.

From integral formulas

$$\int_0^{2\pi} \sin k\alpha \sin^2\alpha \, d\alpha = 0$$

$$\int_0^{2\pi} \sin k\alpha \cos^2\alpha \, d\alpha = 0$$

$$\int_0^{2\pi} \cos k\alpha \sin\alpha \cos\alpha \, d\alpha = 0$$

$$\int_0^{2\pi} \cos k\alpha \sin^2\alpha \, d\alpha = \begin{cases} \pi & \text{if } k=0 \\ -\frac{\pi}{2} & \text{if } k=2 \\ 0 & \text{if } k\neq 0 \text{ and } k\neq 2 \end{cases}$$

$$\int_0^{2\pi} \cos k\alpha \cos^2\alpha \, d\alpha = \begin{cases} \pi & \text{if } k=0 \\ \frac{\pi}{2} & \text{if } k=2 \\ 0 & \text{if } k\neq 0 \text{ and } k\neq 2 \end{cases}$$

$$\int_0^{2\pi} \sin k\alpha \sin\alpha \cos\alpha \, d\alpha = \begin{cases} \frac{\pi}{2} & \text{if } k=2 \\ 0 & \text{if } k\neq 2 \end{cases}$$

it is easy to derive

$$\left.\begin{aligned}
t_{xx}\cos\delta_{xx,II} &= \sum_{n=0}^{\infty}\left(f_{1n}H_{cn} + f_{2n}\frac{\partial^2 H_{cn}}{\partial\theta^2}\right) \\
t_{xx}\sin\delta_{xx,II} &= \sum_{n=0}^{\infty}\left(f_{1n}H_{sn} + f_{2n}\frac{\partial^2 H_{sn}}{\partial\theta^2}\right) \\
t_{xy}\cos\delta_{xy,II} &= \sum_{n=0}^{\infty} f_{2n}\left\{\frac{\partial^2 H_{cn}}{\sin\theta_0\,\partial\theta\partial\lambda} - \operatorname{ctg}\theta_0\frac{\partial H_{cn}}{\sin\theta_0\,\partial\lambda}\right\} \\
t_{xy}\sin\delta_{xy,II} &= \sum_{n=0}^{\infty} f_{2n}\left\{\frac{\partial^2 H_{sn}}{\sin\theta_0\,\partial\theta\partial\lambda} - \operatorname{ctg}\theta_0\frac{\partial H_{sn}}{\sin\theta_0\,\partial\lambda}\right\} \\
t_{yy}\cos\delta_{yy,II} &= \sum_{n=0}^{\infty}\left(f_{3n}H_{cn} - f_{2n}\frac{\partial^2 H_{cn}}{\partial\theta^2}\right) \\
t_{yy}\sin\delta_{yy,II} &= \sum_{n=0}^{\infty}\left(f_{3n}H_{sn} - f_{2n}\frac{\partial^2 H_{sn}}{\partial\theta^2}\right)
\end{aligned}\right\} \qquad (10)$$

equation (10) is the final working formula, here f_n, f_{2n}, f_{3n} are three sets of coefficients depending on n and ψ_0:

$$f_{1n} = \mu\pi R^2\int_{\psi_0}^{\pi}\left\{(E_{\psi\psi}+E_{\lambda\lambda})P_n(\cos\psi) + \frac{1}{(n-1)(n+2)}(E_{\lambda\lambda}-E_{\psi\psi})P_{n2}(\cos\psi)\right\}\sin\psi\,d\psi \qquad (11)$$

$$f_{2n} = \frac{2\mu\pi R^2}{(n-1)n(n+1)(n+2)}\int_{\psi_0}^{\pi}(E_{\lambda\lambda}-E_{\psi\psi})P_{n2}(\cos\psi)\sin\psi\,d\psi \qquad (12)$$

$$f_{3n} = \mu\pi R^2\int_{\psi_0}^{\pi}\left\{(E_{\psi\psi}+E_{\lambda\lambda})P_n(\cos\psi) - \frac{1}{(n-1)(n+2)}(E_{\lambda\lambda}-E_{\psi\psi})P_{n2}(\cos\psi)\right\}\sin\psi\,d\psi \qquad (13)$$

these three sets of coefficients can be evaluated by carrying out numeral integral to equations (11)-(13) based on various values of n and ψ respectively. Once these coefficients and the expansion coefficients of tide height (5) a_{nm}, b_{nm} and a'_{nm}, b'_{nm} are known, the loading tidal strain

caused by remote region beyond ψ_0 may be more easily calculated from equation (10).

The results of gravity tidal observations in China show that Schwiderski's cotidal map coincides with the actual observation much better than other maps, but the local tidal effect of sea coast must be taken into account together. The loading strains at five stations in China are listed in table 1 which are calculated based on the Green functions obtained by G-B model and the tide heights used are taken from Schwiderski's and local M_2 cotidal map of China sea.

TABLE 1. M_2 loading strain

	Shanghai		Beijing		Huangshi		Tangshan		Haicheng	
	$tx10^{-9}$	$\delta°$	$tx10^{-9}$	$\delta°$	$tx10^{-9}$	$\delta°$	$tx10^{-9}$	$\delta°$	$tx10^{-9}$	$\delta°$
T_{xx}	6.4316	-75	0.9902	+36	0.4284	-67	3.5487	-47	10.154	-260
T_{xy}	11.924	+16	0.3194	-18	0.9869	+35	1.2785	-171	14.140	+67
T_{yy}	1.3820	+44	0.2609	-100	1.0230	+24	3.1120	-240	14.759	-82

So summing up the effects of earth tides and of ocean tides, the theoretical strain tides of any stations can be formed as follows:

$$\varepsilon_{ij} = \varepsilon^s_{ij} + \sum_p t^p_{ij} \cos(\omega_p t + \chi_p - \delta^p_{ij})$$

ε^s_{ij} being body tides strain, ω_p, χ_p the angular frequency and initial phase of wave p. In fig. 3 4a, b, theoretical linear strain s (March 16-17, 1983) of body tides and loading tides in Shanghai station (azimuth N60°E) and Beijing station (azimuth E 71°995) are shown. Where loading effect is superposed by four main tides, M_2, S_2, O_1, K_1, according to Schwiderski's definition their phases χ_p are

$$\chi_{M_2} = 2(h_0 - s_0), \qquad \chi_{S_2} = 0$$

$$\chi_{O_1} = h_0 - 2s_0 - 90°, \qquad \chi_{K_1} = h_0 + 90°$$

it is seen from fig. 3 that the effect of oceanic loading to strain almost arrives the same magnitude as those of body tides at sea shore station,

but the effect will be smaller if the station is far from the open sea, Fig. 3, 4(c) represents superposition of both earth and loading tide strain. It may be seen from this chart, the theoretic model of body tides strain will be greatly distorted by the effect of ocean loading, especially, to their phase. Loading effect could be used for different purpose, for example, if the factor of earth tides in somewhere is acquired, we must avoid the ocean tides interaction as far as possible, on the contrary, if our interest lies in the investigation of the crust-upper mantle structure of the earth or of monitoring the precursor of earthquake we shall try our best to observe the bigger loading strain effect because of sensibility against crust-upper mantle. Obviously, the linear strain depends on azimuth of the observation direction, thus we have calculated the body tide and loading strains at various azimuths and shown in fig. 5. It can be easily seen that the strain caused by M_2 and O_1 has quite different characters for example, both body tides and loading tides, for M_2 the NS component is bigger than the EW component, but for O_1 EW component is a little bit bigger than NS component. On the other hand, at the same place, the EW component of O_1 is bigger than that of M_2. These features result from the tidal character and geographic location. From fig. 5b, it shows that the strain direction in Shanghai is just located in the direction which is more sensitive to ocean tides, but the strain direction in Beijing is located in the direction which is not sensitive to ocean tides, for tilt loading tides the same phenomenon has been found. Doubtlessly, it provides some geophysical information to us.

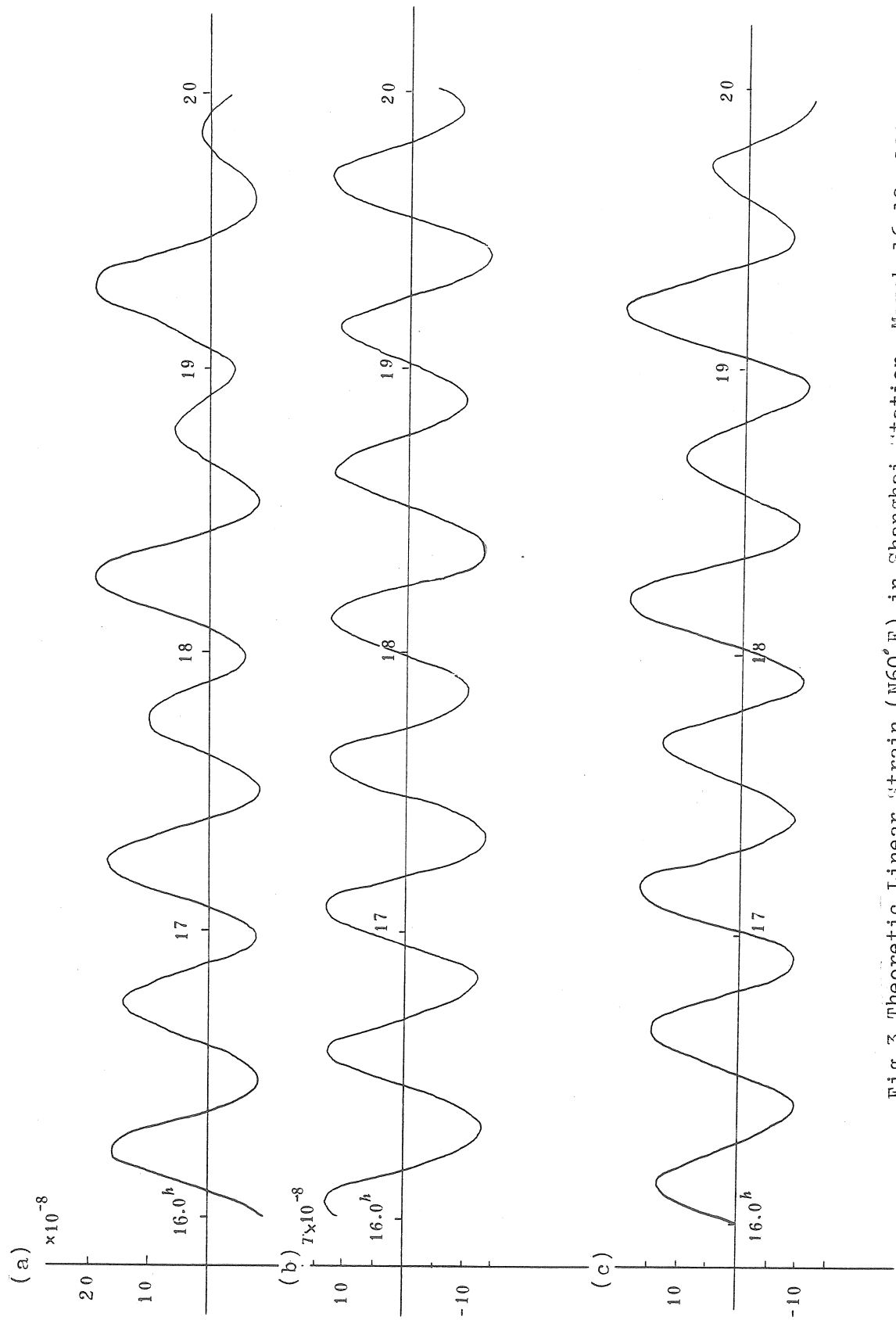

Fig 3 Theoretic Linear Strain (N60°E) in Shanghai Station, March 16-19, 1983

a. body tide b.loading tide c.superposition

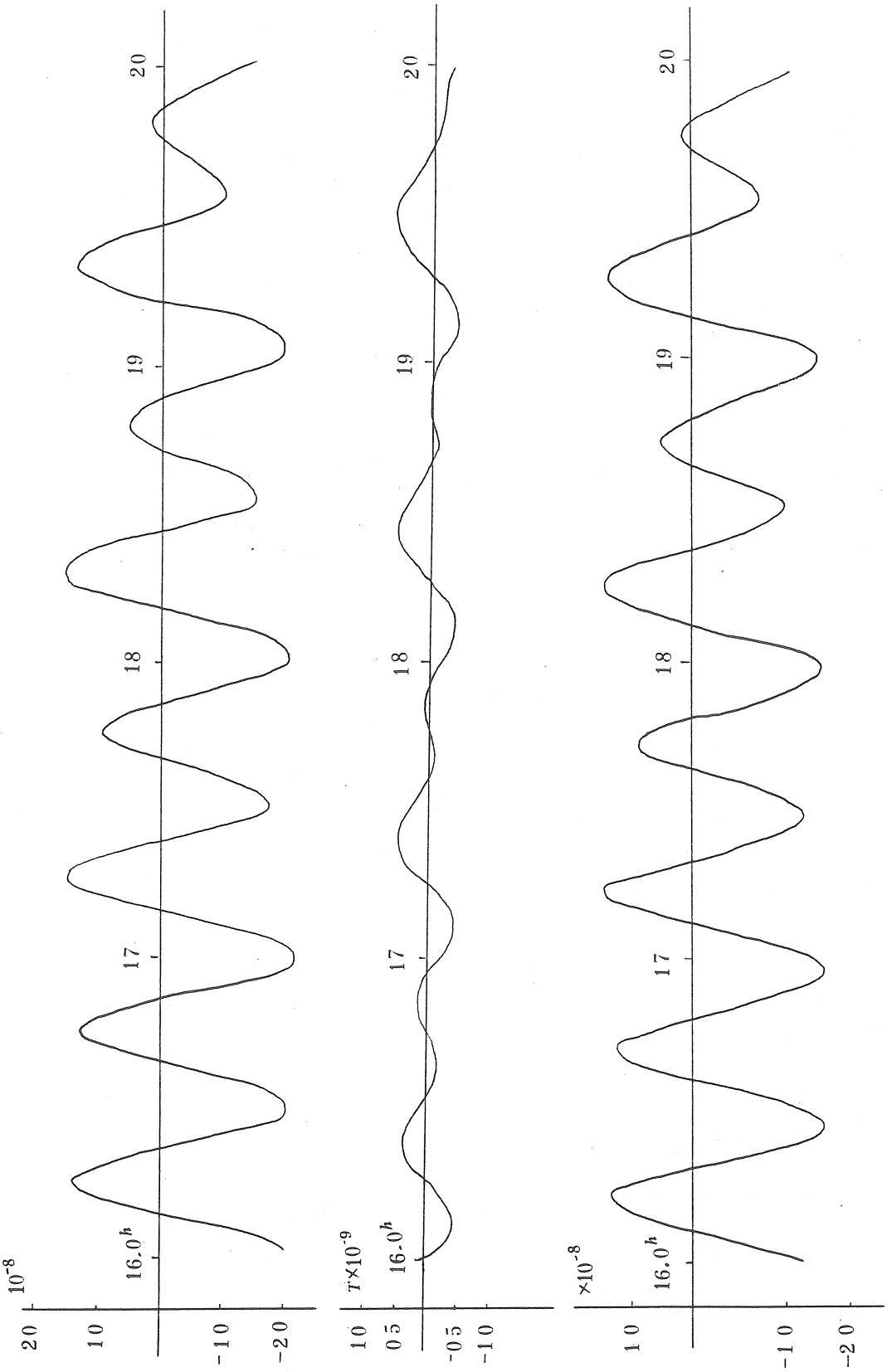

Fig 4 Theoretic Linear Strain (E72.0°S) in Beijing, March 16-19, 1983

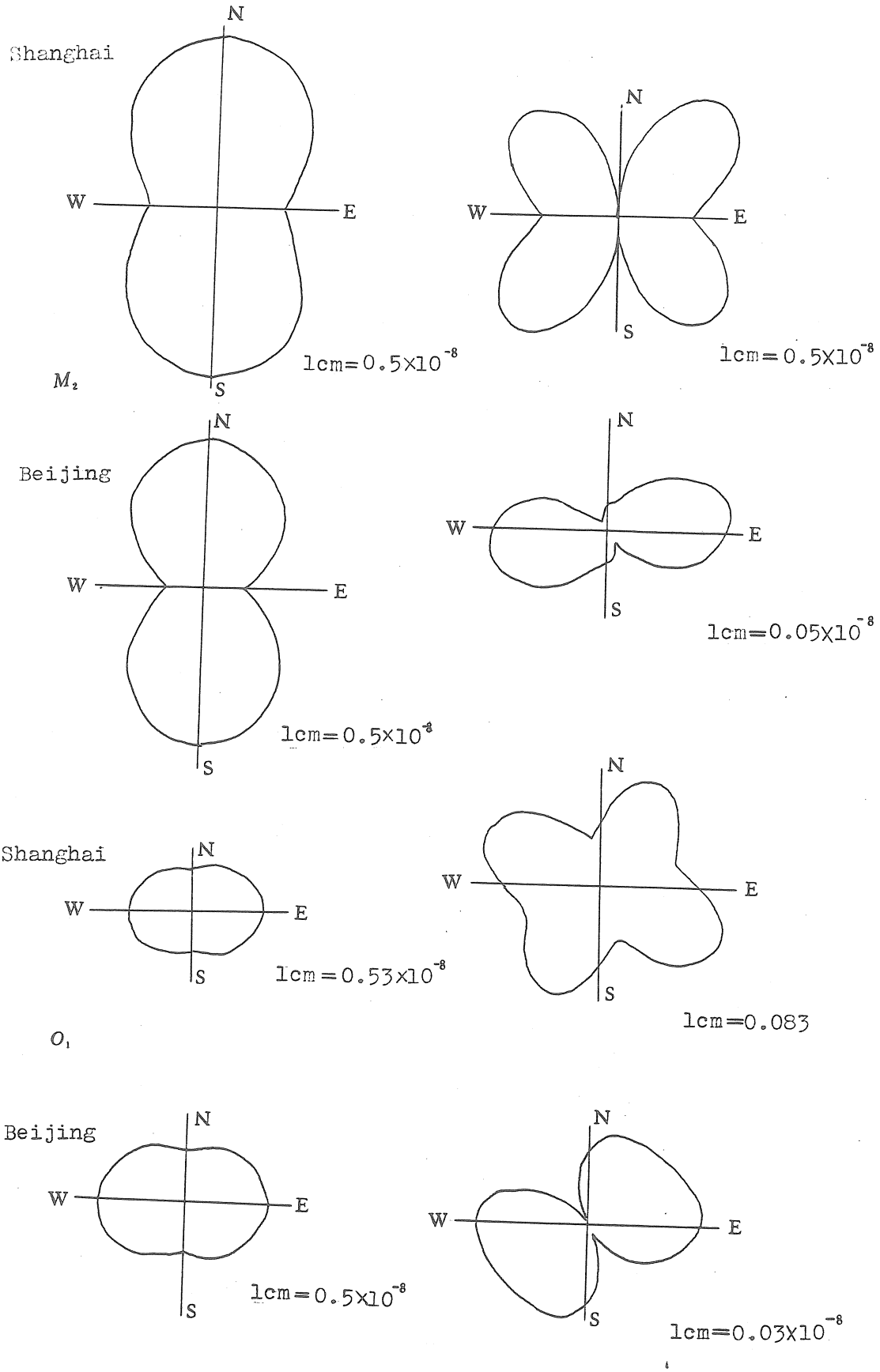

Fig 5(a) body tide strain (b) loading tide strain

REFERENCES

1. HSU, H.T., MAO W.J., ZHANG YONG: Theoretical Model of the Tidal Strain of Earth's Surface (unpublished) 1984.

2. BEAVAN, R.J.: Some Calculation of Ocean Loading Strain Tides in Great Britain. G.J. vol. 38, 63-82, 1974.

3. MAO, W.J.: Static Response of Earth's Surface Mass Acta Geophysica, vol. 27, N°1 74-83, 1984

4. FARRELL, W.E.: Deformation of the Earth by Surface Loads. Rev. Geophys. Space, vol. 10, 761-797, 1972.

5. HSU, H.T., CHENG, Z.B., YANG, H.B.: Effects of Oceanic tides on Tidal Gravity and Tilt Observations Collected Oceanic Works, vol.6, N°2, 43-62, 1983.

6. HSU, H.T., JIANG, F.Z.: On transformation of the Spherical Function Development of Gravity Anomaly. Acta Geodetica et Cartographica Sinica,vol.7,N°4,252-260, 1984

7. HE, MIAAOFU: Second Discussion on transformation of the Spherical Function Development of Gravity Anomaly. Annual Publication of Shanghai Observatory, Academia Sinica, N°4, 1-9, 1982.

8. HSU, H.T., CHENG, Z.B., YANG, H.B.: The Effect of Oceanic Tides on the Gravity Tidal Observation. Acta Geophysica Sinica, vol. 25; N°2, 120-192, 1982.

The influence of the grid structure on the results of loading calculations

by

G. Jentzsch *

1. Introduction

The differences between the theoretical loads calculated by the International Center of Earth Tides (ICET) and the program used in Berlin were the cause to examine some possible sources. Both calculations based on the same version of Schwiderski´s maps, and were used to interprete the results of the tidal gravity measurements along the "Blue Road Geotraverse" in Norway and Sweden (Jentzsch, 1983).

2. Calculated and observed residuals for O1 and M2

In tab. 1 the calculated and observed loads are compared. The observed residuals are based on the results of the final analyses, assuming $\delta = 1.16$. The computations of the theoretical load were carried out in Berlin using a current version of Farrell´s program (Farrell, 1972) and the Schwiderski maps provided by ICET (Schwiderski, 1979; 1980; Ducarme, 1984), where the middle section of the Norwegian shelf was shifted by -15°.

The results for O1 show a good agreement of the theoretical amplitudes, but a significant phase shift of $\sim 7^{\circ}$. Compared to the observations from Nesna and Umbukta the amplitudes are too small at about 45%, whereas the errors of the observations are less than 20% in amplitude and 15° in phase.

* Institut für Geophysikalische Wissenschaften der Freien Universität Berlin, Rheinbabenallee 49, D-1000 Berlin 33

Tab. 1: Observed and calculated load (microgals, degrees)
(station elevation not corrected)

Station	theoretical load from Schwiderski ICET original		Berlin original		Berlin shelf -15°		observed	
O1								
NESNA	.44	133	.45	138.0	—		.853 ± .070	114.65 ± 4.70
HEMNES-BERGET	.43	132	.54	134.1	—		.493 ± .046	134.69 ± 5.35
UMBUKTA	.35	131	.35	138.7	—		.633 ± .146	55.04 ± 13.21
TÄRNABY	.32	131	.32	139.5	—		.347 ± .032	112.89 ± 5.28
M2								
NESNA	2.75	179	3.28	178.1	3.16	-172.9	2.834 ± .056	-171.60 ± 1.13
HEMNES-BERGET	2.69	177	5.75	-178.0	5.67	-173.8	5.635 ± .047	-172.65 ± .48
UMBUKTA	1.60	165	2.05	166.8	1.92	175.8	1.710 ± .079	170.58 ± 2.65
TÄRNABY	1.15	157	1.56	161.7	1.44	170.5	1.429 ± .009	170.04 ± .35

Since the effect of the loading of the Rana fjord area is only small (less than 0.2 μgal for Nesna, and less than 0.1 μgal for Umbukta) errors of the modelling of the local marine tide cannot be responsible for these discrepancies.

The results for the wave M2 are more significant: Both programs calculate different load vectors for Nesna, Hemnesberget, Umbukta and Tärnaby. It can be shown, that a shift of -15° of the middle section of the shelf tides provides a fairly good fit of the theoretical (Berlin) to the observed load. This phase shift is indicated by recent water level records.

According to these differences and with regard to the unexpected high residual from Hemnesberget some possible error sources are examined in the following.

3. Error sources for the computations

Here only the effects of the M2-ocean tidal input will be examined, not the algorithms used in the programs (Jentzsch, 1985).

In the data set for Schwiderski´s maps provided by ICET the coordinates of the mass center of the $1^{\circ} \times 1^{\circ}$ grid are just the mean values between both longitudes (which is correct) and both latitudes. Since esp. in polar regions the shape of a $1^{\circ} \times 1^{\circ}$ element changes approximately from a square to a trapezium the coordinates of the mass center have to be moved towards the equator. For latitude 60° this means a deviation of only ~1 km, for 80° it is ~3 km. The gravity effect is small, and it depends on the amplitude of the tidal load and on the location of the station: For Nesna it amounts to 0.2 μgal and 0.6°, and decreases rapidly for inland stations.

Tab. 2 contains the effects of different ocean patches on the coastal stations, calculated for sea level. It is obvious, that the middle section of the Norwegian shelf tides (about 64° to 70° north) covers more than 65% of the total load. An error of only 10% in amplitude amounts to 0.1 μgal at Tärnaby, 140 km far from the coast. This corresponds to the phase shift of -15° (compare tab. 1).

Near the coast a correct approximation of the coast line is crucial. The $1^{\circ} \times 1^{\circ}$ trapezium of Schwiderski´s map of this area provides about 0.65 μgal, which has to be removed and replaced by the local tidal distribution.

According to these results the estimations of the loading

Tab. 2: Theoretical load for M2 from adjacent seas compared to total load at sea level (microgal, degrees)

Ocean	NESNA	HEMNESBERGET	UMBUKTA	TÄRNABY
Rana fjord (inner)	.18 -169.2	.19 -171.0	.02 -172.8	.01 -174.1
Rana fjord (outer)	.34 -170.1	.21 -172.4	.12 -174.8	.07 -175.4
North Norw. shelf	.35 127.7	.36 126.5	.36 124.0	.33 120.8
Middle Norw. shelf	1.82 -168.5	1.58 -170.5	1.24 -173.2	.98 -173.6
South Norw. shelf	.18 -143.9	.17 -145.0	.15 -146.8	.15 -148.0
Norw. Greenland Sea	.52 -114.9	.49 -113.4	.46 -110.5	.44 -106.7
Total	3.00 177.7	2.62 173.7	1.98 166.2	1.54 161.5

effects closer than 200 km to the coast are influenced to a high degree by the local grid structure.

The unexpected high amplitude of the observed residual at Hemnesberget is due to the attraction effect of the tide. This station was situated on a peninsula in the fjord area at an elevation of 83.3 m. Due to this fact the ratio of the normalized Green´s functions of about 6 to 10 (deformation/Newtonian attraction) is changed to about 1.6, which results in an amplification of the attraction effect by factor 7: The effect of the elevation is greater than 3 μgal.

4. Conclusions

Since the results were obtained from the interpretations of the tidal gravity measurements along the Fennoscandian "Blue Road Geotraverse" (Jentzsch, 1985), they are not representative for all possible stations. Nevertheless, the following conclusions can be drawn:

(1) The coordinates of the ocean cells should be corrected for the true mass center.

(2) Calculations of theoretical load vectors for stations closer than 200 km are meaningless, if no improvement of the grid structure at the coast line is made, and if no local tidal model is used. Between 200 km and 300 km from the coast one has still to be aware of possible local effects.

(3) Depending on the amplitude of the load and the form of the coast line the additional attraction effect of the marine tide for stations higher than sealevel has to be taken into account. This is of special importance for stations within 20 km to the coast, but also stations up to a distance of 50 km may be effected.

5. References

Farrell, W. E., 1972: Deformation of the earth by surface loads.- Rev. Geophys. Space Physics, 10(3), 761-797.

Ducarme, B., 1984: personal communication.

Jentzsch, G., 1983a: A gravity tidal profile along the "Blue Road Geotraverse" - aims of research and present state of the project.- BIM, 89, 5737-5741.

Jentzsch, G., 1985: Auflastgezeiten in Fennoskandien. - Fachbereich Geowissenschaften der Freien Universität Berlin (internal report)

Schwiderski, E. W., 1979: Global ocean tides, part II: The semidiurnal principal lunar tide (M2), tlas of tidal charts and maps.- NSWC, Dahlgren.

Schwiderski, E. W., 1980: Global ocean tides, V. The diurnal principal lunar tide (O1). - NSWC, Dahlgren.

A DATA BANK FOR EARTH TIDES

B. Ducarme[x]

International center of Earth Tides (ICET/FAGS)
Observatoire Royal de Belgique, 1180 Bruxelles, Belgium.

A data bank is operational at ICET. For about 250 tidal gravity stations from which data were made available to ICET it can retrieve :

- a geographical and geological description of the station with the list of all operating instruments, and epochs of observations.
- the analysis results concerning the main tidal waves (up to 35 components depending upon of the registration length).
- the residual vector $\overline{B}$ obtained by subtracting from the observed tidal vectors the gravity tide of the Molodensky I earth model.
- the oceanic attraction and loading vector $\overline{L}$ computed from the Schwiderski oceanic cotidal maps taken as working standards for the waves Q_1, O_1, P_1, K_1, N_2, M_2, S_2 and K_2.
- the eight corresponding final vectorial residues $\overline{X} = \overline{B} - \overline{L}$.

The exploitation programs allow to extract tabulated results for conventional geographical areas as well as for individual stations.

---

[x] Chercheur Qualifié au Fonds National de la Recherche Scientifique